Density Functional and Hybrid QM/MM Calculations of Cu_{13}-Clusters with Alkylthiolate Ligands and their Two-Dimensional Periodic Arrangements

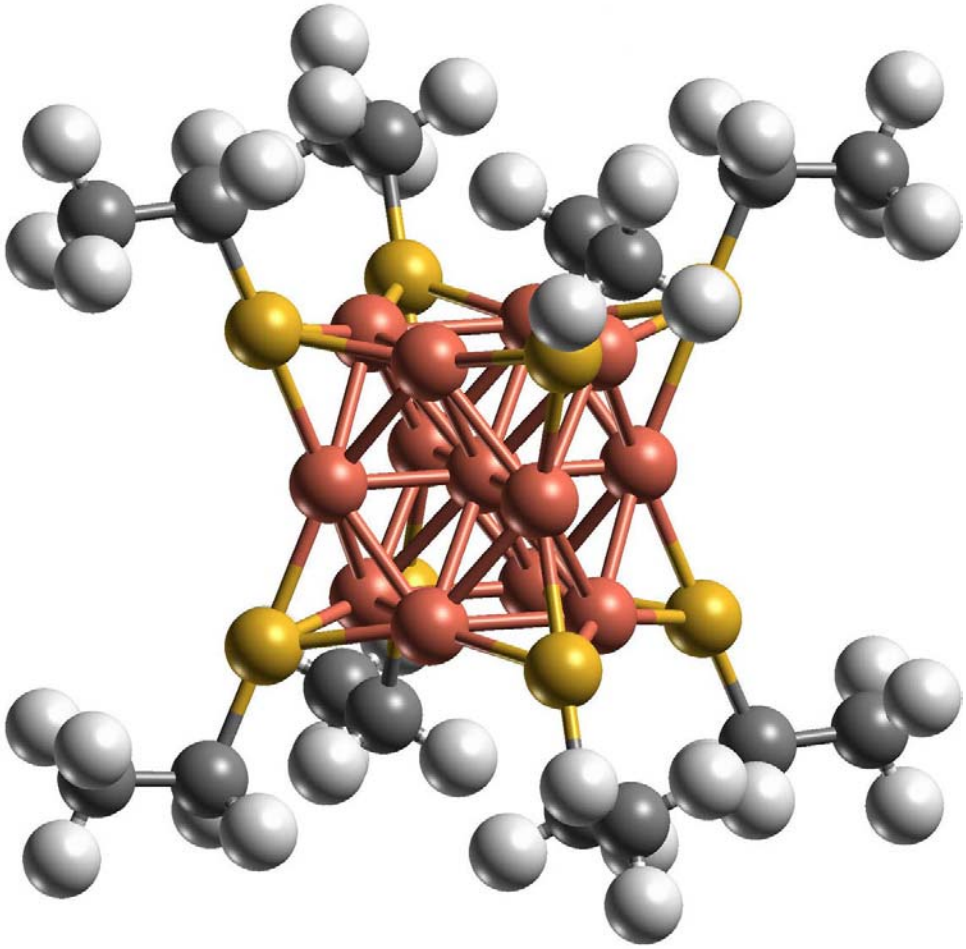

André Woiterski

Institut für Physikalische und Theoretische Chemie,

Lehrstuhl für Theoretische Chemie

der Technischen Universität München

Density Functional and Hybrid QM/MM Calculations of Cu_{13}-Clusters with Alkylthiolate Ligands and their Two-Dimensional Periodic Arrangements

André Woiterski

Vollständiger Abdruck der von der Fakultät für Chemie der Technischen Universität München zur Erlangung des akademischen Grades eines

Doktors der Naturwissenschaften (Dr. rer. nat.)

genehmigten Dissertation.

Vorsitzender:		Univ.-Prof. F. H. Köhler
Prüfer der Dissertation:	1.	Univ.-Prof. N. Rösch
	2.	Univ.-Prof. St. J. Glaser

Die Dissertation wurde am 7. 4. 2003 bei der Technischen Universität München eingereicht und durch die Fakultät für Chemie am 8. 5. 2003 angenommen.

Danksagung

Meinen besonderen Dank möchte ich Herrn Prof. Dr. N. Rösch für die Vergabe des interessanten Themas, die Schaffung optimaler Rahmenbedingungen und sein großes persönliches Engagement bei der Betreuung dieser Arbeit aussprechen.

Ebenso danke ich Herrn Dr. Sven Krüger für seine unermüdliche Bereitschaft zu wissenschaftlicher Diskussion aller Art und seine hilfreichen Ratschläge, die entscheidend zum Gelingen dieser Arbeit beigetragen haben.

Herrn Prof. Dr. W. Domcke und den Mitgliedern seines Arbeitskreises möchte ich ebenso wie den Sekretärinnen Frau I. Braun und Frau R. Mösch für das angenehme Klima am Lehrstuhl sowie die erhaltene Unterstützung danken.

Meinen Kollegen Dr. Habbo Heinze und Herrn Alexander Genest, sowie meinem Zimmernachbarn Herrn Florian Schlosser sei hier besonders für die zahlreichen Diskussionen und Aktivitäten gedankt, die eine freundschaftliche und erfolgreiche Zusammenarbeit angenehmer gemacht haben. Auch meinem Kollegen Dr. Philip Gisdakis danke ich für die freundliche Unterstützung gerade während der Anfangszeit meiner Arbeit.

Mein Dank gilt auch meinen Kollegen, den Damen Dr. M. Garcia-Hernandez, Dr. M. Fuchs-Rohr, Dr. C. Lauterbach, Dr. L. Moskaleva, D. Dogaru und P. Chuichay sowie den Herrn R. Krawczyk, M. Suzen, M. Girju, Dr. R. Malek, A. Matveev, T. Seemüller, Dr. W. Alsheimer, K. Siriwong, PD U. Birkenheuer, Dr. T. Kerdcharoen, Dr. K. Neyman, Dr. A. Voityuk, D. Ganyushin, C. Inntam, K.-H. Lim, Dr. A. Gordienko, Dr. V. Nasluzov, Dr. S. Majumder und Dr. Z. Chen sowie allen Kollegen, die hier nicht namentlich erwähnt sind, für die angenehme Atmosphäre, fachliche und private Diskussionen und interessante Vorträge.

An dieser besonderen Stelle danke ich meiner Freundin Claudia Dahmen, deren Ermunterung und Geduld diese Arbeit entscheidend erleichtert hat. Meinen Eltern, meiner Schwester sowie meiner weiteren Familie danke ich für die Unterstützung, die sie mir Zeit meines Lebens haben zukommen lassen.

Contents

List of Abbreviations

Å	Ångstrøm
au	atomic units
ax	axial
BP	Becke-Perdew
ce	central
covEPE	covalent Elastic Polarizable Environment
DF	Density Functional
DFT	Density Functional Theory
E_B	binding energy
E_f	Fermi Energy
EPE	Elastic Polarizable Environment
eq	equatorial
eV	electron volt
fcc	face centered cubic
GGA	Generalized Gradient Aprproximation
HF	Hartree-Fock
HOMO	Highest Occupied Molecular Orbital
IMOMM	Integrated Molecuar-Orbital Molecular-Mechanic
IP	Ionization Potential
kcal/mol	Kilocalories per mole
k	Boltzmann constant
LDA	Local Density Approximation
LSDA	Local Spin Density Approximation
LUMO	Lowest Unoccupied Molecular Orbital
MM	Molecular Mechanics
n, j, i, k, l	generic variables
nm	nanometer
PCM	Polarizable Continuum Method
pm	picometer
QM	Quantum Mechanics
QM/MM	Quantum Mechanics/Molecular Mechanics

rcut	generic cutoff parameter
rvdw	cutoff parameter of van der Waals interaction
T	temperature
TEM	Transmission Electron Microscopy
vdW	van der Waals
VWN	Vosko-Wilk-Nusair
δ	Kubo-gap

1. Introduction

To model chemical systems of interest in varying degrees of approximation has a long tradition in quantum chemistry. With each consecutive step of model and method refinement, one can gain additional insights in the properties of the respective system. In this thesis methods and models for the computation of ligand covered metal clusters will be developed and applied. Small copper clusters with thiolate ligands of the general composition $Cu_{13}(S(CH_2)_nCH_3)_8$ with n = 1, 2 were chosen as model systems. Two ways of improving the model will be employed. On the one hand, the chemical composition of the clusters will be varied. Beginning with a bare copper cluster which is readily available in physical experiments[1], the model will be extended to clusters protected by an alkyl thiolate shell of varying chain lengths, leading to the ordered layer model of thiolate covered copper clusters. Model ligands (SH) will be used in an intermediary step. Concomitantly, different computational chemistry methods will be applied. They will be compared with respect to their applicability for different model refinements. Bare small transition metal clusters are advantageously described by “ab initio” approaches, such as the density functional (DF) method.[2,3] As the model size increases by incorporation of thiolate ligands in the model, the computational effort of pure “ab initio” methods becomes prohibitively high. A combined quantum chemical and molecular mechanics method (QM/MM) will be applied to such models.[4-6] By way of comparison with "ab initio" results it will be shown, that this approximation actually improves the description of dispersive electron-electron interaction. This combined method will be applied to ordered structures of thiolate protected metal clusters. This thesis will demonstrate the QM/MM approach being an attractive method to compute the properties of complex ligand protected clusters as well as their ordered arrangements.

1.1. Motivation

Ordered structures of ligand protected metal clusters are a new class of chemical systems, which have been systematically developed only recently.[7,8] The first synthesis of thiolate protected metal clusters was conducted with gold as cluster metal.[9] This element forms stable aggregates with alkyl thiolates at the surface of the bulk metal as well as at cluster surfaces.[10] Furthermore, the alkyl chains of these aggregates tend to form self-organized ordered monolayers, called SAMs (self-assembled monolayers).[11-14] This phenomenon has been experimentally observed on metal surfaces of gold, silver, copper and other transition metals.[15] The same behavior was shown in force field

computations of thiolate ligands on gold nanocrystallites by Luedtke and Landmann,[16] where bundles of ligands assemble. Thus, it is obvious to assume that the interaction of the ligands plays an important role in the organization of metal clusters to ordered structures.[16] It was one goal of this thesis to examine the role of ligand interactions in the formation and stabilization of cluster layers. Similarly difficult as the observation of ligand interaction and their conformation is the experimental determination of properties of ordered layers of clusters such as the binding energy of individual ligands, the stabilization energy of a layer and the effective chain length of ligands.[17] These properties are easier accessible in computational investigations.

One-,[18] two-[19] and three-dimensional[20,21] arrays of clusters are known and subject of investigation.[22-32] They have been proposed as the next generation of computational devices.[33] They could be utilized like conventional semiconductors or in a unique way as quantum dots. Clusters may be used in heterogeneous catalysis, because low coordinated surface atoms like edges of specific surface facets, which have been identified as key catalytic sites, make up a large part of the cluster surface.[34] Although thiolate covered copper clusters are known,[35] their ordered structures have not yet been synthesized.

Gold is a difficult element to treat computationally in "ab initio" methods, as it possesses a large number of electrons, which in addition experience substantial relativistic effects. The computational problem scales as a power of the number of electrons. Thus, the limit in reasonable computation time and physical capability of the computer is reached at relatively small system sizes, (Au_n, n = 10-100), depending on the approximations applied. For these reasons, gold was substituted by copper as a simplified model. Its lower number of electrons and negligible relativistic effects allow faster computation of systems of equal size. To keep the computational effort manageable with increasing ligand lengths, only clusters of 13 copper atoms were investigated. Bare copper clusters were easily computable with the DF method this way. The inclusion of the thiolate ligands into the model increased the system size considerably. Therefore, an QM/MM method was implemented and tested on these cluster systems. In this method, only the cluster core and the head groups of ligands are treated by the DF method. The tail groups of the ligands are treated only by molecular mechanics (MM).[36-39] As the MM method is significantly less computational expensive, the hybrid QM/MM approach allows models with realistic ligand lengths.[40] To assess the interaction of ligand shells of neighboring clusters in ordered layers, the periodic model was used.[41,42] One cluster is interacting with periodic images of itself. This

interaction is restricted to the MM part of the QM/MM model. With the newly implemented method it was possible for the first time to compute properties of periodic cluster arrangements with a realistic model.

1.2. Investigated Topics

Chapter 2 will introduce the reader to transition metal clusters. It will discuss computational chemistry methods for treating ligand covered clusters and their ordered structures. Some computational and experimental results will be presented for later reference.

Chapter 3 will detail some important topics of the methods used in the QM/MM approach. The choice of copper as a model for silver and gold will be justified. A sketch of the density functional method and the molecular mechanics approach and their applicability to the computational treatment of metal cluster systems will be presented. The background of the QM/MM approach is highlighted. The special features of the implementation constructed in the course of this thesis will be compared to earlier implementations. The considerations necessary in the implementation of periodic boundary conditions in the QM/MM method will be presented. The results of test calculations using the programs TINKER[43] and DL_POLY_2[44] as MM programs will demonstrate the applicability of the QM/MM implementation to copper clusters and periodic systems. Computational details will be presented in Chapter 4.

Chapter 5 begins with the discussion of the bare Cu_{13} cluster. The result of geometry optimizations with four different symmetries with the LDA functional will be discussed and a geometry of the Cu_{13} cluster as the cluster core model of subsequent calculations will be proposed as a tradeoff between computational accuracy and speed. Subsequently, the $Cu_{13}(SH)_8$ model will be used to determine the binding site dependence of properties of thiolate ligands bound to small copper clusters.

Chapter 6 compares quantum mechanical (DF) results with the treatment of $Cu_{13}(SCH_2CH_3)_8$ in the QM/MM method. The differences in the geometric structure of the various results will be emphasized and rationalized. Total energies and binding energies of the ligands will be discussed with respect to the influences caused by differences in the computational models.

Finally in Chapter 7, the QM/MM implementation using periodic boundary conditions will be applied to two-dimensional arrays of copper clusters with ethylthiolate and propylthiolate ligands. Computed lattice constants for cluster layers in different arrangements will be presented. The energy contributions of different parts of

the model will be examined. Conclusions for the applicability of the QM/MM approach using periodic boundary conditions to metal cluster systems with complex ligand shells will be drawn.

2. Clusters

2.1. General Remarks

In the course of this work the term metal cluster is used as defined by Cotton: [45]

"*Any compound of a finite group of metal atoms participating in direct metal - metal bonds with a considerable overlap of binding orbitals.*"

Ligands may be chemically bound or physically adsorbed to clusters. Properties of bulk metals change very little when the size of a sample is reduced to a few tens of micrometers. This behavior is known as the size invariance of properties of solids.[46] When the size of the metal particle under consideration falls below a material dependent limit, this observation is not true anymore. While for instance, electronic energy levels are so minimally spaced as to be indistinguishable in the bulk, single energy levels gradually emerge when reducing the samples size.[47-52] This leads to a semiconductor like electric conductivity, opening up possibilities of electronic or magnetic research and applications.[53]

Most common metals are arranged in the bulk form in a way that their volume is lowest with maximized overlap of binding orbitals. In the case of copper and late transition metals, this is accomplished in the fcc lattice. Cluster structures mirror this arrangement. Atom arrangements with as few as 6 atoms, order themselves in a way best reflecting a sphere. The geometrical formation of perfectly spherically structures as well the presence of particular numbers of electrons give rise to a special stability of "magic" numbered clusters (6, 8, 13, 19, 20, 38, 40, 44, 55, 58, 85, 92, 138, 147, etc.).[54,55] From a geometric point of view these magic numbers describe arrangements in which closed shells of either icosahedral (13, 55, 147), octahedral or cuboctahedral (6, 13, 19, 44, 55, 85, 147) symmetries are achieved. Important electronic numbers are multiples of full shell numbers of atomic orbitals (2, 8, 20). While magic number clusters are thought to highly symmetric, the geometric conformations of non-magic numbered clusters are generally less easy determined.[56]

Inter-atomic distances between metal atoms fall in the range between the bulk values and the bond lengths in gas phase dimers.[57,58] Surface atoms of small metal particles and metal clusters frequently exhibit different properties than inner atoms, because of lower coordination.[59]

2.2. Metal Clusters of 13 Atoms

In the M_{13} cluster of fcc metals, a bulk like coordination of 12 atoms can be achieved at least for one atom. It was shown for the example of mercury, that additional coordination greatly stabilizes the cluster.[60] Thus, reasonably realistic model for a cluster with surface and bulk atoms consists of at least 13 atoms.

There are two highly symmetric conformations of a 13-atom cluster. One is the icosahedron, with one atom in the center and 12 atoms forming an regular icosahedron at an evenly spaced distance. All 12 atoms of the first shell exhibit the same distance to the central atom. This inter shell distance is not identical with the distance of the first shell atoms to each other. This way, a *n* shell icosahedral cluster possesses at least *n* geometric degrees of freedom.

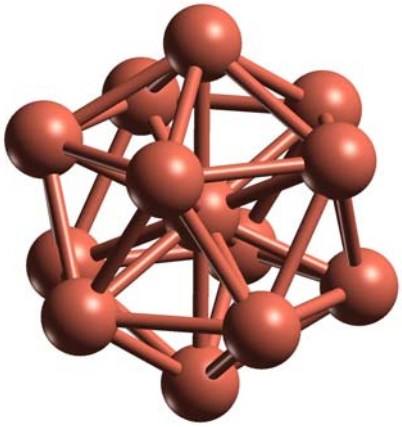

Figure 1 M_{13} cluster in icosahedral symmetry

The high symmetry of the icosahedron allows only a limited number of ways of organizing ligands around this cluster, when retaining all or most symmetry elements. Icosahedral cluster models are seldom discussed.[61] The aim of a relatively flexible ligand arrangement without considerable loss of symmetry prohibited the use of this model in this thesis.

A second way of organizing 13 atoms highly symmetric, is the truncated octahedron or cuboctahedron. It is derived by removing six apex atoms of a 19-atom octahedron (Figure 2 a). A regular cuboctahedron possesses O_h symmetry. The bond lengths between the atoms of the outer shell and the distance between the center atom and the shell are equal. A *n* shell cuboctahedron in octahedral symmetry exhibits at least *n* degrees of freedom. Distorting the cuboctahedron can lower the symmetry to D_{4h}, as shown in Figure 2 b. This conformation shows up to 6 sets of bond lengths. There is no

simple formula to calculate the number of degrees of freedom, as some of these bond length sets may be degenerate.

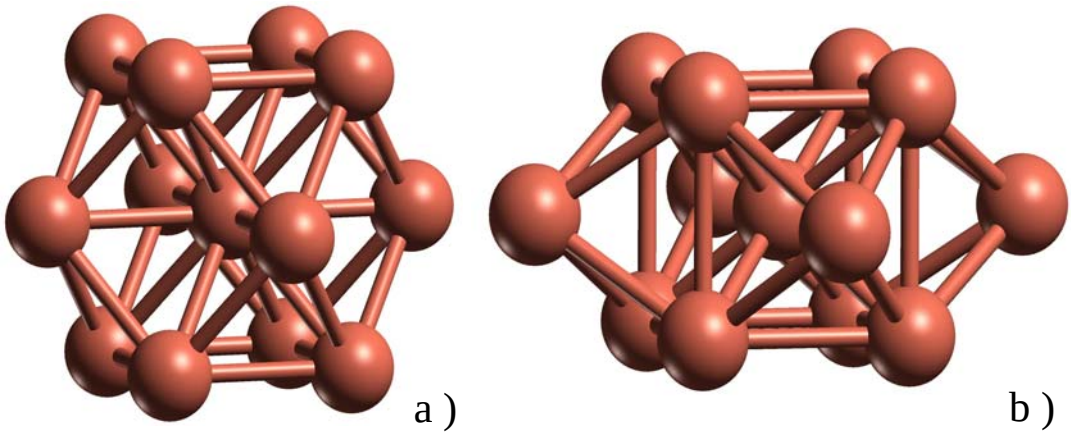

Figure 2 M_{13} cluster in a) cuboctahedral (O_h) and b) upset cuboctahedral (D_{4h}) conformation

Breaking the D_{4h} symmetry of the distorted cuboctahedron leads to D_{2h}, C_{4v} or lower symmetric structures. The resulting cluster exhibits irregular surface facets, as opposed to the O_h cluster.

2.3. Ligand Binding Sites

Clusters are often covered with a stabilizing ligand shell, as they are reactive and unstable otherwise. The position of ligand head groups relative to the cluster surface can be designated by analogy to the terminated surface orientations of bulk lattices. Thus, they are referenced with the corresponding Miller indices. For a comprehensive introduction of the nomenclature of the M_{13} cluster in cuboctahedral conformation and its possible ligand binding sites, the terms central, equatorial and axial atoms are introduced. Their respective positions are illustrated in Figure 3.

In the order of ascending Miller's indices the surface facets are labeled as follows. The facet made up by four adjacent axial atoms is the (100) facet. A fourfold rotation axis passes through the center of this facet. Ligands may bind to this facet in central position above the center. The ligand nomenclature μ_4-(100) was coined, because ligands are bridging four metal atoms this way. Ligands above the triangle facets formed by two adjacent axial atoms and one equatorial atom, the (111) facets, are called to be bridging a threefold-hollow position, or μ_3-(111). As seen in Figure 3, a threefold

axis of symmetry passes through this facet. Other ligand binding sites are the site bridging two axial atoms (bridge; μ_2) and the site on top of one of the axial or equatorial atoms (on-top; μ_1).

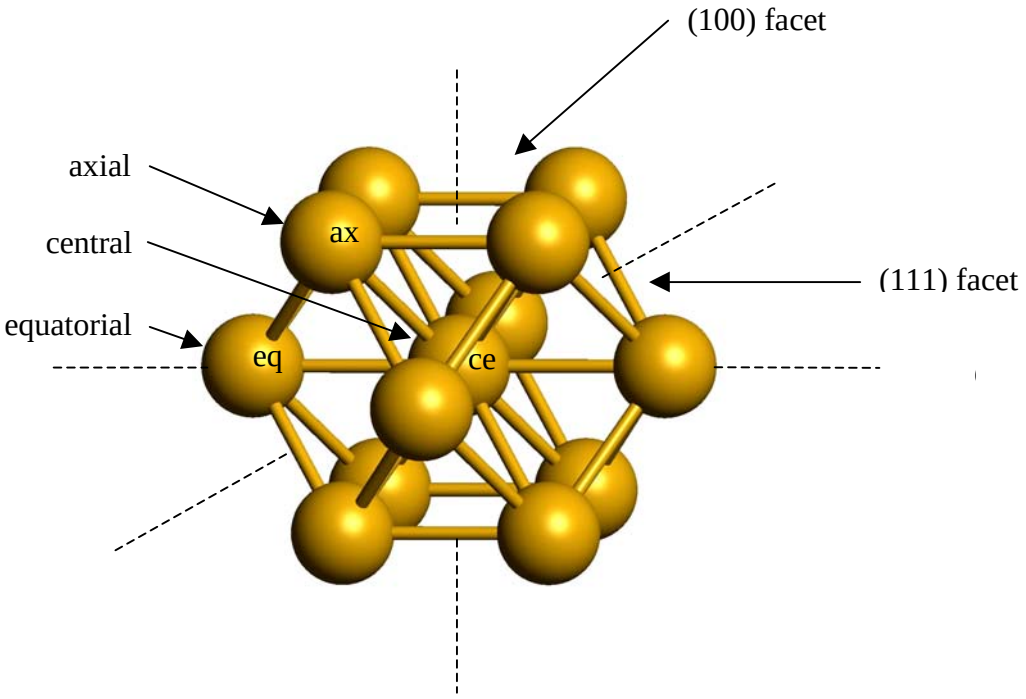

Figure 3 Nomenclature of atoms and facets in a regular M_{13} cuboctahedron

Depending on the geometry and chemical nature of the ligand, the binding site may not be one of the ideal sites indicated above. When ligands occupy intermediate sites not directly associated with crystal facets or symmetry elements, they will be designated with a mixed identifier most closely related to their proposed binding site, such as bridge-hollow, on-top-bridge, etc.

Alkyl thiolates are derived from their respective thioles. The two lone electron pairs of the sp^3 hybrid sulfur lead to a near tetrahedral surface-sulfur-tail angle in the free and adsorbed thiole molecule. The exact mechanism of the thiole adsorption on transition metal surfaces is still subject of investigation.[15,62-66] All models employed in this thesis invoked the vanishing hydrogen theory,[66] where the hydrogen is assumed to dissociate from the thiole and evaporate from the cluster. It should be noted that newer computational hints exist for a model, where the thioles remain intact.[67] The thiolate adsorbate is assumed to prefer μ_2 and μ_3 positions on most transition metal surfaces in most models.[68] Under the influence of the morphology of the underlying surface and the ligand coverage of the cluster even on top sites may be occupied, as suggested in

computations of $Au_n (S(CH_2)_xCH_3)_m$ clusters.[16] The conformation of the alkyl chains is thought to adapt to the chemical environment.

2.4. Electronic Properties

The electronic structure of a metal cluster depends on its size. For small metal particles, the density of states (i.e. the spacing of electronic energy levels) is not (quasi-)continuous as in the bulk material, but discrete. This is due to the confinement of the electron wavefunctions because of the finite size of the particle. The average electronic energy level spacing of successive quantum levels within a band is known as the Kubo gap δ. Its dependence is given by:

$$\delta = 4\,E_f / 3n\,, \qquad (2.1)$$

where E_f is the Fermi energy of the bulk material and n is the total number of valence electrons in the nanocrystal.[69] For copper metal, the Fermi energy at room temperature is 7.03 eV.[70] Therefore, a copper cluster of 1000 atoms has a Kubo gap of ~10 meV. Thus, this copper cluster of ~3 nm diameter is metallic at room temperature, where the thermal energy of electrons is kT ≈ 25 meV. A copper cluster of ~380 atoms, however would have a Kubo gap equaling the thermal energy of the electrons, and smaller clusters would be clearly non-metallic with semi-conductor properties.

Among other influences, the HOMO-LUMO gap of a metal particle is particle size dependent as well. Photo-electron spectroscopic measurements on mass selected Hg_n (n = 3 – 250) particles in the gas phase revealed, that the characteristic HOMO-LUMO gap decrease gradually from ~3.5 eV for n = 3 to ~0.2 eV for n = 250. Band gap closure (HOMO-LUMO gap < kT)was predicted for n ~ 400.[71] It is expected, that the observation of a HOMO-LUMO gap shrinking with cluster size will be true for copper as well. Another observation about the binding behavior of Hg_n cluster will not be transferable to copper cluster. The closed shell metal Hg (ground state configuration $6s^2$ $5d^{10}$ $6p^0$) is non-binding leading to van der Waals binding for clusters with n < 13 atoms. At cluster sizes of >13 atoms, the 6p and 6s levels broaden into bands and an insulator-metal transition occurs.[60] This finding will not be reproduced as such in copper clusters as the atoms have a $4s^1$ $3d^{10}$ electronic ground state with readily available diffuse s orbitals to ensure chemical binding even for small clusters.

The classic description of a cluster with ligand shell is that a metal particle is surrounded by weakly interacting ligand molecules with no strong chemical binding between these subsystems.[72] Investigations showed, that back-donation mechanisms

play an important role in the binding of not only small second row ligands as CO and NO but third row ligands such as phosphines as well.[73,74] Anti-binding electrons of the ligand populate binding molecular orbitals resulting in a reduction of the total energy. This back donation has a stabilizing effect on ligand covered clusters.

2.5. Ordered Arrangements of Ligand Protected Transition Metal Clusters

Just as individual atoms and ions assemble to form crystals, clusters may act as building blocks to form ordered arrangements, often referred to as superlattices.[75] Thus, monodispersed clusters covered by suitable ligands such as alkanthioles spontaneously assemble into two-dimensional lattices when transferred to a flat substrate.[76-80] Figure 4 shows typical arrays of Pd clusters of 4.5 nm diameter coated with varying thioles.

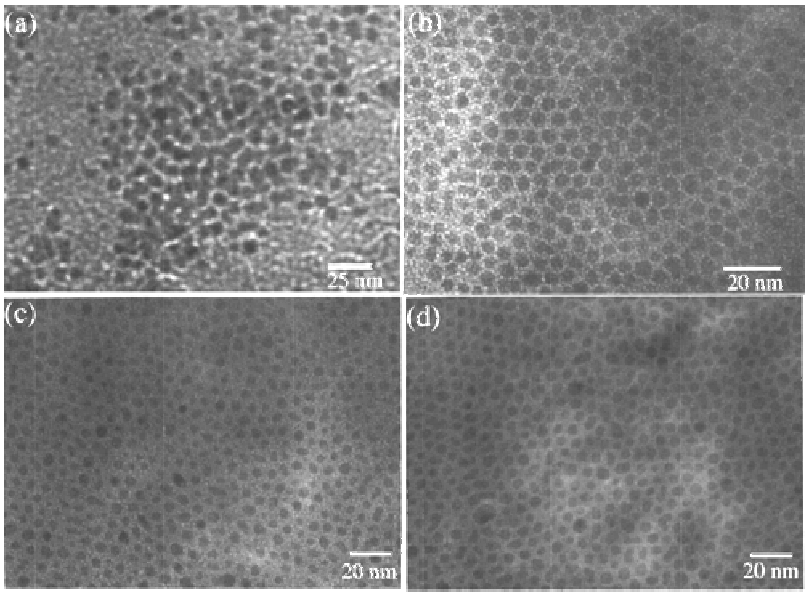

Figure 4 TEM micrographs showing Pd nanocrystals of mean diameter 4.5 nm organized into two-dimensional lattices using different thioles: (a) butanethiol, (b) octanethiol, (c) dodecanethiol, and (d) hexadecanethiol, from Ref. 81

The diameter, *d* of a cluster and the length *l* of the protecting ligands determine the nature of the assembly to a large extent.[82,83] In a phase diagram, Rao et al. compared the relative stability of ordered arrangements of Pd clusters of varying sizes *d* and alkyl thiolate chain lengths *l*. They observed a area, where the ratio *d*/*l* favorably influences the formation of ordered layers.[81] They concluded that the *d*/*l* values of the favorable region are in the range 1.5-3.8. These experimental results have been compared with

empirical calculations based on a soft sphere model, involving an attractive van der Waals term and a repulsive steric term.[84] The areas, where stable ordered layers are to be expected, coincide fairly well (see dashed line in Figure 5).

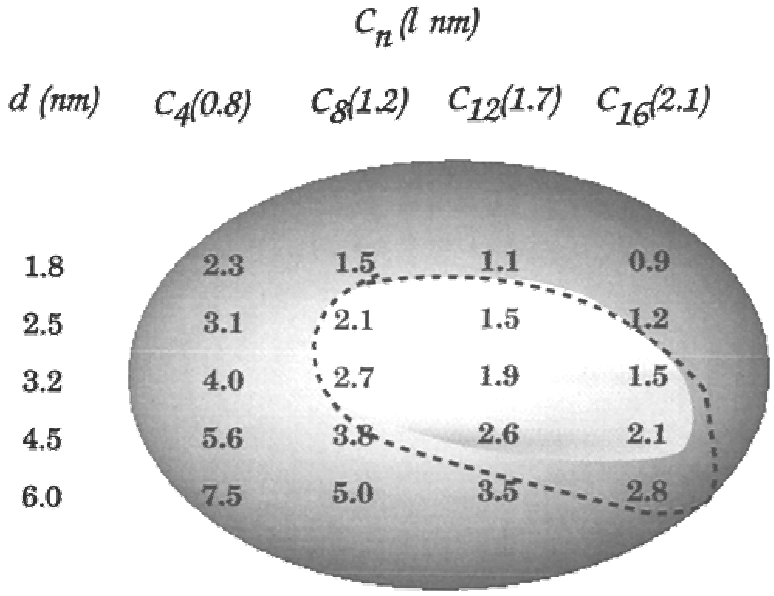

Figure 5 The *d-l* phase diagram for Pd clusters covered by different alkanthioles. The mean diameter *d* was obtained from TEM measurements on as-prepared sols. The length *l* of the thiole is estimated by assuming an all-trans conformation of the alkan chain. The type of thiole is indicated by the number of carbon atoms, C_n. The bright area in the middle encompasses systems which form close-packed organizations of clusters. The surrounding darker area includes disordered layers of clusters. The area enclosed by the dashed line is derived from calculations from the soft sphere model; from references 81, 84

Measurement of magnetic properties of Co clusters (5.8 nm) showed that, accompanying lattice formation, the blocking temperature increases.[85-87] This means that small metal particles exhibit stable magnetism at higher temperatures only by arranging themselves! FePt alloy clusters yield ferromagnetic assemblies for which the coercivity is a function of the Fe:Pt ratio and the particle size.[88] Various investigations were carried out on the electrical transport properties of cluster lattices.[89-93] Kagan et al. showed the electron transfer of proximal CdSe quantum dots by dipole-dipole inter-particle interaction.[91] Snow and Wohltjen concluded that the ligand shell thickness of thiolized gold clusters manifests a very strong effect on electrical conductivity as a resistance barrier between contacting clusters.[92] These observations open up a variety of

applications of the tailored materials envisaged. The development of suitable computational methods and models will help the understanding of the interaction of protected clusters, ligand composition and coverage better, enabling the preparation of ordered arrangements of clusters with defined properties.

3. Computational Chemistry Background

3.1. Density Functional Method

Electronic structure calculations performed in this thesis used density functional (DF) methods.[2,3] In density functional theory (DFT), one determines the total energy of a system as a functional of its three-dimensional electron density. Hohenberg and Kohn proved that the total energy of an electron gas, even in the presence of a static external potential, is a unique functional of the electron density.[2] The minimum value of the total-energy functional is the ground state energy of the system, and the density that yields this minimum value is the exact single-particle ground state density.[2] Kohn and Sham then showed how it is possible to replace the many-electron problem by an exactly equivalent set of self-consistent one-electron equations.[3,94-96] the Kohn-Sham total-energy functional for a set of doubly occupied electronic orbitals ψ_i can be written:

$$E[\{\psi_i\}] = 2\sum_i \int \psi_i \left(-\frac{\hbar^2}{2m}\right)\nabla^2\psi_i \; d^3r + \int V_{ion}(r)\,\rho\,(r)\,d^3r + \frac{1}{2}\int \frac{\rho\,(r)\,\rho(r')}{|r - r'|}\,d^3r\,d^3r' + E_{XC}[\rho(r)] + E_{ion}[\{R_{ion}\}] \quad , \tag{3.1}$$

where the first term is the kinetic energy of non-interacting particles, V_{ion} is the static total electron-ion potential, the third term is the classical Coulomb interaction between electrons

and other electrons, E_{ion} is the Coulomb energy of the nuclei (or ions) at positions $\{R_{ion}\}$, E_{xc} is the exchange-correlation functional and $\rho(r)$ is the electron density given by:

$$\rho(r) = 2\sum_i |\psi_i(r)|^2 \quad . \tag{3.2}$$

At the minimum value, the Kohn-Sham energy functional is equal to the ground-state energy of the system. To determine this ground state energy, it is necessary to construct a set of orbitals ψ_i that minimize the Kohn-Sham energy functional. For a closed-shell system these are given by the self-consistent solutions to the Kohn-Sham equations[3]:

$$\left[-\frac{\hbar^2}{2m}\nabla^2 + V_{ion}(r) + V_H(r) + V_{XC}(r)\right]\psi_i(r) = \varepsilon_i\psi_i(r) \quad , \tag{3.3}$$

where ψ_i is the one-electron Kohn-Sham orbital of electronic state i, ε_i is the Kohn-Sham eigenvalue and V_H is the Hartree potential of the electrons given by:

$$V_H(r) = e^2 \int \frac{\rho(r')}{|r - r'|} d^3r \quad . \tag{3.4}$$

The exchange-correlation potential, V_{XC}, is given by the functional derivative:

$$V_{XC} = \frac{\delta E_{XC}[\rho(r)]}{\delta \rho(r)} \quad . \tag{3.5}$$

The Kohn-Sham equations represent a mapping of the interacting many-electron system onto a system of non-interacting electrons moving in an effective potential due to all other electrons. If the exchange-correlation energy functional were known, then taking the functional derivative with respect to the density would produce an exchange-correlation potential that included the quantum many-particle effects exactly. The Kohn-Sham equations must be solved self-consistently so that the occupied electronic orbitals generate a charge density that produces the electronic potential that was used to construct the equations. The sum of the single-particle Kohn-Sham eigenvalues does not give the total electronic energy because this overcounts the effects of the electron-electron interaction in the Hartree energy and in the exchange-correlation energy. The Kohn-Sham eigenvalues are not the energies of the single-particle electron states, but rather the derivatives of the total energy with respect to the occupation numbers of these states (Janak's theorem).[97] Accordingly, the eigenvalue of the highest occupied orbital in an atomic or molecular calculation is the vertical ionization energy for that system,[98] analogous to Koopman's theorem in wave function based methods.[99]

The exchange-correlation functional, E_{xc}, is the difference of the quantum mechanical and the classical e-e energy functional, plus part of the kinetic energy. Thus far, no explicit form of the exchange-correlation functional is known. Three types of approximations are commonly used. The local density approximation, LDA, assumes that E_{XC} is a local function of ρ.[3] A generalization for open shell systems is the local spin density approximation (LSDA). The generalized gradient approximation (GGA) additionally takes into account the gradient of the local electron density. Hybrid functionals mix exact HF exchange and XC functionals results according a given ratio. Several implementations for LDA[100,101], GGA[102-104] and hybrid functionals[105-107] exist. LDA functionals reproduce geometrical data well, but overestimate fragmentation energies, while GGA functionals are better suited to reproduce fragmentation energies. Hybrid functionals aim to achieve both.[96]

3.2. Molecular Mechanics Method

The Molecular Mechanics[108] (MM) ansatz starts from the notion that it is not necessary to know the exact electronic structure of a molecule to deduce most of its basic properties like bond lengths and angles, etc. or heats of formation and certain spectroscopic data.[109-112] If these properties of a calibrating set of molecules are known, similar molecules would exhibit similar properties.[113-115]

In the ball-and-spring model underlying most molecular mechanics approaches, atoms are considered as point masses. Depending on the level of the respective model they may as well be assigned a certain charge, implicit dipole moment, van der Waals potential or other one particle properties. Bonds will be represented as spring-like potentials between two such mass points, where the energy contribution is solely a function of the distance between them. Other interactions as potentials dependent on bond angles, dihedral angles, dihedral-dihedral interactions, bond-angle interactions, or two-, three-, and four-body non-bonded interactions, like electrostatic and van der Waals interactions, are implemented in a similar fashion. The energy of a given system may then be simply defined as the sum over all those elementary interactions:

$$
\begin{aligned}
E_{tot} = & \sum_{i_{bond}} E_{bond}(i_{bond}, \vec{r_a}, \vec{r_b}) + \sum_{i_{angle}} E_{angle}(i_{angle}, \vec{r_a}, \vec{r_b}, \vec{r_c}) + \sum_{i_{dihedral}} E_{dihedral}(i_{dihedral}, \vec{r_a}, \vec{r_b}, \vec{r_c}, \vec{r_d}) \\
& + \sum_{i=1}^{N-1} \sum_{j>i}^{N} E_{pair}(i, j, \left|\vec{r_i} - \vec{r_j}\right|) + \sum_{i=1}^{N-2} \sum_{j>i}^{N-1} \sum_{k>j}^{N} E_{3\,body}(i, j, k, \vec{r_i}, \vec{r_j}, \vec{r_k}) \\
& + \sum_{i=1}^{N-3} \sum_{j>i}^{N-2} \sum_{k>j}^{N-1} \sum_{n>k}^{N} E_{4\,body}(i, j, k, n, \vec{r_i}, \vec{r_j}, \vec{r_k}, \vec{r_n}) \\
& + \sum_{i=1}^{N} E_{external}(i, \vec{r_i}, \vec{v_i}) \\
= & \sum_{i} E_i(\{\vec{r}\}) \quad , \qquad (3.6)
\end{aligned}
$$

where E_{tot} is the total (Molecular Mechanics) energy of the system depending on the included energy contributions and the underlying model. The E_i are the partial energy contributions included in the model of the respective MM theory implementation. The set variables i_x specifying which atoms take part in which interactions. The functions detailing the energy dependence of a given interaction as well as their parameters have to be well conceived and tuned to allow this method to be used.[116-118] Modern Molecular Mechanics methods are capable of treating a wide variety of different types of

compounds. They range from simple atomic system, e.g. mixtures of noble gases[119] to macromolecules with flexible bonds embedded in a polarizable solvent.[120]

The term **force field**[121] is thus defined to specify the sum of all functional dependencies, atom type definitions as well as the parameter sets used in such a implementation of a MM ansatz. To provide the functional dependencies in force fields, two ways of developing rules and parameter sets exist. The first tries to fit the best available experimental data to specifically designed interpolation functions, to improve the accuracy of prediction for a predefined set of reference compounds, without trying to reflect the underlying quantum mechanics. The application of this approach to an ever increasing number of reference compounds leads to the introduction of different parameter sets for atoms of one element in different chemical environments (atom types). Factors to be taken into account when assigning a type to an atom include hybridization, bond multiplicity, bond partners of first, second and even third order or the presence of hydrogen bonds or π back bonding. Force field implementations like MM2,[122-124] MM3[125-130] and AMBER[131-133] belong to this type of approach. Although able to describe compounds chemically similar to reference compounds very well[134], their disadvantage is the increasing number of parameter sets necessary and the loss of generality for unknown classes of compounds. The MM3 force field for instance includes 5 different types of carbon parameter sets and 3 different for sulfur, depending on the chemical environment.[125,127,128,130,135] Even so, sulfur bound to metals is not taken into account. While many classes of organic compounds,[108] including heterocycles,[136] may be accurately described using this force field, much of the inorganic chemistry is neglected as opposed to other force field implementations.[137]

The other parameterization strategy deals with exactly this problem. It assigns a higher priority to the generality of the parameters than to accuracy. Each element is assigned exactly one set of parameters regardless of the chemical surrounding it may experience. The functional form as well as their parameters are defined in a way to reflect the physical properties of the element considered as good as possible. If a parameter set for each element is derived, any compound is computable. The better the description of the reality by the function and parameter sets, the better results can be expected. Examples of this approach are the DREIDING[138] and the UFF[139,140] force field implementations.

3.3. Periodic Boundary Conditions

In pertinent experiments, clusters with ligand shells are often located in a chemical matrix. In such a situation, the model of a solitary cluster may lack essential features, as the interaction with a matrix can introduce a strain not present in the former model. The problem of incorporating a chemical matrix in a computational model is not a new one. MD simulations of liquids or solids routinely handle this problem.[141] There, the models are often based on the assumption of a infinite, isotropic material. System boundaries are thought to be conveniently far away from the boundary of the model. For this model boundary the term "box" has gained widespread acceptance. It is not always possible to model a large enough box of the system under consideration in order to describe adequately all interactions nor is one always able to neglect boundary effects. The computational cost accompanying such large models may be too high even in force field based approaches. A small model may have two consequences. If movement of particles is not restricted to the box, they could exit, effectively evaporating from the model. If the movement is restricted to the box, unphysical forces would be introduced (artificial pressure). A practical solution is to assume spatial periodicity of the model.[142] As a result of periodicity, for any particle moving out of a box in one direction, another particle enters the box along the same vector at the opposite wall of the box with equal momentum. As the number of particles in the box is constant this way, the number density and the material density of the model are conserved. This situation is illustrated in Figure 6, simplified for the two-dimensional case. The central box contains the original model particles. Boxes A through H are derived by translating this central box along one or both of the cell vectors $\overrightarrow{L_1}$ and $\overrightarrow{L_2}$ as exemplified in box image H. Particle 1 is shown leaving the central box into box B. Images of particle 1 copy this movement. Thus, an image of particle 1 enters the central box from G. By application of translational symmetry, the model becomes effectively infinite.

The perpetuation of particles does not impose any principal problems. Interactions between particles in different boxes however do. Including all images of a particle in the calculation of interactions is very difficult, as sums over a potentially infinite number of particles and their interactions in a periodic model require special consideration. Some way of restricting the number of interactions has to be found; equivalently, the interaction with an indefinite number of surrounding particles has to result in a finite value which has to be determined by an efficient strategy. A customary way to do this is to limit the range of interactions. The physically correct description of the model then

hinges on the sufficient "cutoff" range *rcut*. An easy way is to define this cutoff as the length of one of the cell vectors $\overrightarrow{L_1}$ or $\overrightarrow{L_2}$, whichever is shortest. A situation like this is sketched in Figure 7.

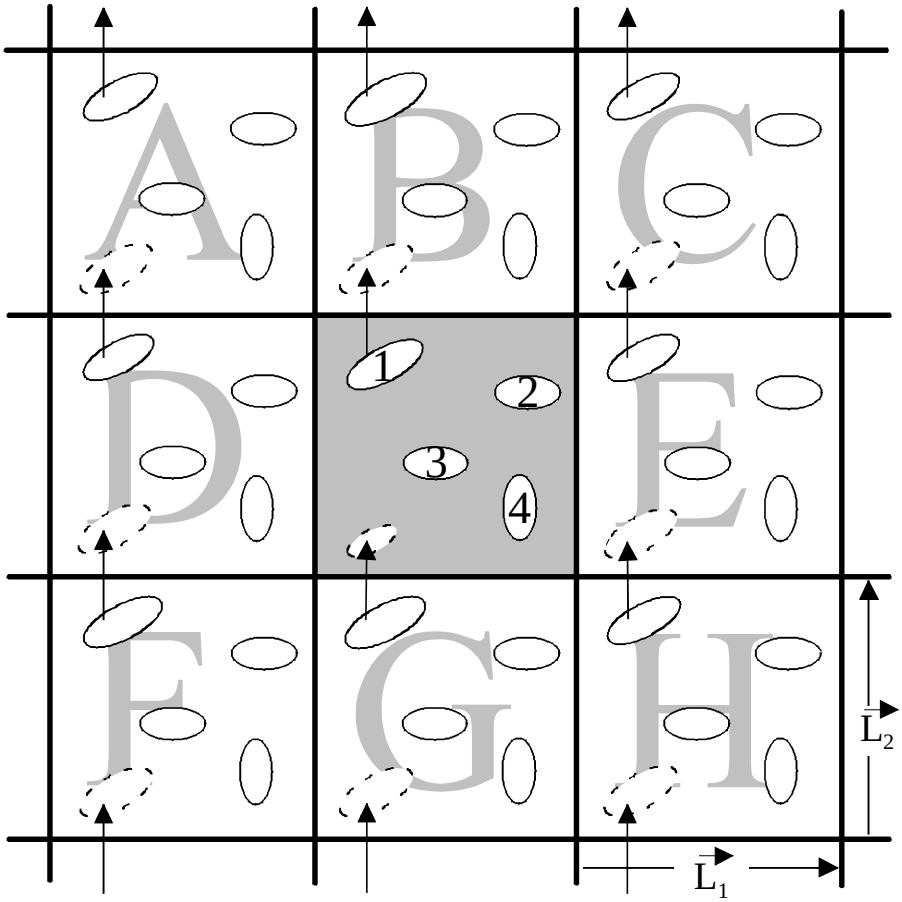

Figure 6 A two-dimensional periodic system. Particles can leave and enter each box across each of the four edges.

While short-range interactions usually do not suffer from this approach, the error introduced in long range interactions such as van der Waals interaction should be corrected by an analytical term. Periodic boundary conditions used in the description of an isotropic model can introduce a periodicity of its properties. The loss of isotropic behavior in liquids is the result.[141] When modeling a non-periodic system with periodic boundary conditions, *rcut* is often set to $rcut < \left[\mathrm{Min}(\overrightarrow{L_i})\right]/2$ to avoid that. One the other hand, periodic effects stemming from too low a choice of *rcut* have also been shown to result in other adverse effects, i.e. suppressing density waves with a wavelengths greater than $\overrightarrow{L_i}$.[141]

However, this influence of *rcut* was demonstrated to be negligible, when the potentials in question are either truly short-ranged ($r_{interaction} << \vec{L_i}$) or, as in the case of ordered arrangements of metal clusters interacting with their images in adjacent cells, suppression of periodicity of properties is unwanted.

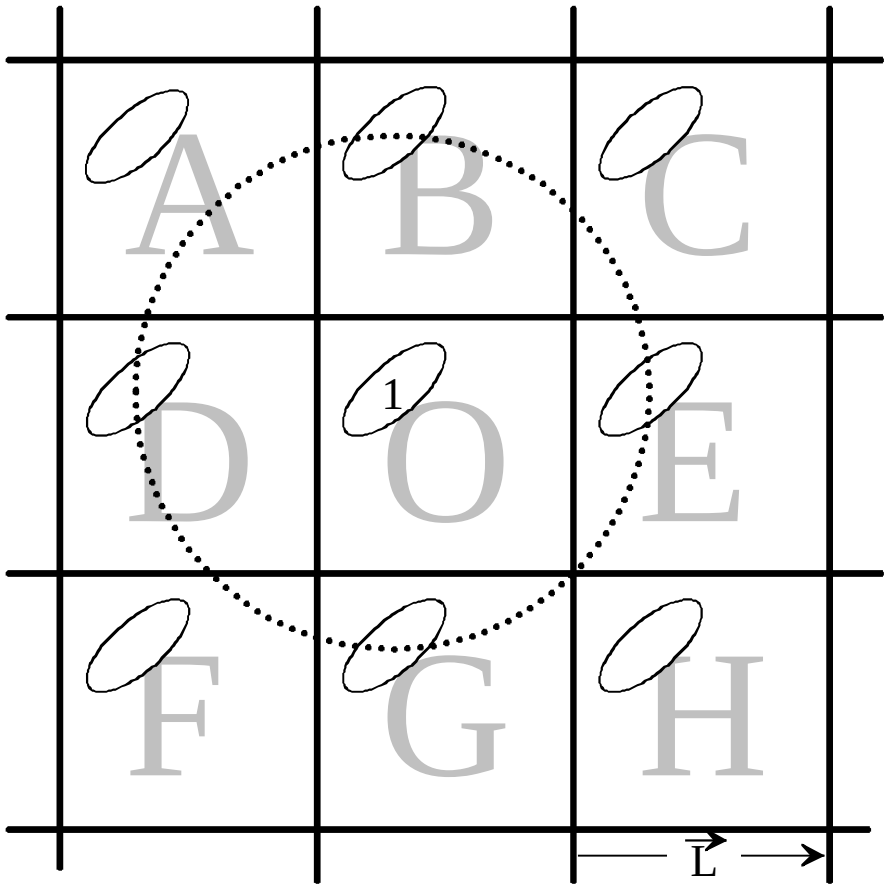

Figure 7 Cell O and 8 symmetric images in a two-dimensional square lattice. The interaction range is indicated by a circle of radius *rcut* = $\left|\vec{L}\right|$, indicated by a dashed line. Some images of particle 1 fall within that radius.

To increase the system size, one could, for example, unify cells A through H with cell O, including translated images of the cluster with copied geometries. Technically, this would be an awkward approach. Thus, *rcut* can be chosen equaling the shortest cell vector length in inherently periodic systems.

3.4. Hybrid Quantum Mechanics and Molecular Mechanics Methods (QM/MM)

3.4.1. General Background

An interesting approach to compute larger chemical systems is to partition them into two or more subsystems which are treated with different computational methods varying in their computational demand.

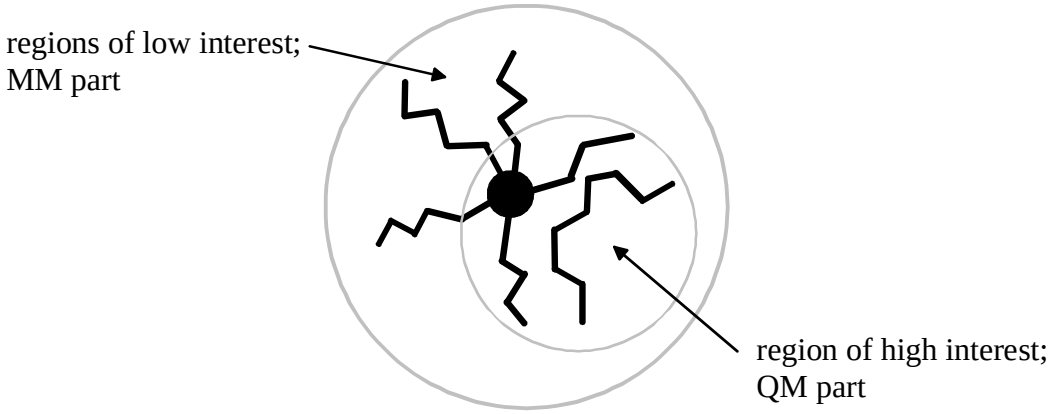

Figure 8 Partitioning a system according regions of interest into QM and MM part

While one system is smaller, it holds the region of immediate interest of the system and is treated accordingly with a quantum mechanical method such as Hartree-Fock[143] (QM part) or a related high level of theory method with exchange-correlation treatment.[144-156] At the same time, the larger system(s), which holds not as much valuable information, is treated with an appropriate method such as a semi-empirical method or with molecular mechanics (MM part). These lower level methods usually have the advantage of lower computational demand.[115] Its feedback on the smaller system would then have to be taken into account at an appropriate level of approximation. The energy of the combined system X+Y, QM (X) and MM (Y) is then:[157-159]

$$E(XY) = E_{high}(X) + E_{low}(Y) + E_{int}(XY) \qquad (3.7)$$

where E(XY) is the total energy of the complete system XY, $E_{high}(X)$ and $E_{low}(Y)$ are the energies of the subsystems X and Y respectively, and $E_{int}(X,Y)$ provides a correction for the interface between the two subsystems. When an explicit form for the interface system correction term is not known, it has been suggested to "extrapolate" the total energy in the form:[5]

$$E(XY) \approx E_{app}(XY) = E_{high}(X) + E_{low}(XY) - E_{low}(X), \qquad (3.8)$$

where E_{app} is the approximated total energy.

This is true only when:

$$E_{int}(X,Y) = E_{low}(XY) - E_{low}(X) - E_{low}(Y) \quad (3.9)$$

According to their respective derivation, the first approach, connecting both parts via an explicit term E_{int}, is called the connection scheme, while the latter, extrapolating this term, is called extrapolation scheme.[159] Depending on the parameterization of the MM implementation (force field) used, the energy differences between similar systems can be used as an extrapolation of the difference of the total energy of both systems treated at the high level of theory.

In the basic QM/MM concept, both regions do not need to be connected via chemical bonds. Furthermore, the QM region does not need to be completely surrounded by the MM region. All that needs be taken care of is the correct proliferation of influences (forces, electronic coupling of the subsystems) of the QM part to the MM part and vice versa and the energy expression for the complete system.[159] If there are no chemical bonds connecting the two subsystems, most approximate descriptions of non-bonded interactions are surely accurate within chemical accuracy.[115] If however chemical bonds are cut separating the subsystems X and Y, this "dangling" bonds have to be saturated in the QM part ($E_{high}(X)$). The energy contribution to the QM energy of non-saturated bonds would otherwise introduce a undetermined source of error.[160] Two techniques have been proposed to avoid such artifacts. The first one saturates the remaining bonds with an extra atom ("atom capping" or "link atom")[157], while the other uses pseudo-orbitals specifically designed to be "chemically similar" to the atom cut ("orbital capping").[147] Although the extrapolation scheme is indifferent to the capping technique used, most applications up to today implement the link atom approach. In fact, the QM treatment an orbital capping approach would be preferable as it does not introduces an additional, unphysical moiety. But, the respective auxiliary orbital would have to be parameterized to reflect the physical and chemical properties of the bond as well as the molecular fragment that is to be replaced. The terms necessary to adequately describe this fragment with a single orbital are so wide ranging, that the only pseudo-orbital able to claim accurate treatment of the subsystem would be the respective subsystem itself.[160] This may explain the reluctance to employ the orbital capping approach in all its consequences. The effort accompanied with the "orbital capping" scheme seems to exceed the gain of accuracy to be achieved.[161,162] Although it is expected that the introduction of an link atom to saturate the bond introduces a energy

distortion that is not physically (or chemically) warranted, this should not interfere in the examination of isodesmic reactions or energy differences of conformers. Even the distinctive features of the energy hypersurface are thought to be, at least qualitatively, preserved. Thus, the QM/MM approach has been successfully used in the exploration of reaction paths and transition points.[6] However, there is no guarantee that the hypersurfaces of real and approximated system are identical or even parallel.[160] To circumvent associated problems, important degrees of freedom should reside well inside the QM part of the model.[160]

To facilitate understanding of the basic QM/MM implementation five sets of atom coordinates are introduced (Figure 9).

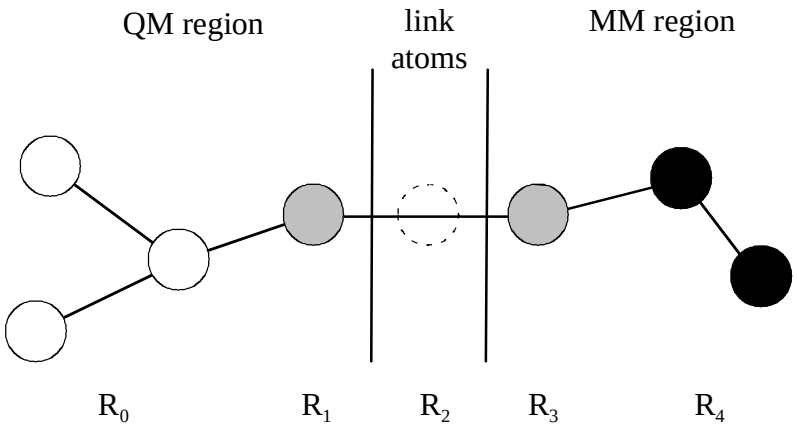

Figure 9 Sketch of a system and its subdivision in the QM/MM approach; The various types of atoms as referenced by their coordinates are: R_0 = interior QM ; R_1 = frontier QM ; R_2 = link atoms ; R_3 = frontier MM ; R_4 = interior MM

In the following, the term "frontier-bond" describes the bond that is cut by the partitioning of the system into a QM and a MM system. It is defined to be formed by a QM frontier atom (R_1) and a MM frontier atom (R_3). Thus, "link-bond" refers to the bond between a QM frontier atom (R_1) and a link atom (R_2).

To model the interactions between the QM and MM subsystem, the simplest approach is mechanical embedding,[163] which will be discussed in more detail later on. Besides the mechanical embedding, three approaches have been proposed to treat the electrostatic interaction of QM and MM parts. These are electrostatic embedding,[163] polarized embedding[163] and self-consistent polarized embedding.[164] In the electrostatic embedding approach the MM part appears as a charge distribution, e.g. a set of point charges, to the QM Hamiltonian. The polarization of the QM part by the MM charge distribution thus occurs as part of the QM electronic structure calculation. The partial

charges used to describe the MM section of the system are frequently taken to be those used in the force field,[40,145,165] relying on electrostatic properties as described by the force field. In "ab initio" schemes, the electrostatic embedding scheme can be implemented by adding the MM point charge contributions to the one-electron Hamiltonian.

In the polarizable embedding approach, the polarization of the MM region in response to the QM charge distribution also taken into account. Intuitively, this makes the most sense when the force field incorporates polarization as unpolarized force fields implicitly incorporate MM polarization in their parameterization, and care must be taken to ensure such implicit contributions to not occur in QM/MM potential. A variety of models for polarization are available, including the shell model,[166] and coupled distributed atomic polarizabilities.[167] Polarizations of MM atoms close to the QM region (e.g. those connected by link-atom terminated bonds) were found to be unphysically large, leading to the suggestion that these atoms be treated as unpolarizable.[160] The self-consistent polarizable embedding approach extents the preceding approach in that QM and MM polarizations are made self-consistent, either by iterative solution of the SCF and polarizability problems,[168] or by matrix inversion techniques, as exemplified by the Direct Reaction Field (DRF) model.[169-172]

In the mechanical embedding approach, the QM calculation is essentially performed in the gas phase, without electronic coupling to the environment. The electrostatic interaction between QM and MM regions is either omitted or performed by the MM code, using a classical point charge model for the QM charge distribution (e.g. a potential derived charge model).[145] The energy expression Eq. (3.8) may be reformulated for a purely mechanical embedding as:

$$E(R_0,R_1,R_3,R_4) = E_{QM}(R_0,R_1,R_2) + E_{MM}(R_0,R_1,R_3,R_4) - E_{MM}(R_0,R_1,R_2) \quad , \qquad (3.10)$$

where

$$R_2 = R_2(R_1,R_3) \quad . \qquad (3.11)$$

Keeping the link atom (R_2) degrees of freedom independent of the physical atom coordinates would introduce artificial degrees of freedom. The resulting energy gradient expression is :

$$\nabla E_{total}(R_0,R_1,R_3,R_4) = \nabla E_{QM}(R_0,R_1,R_2)\, J(R_2{:}R_1,R_3) - \nabla E_{MM}\,(R_0,R_1,R_2)\, J(R_2{:}R_1,R_3) + \nabla E_{MM}(R_0,R_1,R_3,R_4) \quad , \qquad (3.12)$$

where $J(R_2:R_1,R_3)$ is the Jacobian matrix associated with the transformation of gradients with respect to coordinate sets R_2 to sets R_1 and R_3. The original IMOMM[5,6,173] implementation did not include the coordinates R_3 in the energy expression. It rather defined R_3 as dependent of R_2.[6] This was because the coordinate sets of QM and MM part were optimized independently by the corresponding programs. The QM part coordinates were kept fixed during the MM part optimization. This approach obtained more flexibility in the MM part optimization. As the MM structure is equilibrated at every QM step, this amounts to quasi molecular dynamics runs, as the energetically most favorable structure for the MM part is used instead of a structure itself in need of optimization. Because the implementation designed in this thesis intends to examine ground states rather than transition states, which would necessitate a higher flexibility, it was decided to use the schemes presented here. The use of this variational scheme with a single energy expression promised consistent results in a ground state and conformational search.

Three options have been pursued in the mechanical embedding approach to determine the link atom coordinates R_2, all of which constrain the link atom to the frontier-bond vector:

(a) Fixed link-bond length R_{12} and fixed frontier-bond length R_{13}

If link-bond length and frontier-bond length are kept fixed, no transformation of gradients of the link atom to the frontier atoms is required. This option, although simple and popular in earlier IMOMM implementations,[173] freezes the frontier bonds, artificially restricting the geometry of the combined system. This restriction can be one of the reasons for the energy hypersurfaces not being parallel to those of the system treated homogeneously with a single method.

(b) Scaled link-bond length to flexible frontier-bond length[174]

This approach allows a change of the link-bond length according to the length of the frontier-bond length:

$$R_2 := R_1 + g(R_3-R_1) \qquad (3.13)$$

where g is a constant scaling factor. It is often chosen as the ratio of the respective bond lengths in QM and MM reference calculations of small test systems. Although the introduction of the parameter g is somewhat arbitrary, tests showed that the resulting bond lengths are accurate to a few hundredth of an Å. This includes the simulation of

bond stretching effects in sterically stressed compounds propagating these effects into the QM part.

(c) Fixed link-bond length and flexible frontier-bond length[175]

Here, the link-bond is kept fixed at some pre-defined value R_{12}^0,

$$R_2 := R_1 + \frac{R_{12}^0}{|R_3 - R_1|}(R_3 - R_1) \quad . \tag{3.14}$$

By expanding the Jacobian matrix in Eq. (3.12), the explicit gradients for each type of coordinates in a QM/MM calculation can be written as follows:

$$\frac{\partial E}{\partial R_0} = \frac{\partial E_{QM}(R_0,R_1,R_2)}{\partial R_0} + \frac{\partial E_{MM}(R_0,R_1,R_3,R_4)}{\partial R_0} - \frac{\partial E_{MM}(R_0,R_1,R_2)}{\partial R_0}$$

$$\frac{\partial E}{\partial R_1} = \frac{\partial E_{QM}(R_0,R_1,R_2)}{\partial R_1} + \frac{\partial E_{QM}(R_0,R_1,R_2)}{\partial R_2}\frac{\partial R_2(R_1,R_3)}{\partial R_1} + \frac{\partial E_{MM}(R_0,R_1,R_3,R_4)}{\partial R_1} - \frac{\partial E_{MM}(R_0,R_1,R_2)}{\partial R_1} - \frac{\partial E_{MM}(R_0,R_1,R_2)}{\partial R_2}\frac{\partial R_2(R_1,R_3)}{\partial R_1}$$

$$\frac{\partial E}{\partial R_3} = \frac{\partial E_{QM}(R_0,R_1,R_2)}{\partial R_2}\frac{\partial R_2(R_1,R_3)}{\partial R_3} + \frac{\partial E_{MM}(R_0,R_1,R_3,R_4)}{\partial R_3} - \frac{\partial E_{MM}(R_0,R_1,R_2)}{\partial R_2}\frac{\partial R_2(R_1,R_3)}{\partial R_3}$$

$$\frac{\partial E}{\partial R_4} = \frac{\partial E_{MM}(R_0,R_1,R_3,R_4)}{\partial R_4} \quad . \tag{3.15}$$

For option (b), the Jacobian transformations in Cartesian coordinates is:

$$\frac{\partial R_{2,i}}{\partial R_{1,j}} = (1 - g)\,\delta_{ij}$$

$$\frac{\partial R_{2,i}}{\partial R_{3,j}} = g\,\delta_{ij} \quad , \tag{3.16}$$

where i and j denote Cartesian components x, y and z, and δ is the Kronecker symbol. The transformation Jacobian for option (c) may be written as:

$$\frac{\partial R_{2,i}}{\partial R_{1,j}} = \delta_{ij} + \frac{R_{12}^0}{|R_3 - R_1|}\,e_i e_j - \frac{R_{12}^0}{|R_3 - R_1|}\,\delta_{ij} \quad \text{and}$$

$$\frac{\partial R_{2,i}}{\partial R_{3,j}} = - \frac{R_{12}^{0}}{\left|R_3 - R_1\right|} e_i e_j + \frac{R_{12}^{0}}{\left|R_3 - R_1\right|} \delta_{ij} \quad , \tag{3.17}$$

where e_i and e_j are the components i and j of the unit vector e:

$$e = \left(R_3 - R_1\right) / \left|R_3 - R_1\right| \ . \tag{3.18}$$

As mentioned above, option (a) is not used anymore for examination of chemical problems as it introduces an artificial strain on QM and MM part of the system alike. As this strain can not be quantified, it contributes to the interface energy E_{int} in an unknown fashion. In a similar way, option (c) puts a strain on the QM part and neglects steric contribution of the MM part. Option (b) on the other hand, even when applying only an approximate distance ratio, joins QM and MM part in a way, where effects of one part are propagated to the other. It can be seen as a valid approximation as the correct ratio of link-bond to frontier-bond is not known. A good guess for g was proposed by Morokuma as the ratio of the respective bond lengths in a MM force field.[174] In the present work, it turned out that option b results in reasonable geometries as well as energies when applied to copper-organic model species where the QM/MM boundary intersects a carbon-carbon bond.

3.4.2. Implementation

In the development of QM/MM schemes, two approaches regarding the update of the geometries of the QM and MM part were pursued. One procedure kept the QM part coordinates R_0 and R_1 as well as part of the MM part R_3 coordinates fixed during the MM optimization, and updated them only after MM convergence had been reached. Alternatively, one updates the complete coordinate set according to the combined gradients of QM and MM calculations. This scheme was used in the present implementation of the QM/MM approach. Figure 10 represents an overview of the implementation structure; the coordinate sets were substituted with convenient abbreviations. R_0, R_1 and R_2 together are R(central), R_0, R_1, R_3, and R_4 are represented as R(total) and R_2 as R(link).

A typical run comprises the following steps. First, input for both QM and MM program as well as the set of link atom coordinates are constructed. Then, R(central) and R(total) are established. Next, the three "partial" energies are computed by specialized programs independently of each other. Afterwards, the energies and gradients are combined according the invoked gradient coupling scheme. The structure optimizer program, part of the PARAGAUSS package is then called to update the structure according to energy and gradients. If the resultant structure was converged

according to pre-defined conditions, the run terminates. Else, the loop starts anew with the updated coordinate set.

A central idea underlying the implementation of the QM/MM scheme realized in the present work was to ensure usability of existing programs for the respective tasks with modifications reduced as much as possible. Thus, the input structure of the individual programs had not to be changed. Any control of the QM/MM run itself and accompanied data is handled by a higher level input, which contains the necessary information of the specialized programs in a meta-format. The operating system specific framework of the respective runs had to be predetermined by a top-level script, called qmmm.script.

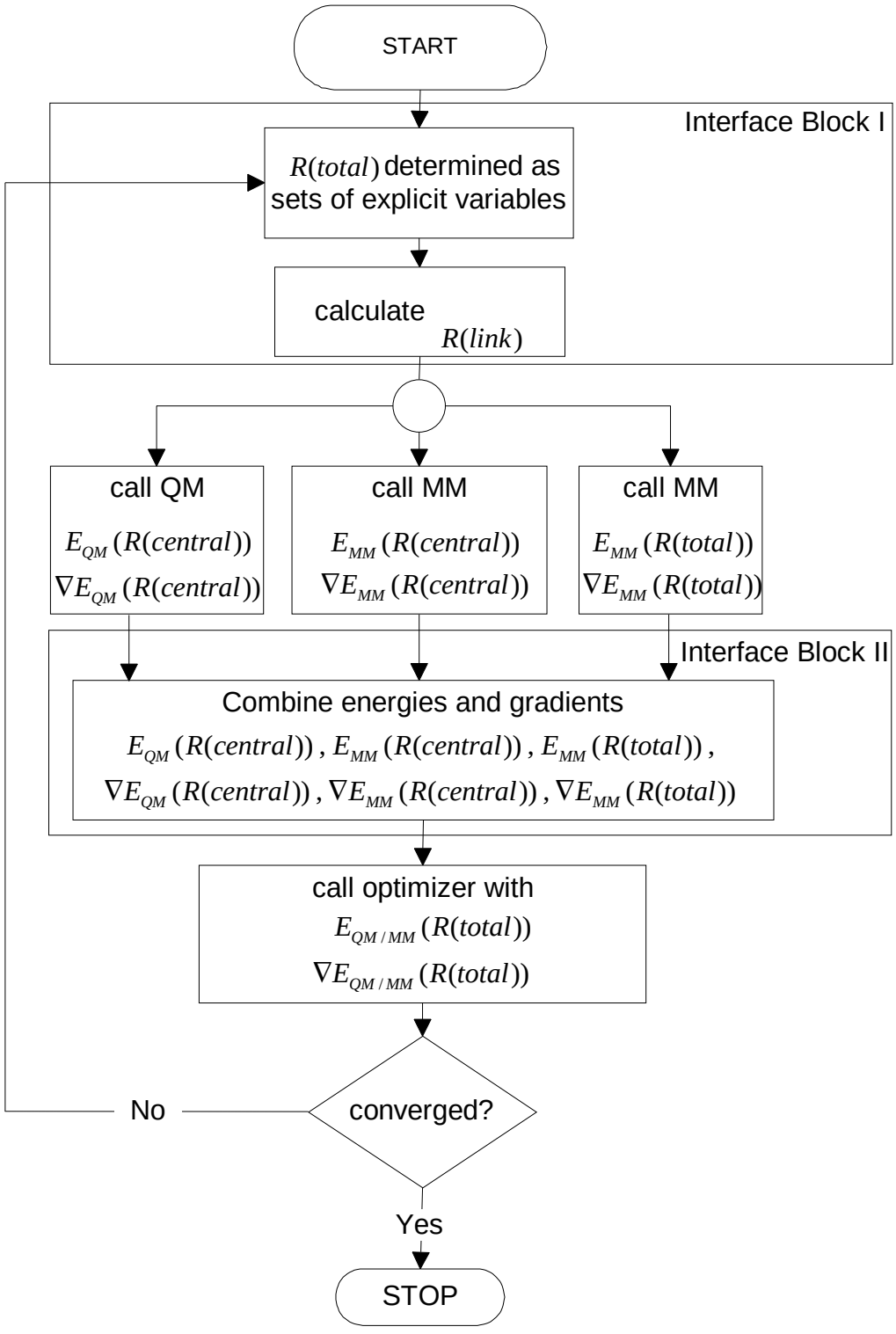

Figure 10 Flow diagram of qmmm.script combining QM and MM programs; interface blocks I and II indicated for future reference

In a normal PARAGAUSS run the PARAGAUSS executable and the optimizer program are called by the ttfs_script, which in turn would transfers its environment variables to the program called. In a qmmm.script run this is not possible, as both QM and MM programs are called independently. The ttfs script is only used to acquire environment data and call the PARAGAUSS executable separately. The transfer of environment variables is achieved by saving the output of a call of a special script (*ttfs -environment*) in a file and reading this file for the profit of the optimizer program. The following figure compares the two approaches.

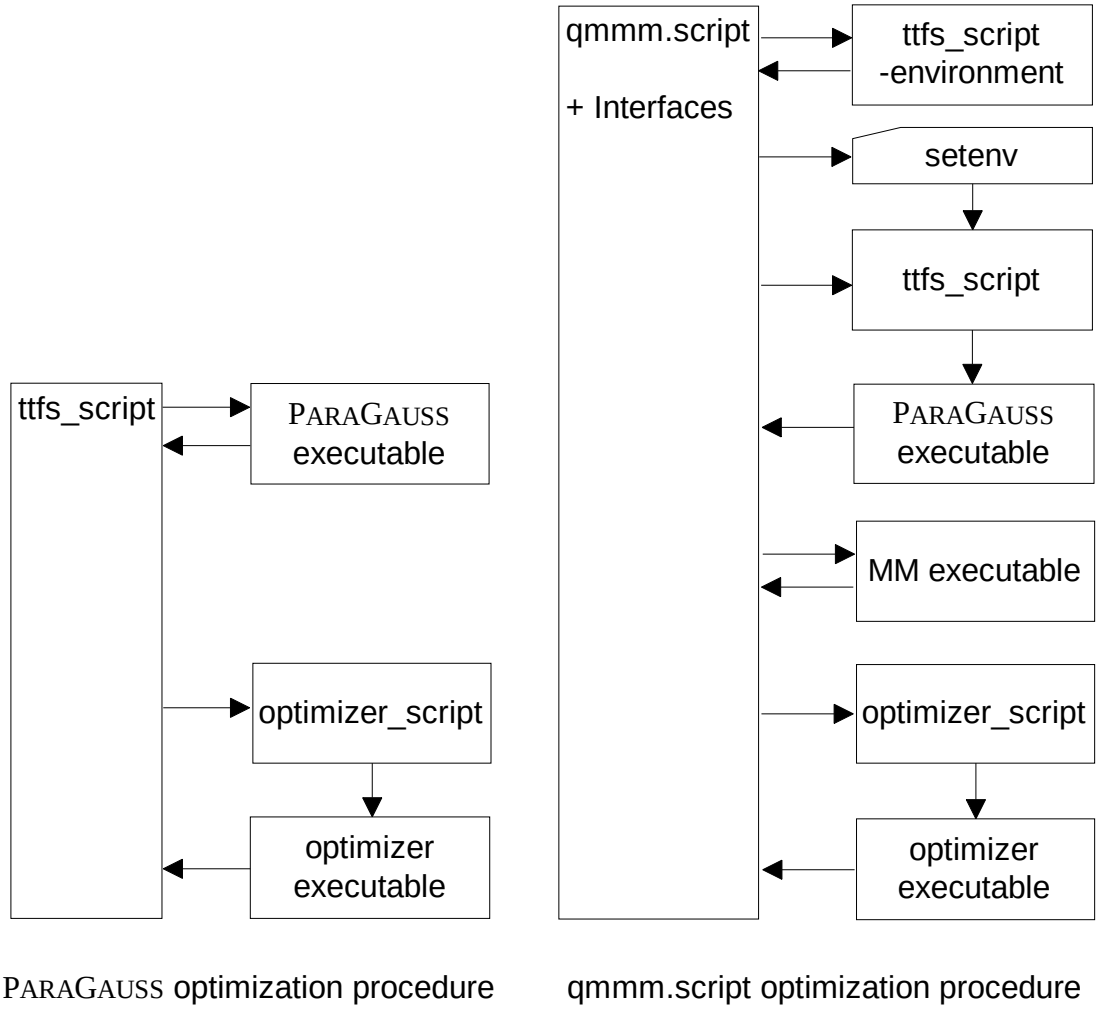

Figure 11 Comparison of DF (ttfs) and QM/MM (qmmm.script) optimization procedures

To allow the interface processing as indicated in Figure 10, a suite of F90 programs (interfaces) was written to be called by the qmmm.script in addition to the QM and MM programs. Their respective duties are indicated in Figure 12, and will be explained in detail later on in this work.

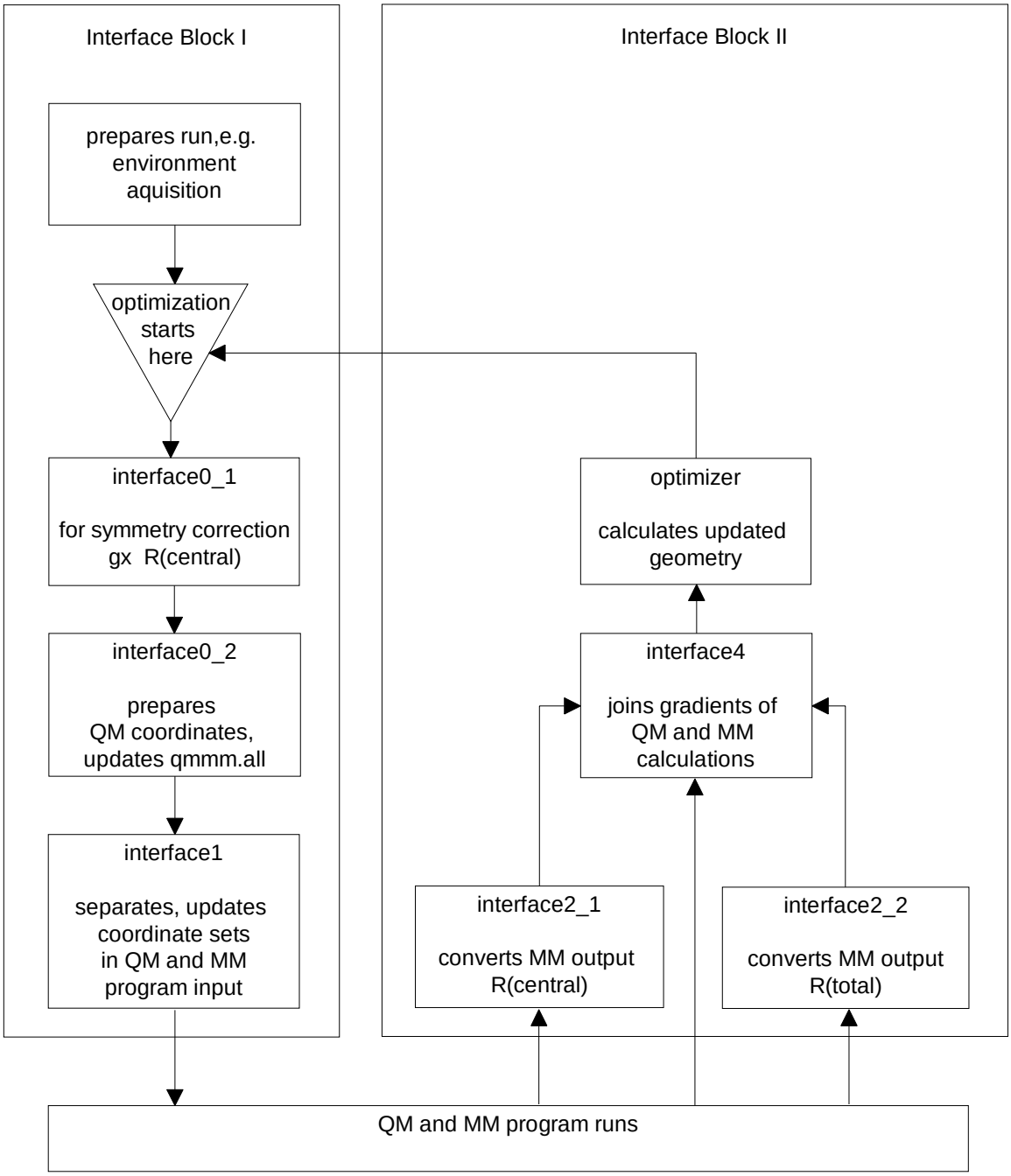

Figure 12 Tasks of the interface programs called by qmmm.script

Before detailing the inner workings of the qmmm.script, the driving program of the QM/MM run, a few general remarks shall explain the terminology used. The individual interfaces programs were named interface*x_y*, where *x* and *y* indicate the respective position in the execution hierarchy. The only PARAGAUSS specific files mentioned are the input/output files furnishing the z-matrix and the gradients. The MM program will be provided with its set of geometry and gradient containing input and output files as well. Note that two sets of these files exist for the MM treatment of R(central) and

R(total), respectively. As their names are MM program specific, they shall not be mentioned here to avoid confusion. Intermediate files constructed by some of the interfaces will be addressed by their function as well. For the actual naming conventions and content of the individual files, see the QM/MM Users Guide.[176]

MM programs usually do not enforce any symmetry restrictions of the system computed. In QM calculation, symmetric models are often used as a means to reduce the computational effort (see Chapter 2.2). To retain symmetry during the update and in parallel allow non-symmetric models in the MM part, the QM part of the model is frequently symmetry adapted. Thus symmetry restrictions of the QM part are independent of the restrictions in the MM part and vice versa. The optimizer program itself does not observe any symmetry restrictions. In this way it is possible to set up a calculation with "partial" symmetry. This approach allows a more flexible treatment of the MM system, but increases planning effort in the construction of the z matrix.

At the start of a qmmm.script run, a loop evaluates the command line parameters and decides for instance which MM program to use. The first step towards an actual calculation is the execution of program interface*0_1*. When called the first time it reads a general system definition file and an MM system defining files and then it combines these files to a meta-file, containing all necessary atom type and position information necessary to describe both subsystems in their appropriate formats. Later computations will reference this file for all geometry updates. Likewise, interface*0_1* will prepare a z-matrix file for the QM subsystem. This file is used in a first PARAGAUSS run to check if the atom definitions conform to the selected symmetry. Deviations of atom positions of up to 10^{-5} au (~$5*10^{-6}$ Å) are corrected, if necessary.

After some cleanup operations of the QM symmetry run, the actual optimization cycle begins. First within the optimization loop is an additional symmetrization step, just as the one described above. The symmetry corrected atom positions from a geometry update (cycle 2 and above) are read into interface*0_2* which in turn updates the meta-file. In interface1, these updated positions are used to compute the new positions of the link atoms. The coordinate sets R(central) and R(total) are written to the QM program and MM program input files. This new computation of the complete coordinate set is required because the necessity to adapt the link atom positions have to be adjusted to the symmetry-adapted R(total), computed in interface*0_1*.

Subsequently, the PARAGAUSS run and the two MM program runs of central and total system are performed. The MM program and the accompanying preparatory work are chosen according to the parameters supplied to the script in the first step. The two

programs interface*2_1* and interface*2_2* convert the MM program output coordinates and gradients to a format compatible with the optimizer program. In this way, one can check the computed energy and gradients for possible errors; also, this strategy allows a uniform approach in future extensions. The respective information is written into a file holding the results of the MM calculations in a PARAGAUSS convenient format. The program interface*4* combines the gradients of the QM and the two MM calculations in a z-matrix and gradient file. This combination is carried out according to the link atom and gradient combination scheme chosen (see Eqs. 3.13-3.18). The energies of the subsystems are combined according to Eq. 3.10. The combined gradients and energies of the independent calculations are turned over to the optimizer program which generates a new geometry. If convergence according to some predefined conditions is met, the optimization stops here. Otherwise, the cycle is resumed with the symmetrization step in interface*0_1*.

3.4.3. QM/MM Test Calculations of Pentane

Pentane was chosen as the first to test the QM/MM implementation based on the MM code DL_POLY_2. The goal of this study was to reproduce results obtained with the implementation based on the MM program TINKER. Attention was paid mainly to get good agreement of the geometry and the total energy, although the total QM/MM energy does not possess a physical meaning because of the MM component.

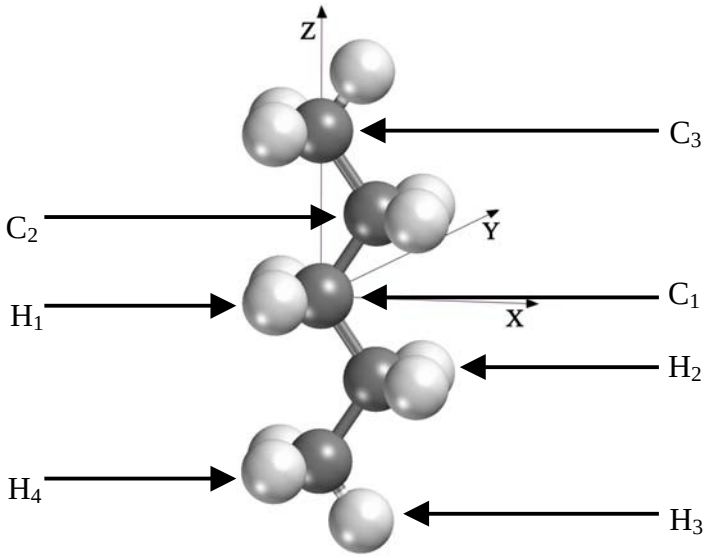

Figure 13 Pentane in a C_S symmetry conform orientation. Coordinate axes and unique atoms indicated

The model used C_s symmetry constraints. In this way, there were 7 groups of atoms not equivalent by symmetry, as illustrated in Figure 13. The boundary between QM and MM part was chosen to cut the bond between the atoms C_1 and C_2, which were replaced by hydrogen link atoms to form methane in the QM part. For both calculations, the computational parameters for the programs PARAGAUSS, TINKER and DL_POLY_2 were used as set forth in Chapter 4.

Table 1 Characteristic bond lengths of pentane in Cs symmetry; example DF (LDA) optimized geometry and end geometries of QM/MM optimizations; accuracy exaggerated to highlight the identity of QM/MM results; in Å

bond length	multiplicity	end value [Å] DFT	end value [Å] Tinker	end value [Å] DL_POLY_2
C_1-H_1	2	1.1096	1.1036	1.1036
C_1-C_2	2	1.5157	1.5253	1.5253
C_2-H_2	4	1.1078	1.1141	1.1141
C_2-C_3	2	1.5156	1.5333	1.5333
C_3-H_3	2	1.1050	1.1130	1.1130
C_3-H_4	4	1.1033	1.1130	1.1130

In the analysis of the results, the identity of the two QM/MM calculations is striking. Both implementations even needed the same number of steps to reach convergence. Only an inspection of the of the atomic positions in the respective end geometry revealed that differences in the order of 10^{-3} Å existed for the positions of the H_4 atoms. And these are the atoms exhibiting the highest difference between the QM/MM calculations with the TINKER and DL_POLY_2 MM program respectively.

One could argue, that the identity between the respective QM/MM calculations is the result of an accidentally good starting geometry. But, the H_4 atoms were moved ~0.25 Å between start and end geometry in the course of the optimization, ruling out this possibility.

Indeed, the similarities did not end in the geometry of the molecules computed. Total QM/MM and even the partial energies were equal to at least 5 decimal places (see

Table 2). The implementation of the QM/MM approach with DL_POLY_2 proved to be successful in any way.

Table 2 Total and partial energies of pentane in QM/MM in TINKER and DL_POLY_2 implementations; in au

method	coordinate set	DL_POLY_2 [au]	TINKER [au]
QM	R(central)	-40.1144123	-40.1144109
MM	R(central)	0.0004549	0.0004510
MM	R(total)	0.0048359	0.0048309
QM/MM	R(total)	-40.1100313	-40.1100310

It was only an intermediate goal to reproduce QM/MM geometries and energies calculated with the TINKER implementation by means of the DL_POLY_2 implementation. The more far reaching goal was to compute QM/MM systems with periodic boundary conditions, as the systems of interest in this thesis, copper clusters, were to be computed arranged in a grid-like pattern.

With this goal in mind, it was considered sufficient to chose pentane from the functional test above as first simple test case. A model was set up containing the pentane molecule in a periodic box in triclinic periodicity. In x and y direction the box length was set to 100 Å. In z-direction the cell vector was lowered from 40 Å to 9 Å in a stepwise fashion. The pentane molecules thus form a chain, where only the end groups, consisting of the C_3, H_3 and H_4 atoms, come in close contact with their periodic images. The interaction of the molecules was limited this way, allowing a comprehensive analysis of possible errors. The gas phase geometry of pentane was chosen as the start geometry of every step. The van der Waals cutoff radius was set to the respective z-direction cell vector length (see Chapter 3.3).

The relative total QM/MM energies at different distances between molecular centers were collected in Figure 14. The calculations found a minimum of the QM/MM total energy at a molecule center distance of approx. 9.5 Å with a minimum energy in the order of 0.1 kcal/mol. This value was confirmed to be sensible by comparison with a reference calculation, consisting of an explicit evaluation of the van der Waals potential of two methyl groups.

The contributions of the individual subsystems to the QM/MM total energy are detailed in Figure 15. The non-bonded interaction energy is provided by the outer part of the model only. The QM energy of the central part (QM part) depends mostly on the deformation of the QM model molecule, methane, by the interactions with the end groups and does not reflect a physical observable in the QM/MM context. At intermolecular distances higher than 9 Å, the QM part is not deformed at all. At 9 Å intermolecular center distance, pertaining to a H_3-H_3' distance of 2.2 Å, the QM part is deformed accidentally into a energetically favorable geometry by the MM part due to the link atom positions.

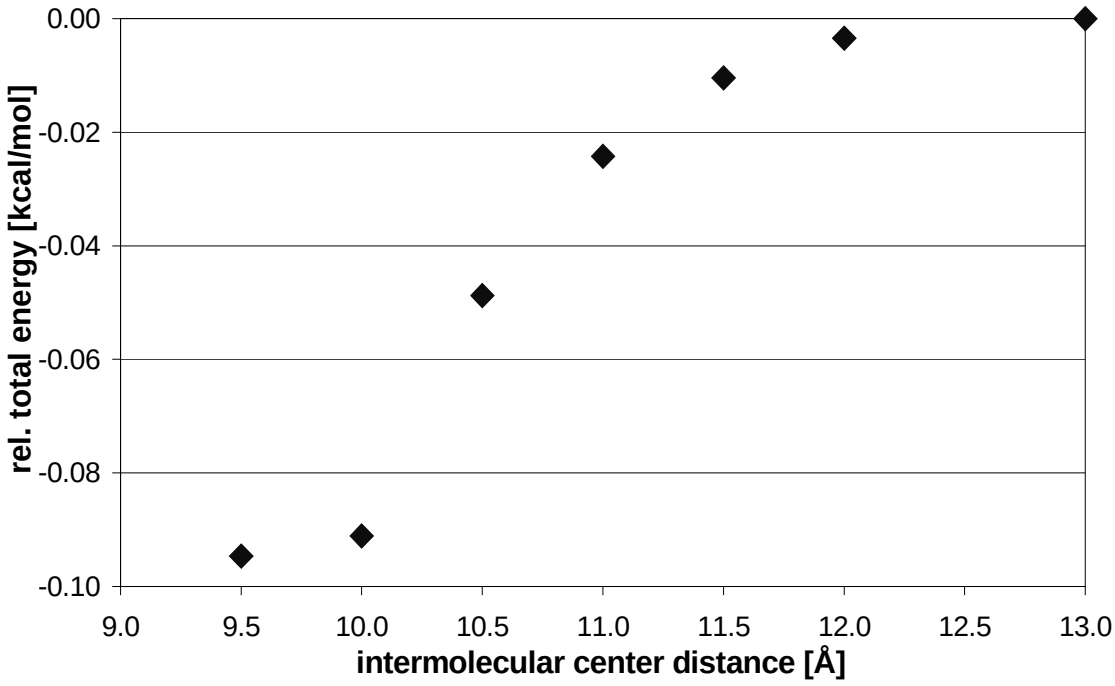

Figure 14 Relative total QM/MM energy of a chain of pentane molecules; in kcal/mol; relative total energy at 9.0 Å = + 0.5 kcal/mol omitted for clarity; QM/MM total energy of the gas phase geometry is -40.114546497019 au

The MM energy of the central part mirrors the results of the QM energy. It is assumed, that the decrease in relative energy is at least in part caused by van der Waals interaction between the central parts in MM description. This interaction is not completely cancelled.

The MM energy of R(total) shows the behavior of a typical van der Waals interaction. A slow decrease of the partial energy towards the intermolecular center distance of strongest van der Waals interaction is followed by a steep increase at shorter distances. The minimum of the MM energy of the total model is found at a

intermolecular center distance of 9.6 Å, pertaining to a H_3-H_3' distance between molecules of 2.7 Å. The results obtained in these calculations will help in the interpretation of the results of larger systems.

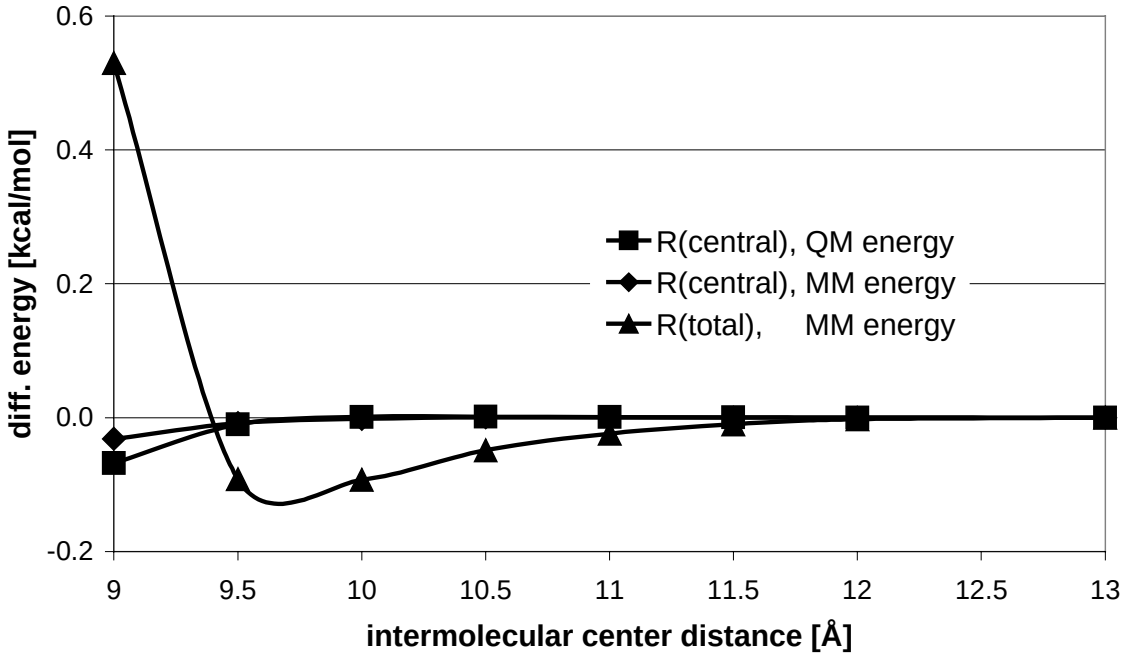

Figure 15 Partial energies used in the calculation of the QM/MM energy of pentane in periodic boundary conditions

As another test, one can study whether the geometry of the pentane molecule would deform according to the forces exerted by the van der Waals interaction between periodic images. A deformation should result only when the van der Waals interaction energy is high, i.e. at intermolecular hydrogen-hydrogen distances H_3-H_3' below 2.5 Å. For this purpose, the intermolecular center distance was correlated with the z coordinate of the H_3 atom relative to the gas phase geometry.

$$\Delta r(H_3) = \left| \vec{r}_{inf}(H_3) - \vec{r}_{\vec{c}}(H_3) \right| \qquad (3.19)$$

with ($\vec{r}_{inf}(H_3)$) being the coordinate vector of atom H_3 in the gas phase geometry and ($\vec{r}_{\vec{c}}(H_3)$) at the respective value of $\vec{c}$, the cell vector in z-direction.

At intermolecular center distances higher than 9.5 Å the molecule is widened minimally by the attractive van der Waals interaction between molecules. At lower distance it is compressed according the now repulsive interaction. This compression is

rightly the highest at the lowest intermolecular distance considered (9 Å). The deformation of the molecular geometry follows the expectation.

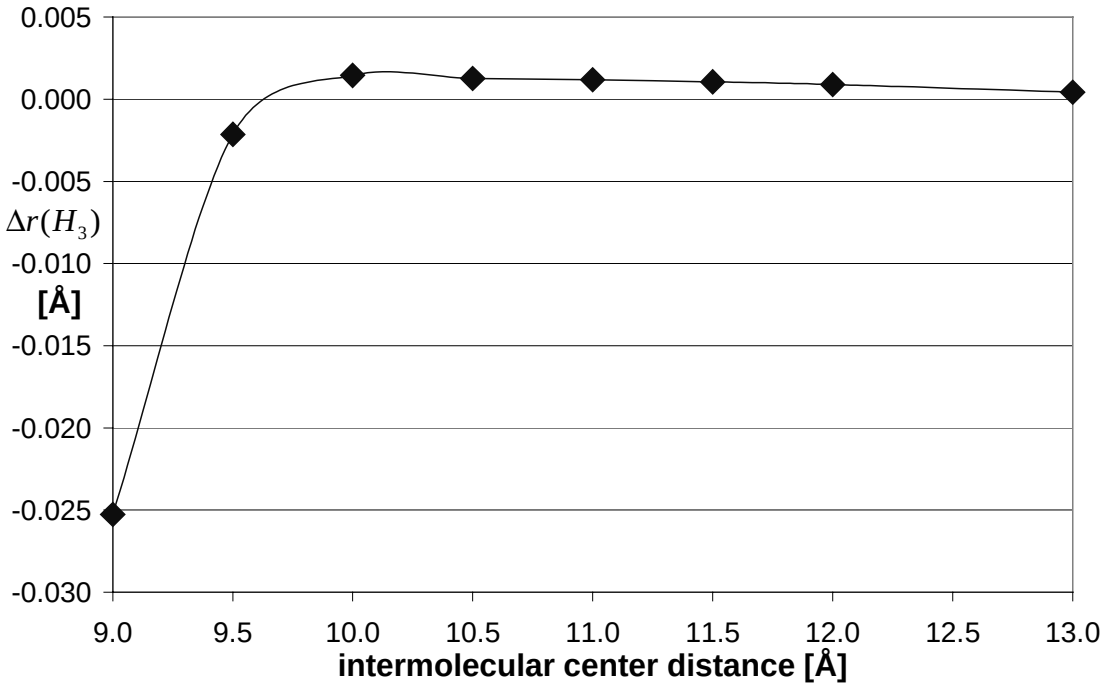

Figure 16 Deformation of the pentane molecule in periodic boundary conditions at given intermolecular center distances exemplified by the difference of H_3 atomic positions relative to the gas phase geometry

The tests discussed above showed that the DL_POLY_2 QM/MM implementation was able to reproduce geometric and energetic properties of the TINKER QM/MM implementation with high accuracy. Furthermore, the capability of the DL_POLY_2 based QM/MM implementation to conduct calculations with periodic boundary conditions was demonstrated. The extensive discussion proved the reliability of the results in every case.

4. Computational Details

For the DF calculations of this course of this work the PARAGAUSS program was used exclusively.[177] It employs a variant of the Linear Combination of Gaussian Type Orbitals – Fitting Function – Density Functional approach.[178] It uses an auxiliary basis to represent the electronic density for evaluating the Hartree contribution of the electron-electron interaction in an efficient fashion by means of three-center integrals.[179] Distinguishing features of PARAGAUSS are the consequently parallel implementation of every task, efficient relativistic treatment of heavy atoms, and various approaches for describing the interaction of a system with its surrounding. These interaction approaches include, for instance, cluster embedding in an elastic polarizable environment (EPE) and its extension covEPE to covalent substrates,[180] the polarizable continuum method (PCM)[181] and the QM/MM method.[182,183] A feature most helpful for the application in this thesis was the utilization of symmetry in almost every part of the program, which allowed speedup of the calculations for symmetric models. The geometry optimizations (ground state search only), were carried out with the LDA functional as suggested by Vosko-Wilk-Nusair (VWN).[101] Many studies showed that the VWN functional yields reasonable ground state geometries for transition metal cluster systems.[56,184] Energetic properties were computed using the BP86[102,185,186] functional of the GGA type. GGA-type exchange-correlation potentials tend to overestimate bond lengths for transition metal clusters,[57] but are superior to VWN functionals in terms of energetic accuracy.[58] All systems studied had an odd number of electrons. Thus, spin-polarized calculations were performed throughout this work. Relativistic effects were expected to be comparable to those found in an earlier work on Ni clusters[187] where, for clusters with 4 and 55 atoms, nearest-neighbor distances were found to contract about 0.02 Å, accompanied by an average increase of binding energies of about 5 %. These effects were considered negligible in the framework of the current investigation. The molecular orbital basis set for copper comprised 15 s-, 11 p-, and 6 d-type Gaussian exponents, contracted to [6s,4p,3d] using atomic Kohn-Sham eigenvectors obtained in a spin-restricted atomic calculation employing I_h symmetry restriction.[188] The corresponding auxiliary basis set was constructed in a standard fashion.[189] Basis sets of other elements used in this work received similar treatment to ensure an equal quality of basis sets for every element, Table 3 provides an overview. The grid for numerical integration was chosen as a superposition of atom-centered spherical grids according to Becke;[190] the parameters are also listed in Table 3. The grid construction implies a Lebedev angular integration grid of order 17 (locally accurate up to angular momentum

L = 17).[191-193] The resulting number of grid points, as listed in Table 3, varies because of symmetry considerations in the construction of the grid. Geometry optimizations were performed using the *optimizer* subprogram of the PARAGAUSS program suite. This program employs a quasi-Newtonian minimum search algorithm[194] using a consecutively refined Hessian matrix from an initial guess of an unit matrix. [194-201] In all cases the geometries were relaxed until the components of the Cartesian gradients were found to be smaller than 10^{-5} au.

Table 3 Parameters used in the QM calculations. Numbers in parenthesis denote the uncontracted basis set, numbers in square brackets the contractions derived thereof. NRAD is an implementation specific grid parameter used in the construction of the Lebedev integration grid; approximate size of grid indicated by number of grid points

element	basis set		NRAD	appr. number of grid points
Cu	(15, 11, 6)	→ [6, 4, 3]	51	6660
S	(12, 9, 2)	→ [6, 5, 2]	71	6710
C	(9, 5, 1)	→ [5, 4, 1]	51	3480
H	(6, 1)	→ [4, 1]	71	6820

The MM calculations were carried out with the programs TINKER[43] and DL_POLY_2[44] using the MM3 force field of Allinger et al.[125-130] In the case of DL_POLY_2 some conversions and adaptation were necessary which are described in Appendix A. Gradients and total energies were calculated with an accuracy of $8 \cdot 10^{-7}$ au, their respective geometry optimization (TINKER) or update (DL_POLY_2) facilities were not used in favor of the *optimizer* program. In computations using periodic boundary conditions, an adapted cutoff strategy was used for van der Waals interactions; their corresponding minimal values are collected in Table 4.

Table 4 Listing of appropriate values of *rvdw* for a maximum value of 0.001 kcal/mol at cutoff distance of an arbitrary potential; highest value applies where multiple types present

vdW atom pair	minimum rvdw [Å]
H - H	6.11
H - S	9.46
H - Cu	10.33
Cu - Cu	13.36

5. Calculations of Small Systems

5.1. Cuboctahedral Cu_{13} Clusters in Different Symmetries

The cluster Cu_{13} corresponds to a complete coordination shell surrounding a central atom and is thus the smallest cluster with a bulk-like coordination shell of at least one atom. Clusters of this nuclearity are expected to be particularly stable.[202] Optimizing the structure of the cluster under different symmetry constraints was supposed to show the minimum energy structure. Reference data would be provided for the calculations of ligated clusters. O_h symmetry was presumed as a reasonable starting point for the investigation, as detailed in a *X*α study of Cu_{13} by Messmer et al.[203] They assumed that a Cu_{13} cluster would inherit the O_h symmetry present in the cutout of the fcc bulk metal lattice. Therefore, they restricted their model to a cuboctahedron at fixed bond lengths. Later density functional studies of smaller Cu_n species with $n \leq 10$ however showed the tendency of copper clusters to form ellipsoidal, flat, geometries.[204-206] To test if this tendency would prevail in Cu_{13}, lower symmetry models were studied. A successive reduction of symmetry constraints from D_{4h} to D_{2h} and C_{4v} would allow the cluster to adopt such an optimum structure.

The geometry of Cu_{13} clusters was optimized using the VWN (LDA) functional.[101,207,208] GGA total energies were then calculated in single point fashion using the BP86 functional.[102,186] The validity of model and computational parameters was assessed by comparison with available computational and experimental data. Symmetry constraints to the model were compared based on their effect on the cluster geometry. The optimum geometry of the Cu_{13} cluster was to be used as the cluster core in further calculations, which would contain a ligand shell model.

5.1.1. Computational Details

The O_h computation was started with a cuboctahedral cutout of the fcc lattice of copper of 13 atoms, using the bulk nearest neighbor distance of 2.556 Å.[209,210] For each of the symmetry constraints lower than O_h, the atomic positions were modified by ~10^{-2} Å in the appropriate degrees of freedom to facilitate convergence of the electronic structure in the subsequent geometry optimization.

In the Cu_{13} cuboctahedron (O_h) only two sets of symmetry inequivalent atoms exist. (Figure 17) In symmetry D_{4h}, mainly applied in this work, cluster atoms fall into three such sets. The central atom will be called just that. The four atoms located on the x

or y axes, with z = 0, will be referred to as equatorial atoms or Cu_{eq}. The remaining 8 atoms are termed axial atoms Cu_{ax}, reminiscent of the nomenclature in e.g. carbohydrates or complexes.[211-213] When reducing the symmetry from O_h to D_{4h}, the bond lengths of equatorial and axial atom to the central atom become disparate. In a further reduction of symmetry from D_{4h} to D_{2h}, and the change from D_{2h} to C_{4V}, of the axial and equatorial atom groups split up further. In D_{2h}, diagonal axial atoms together with their horizontal images constitute two groups. In C_{4v}, the axial atoms above and below the x-y-plane constitute separate groups.

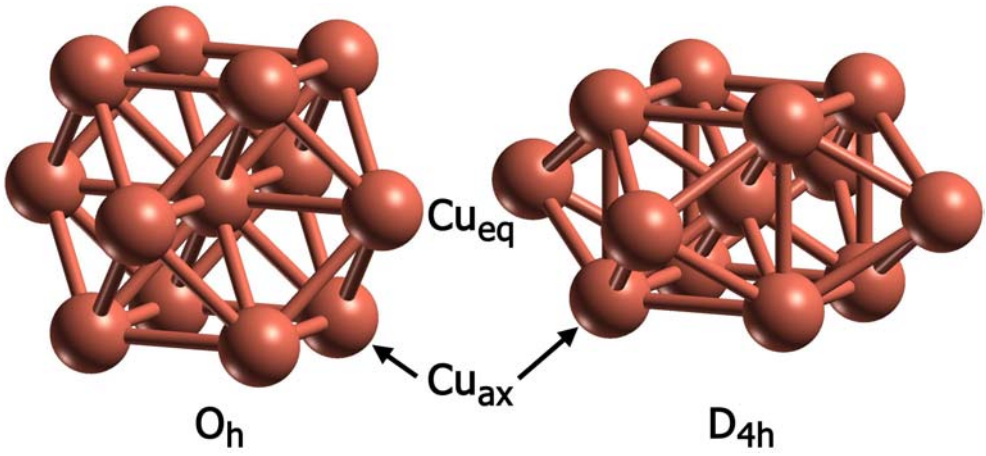

Figure 17 Cu13 in O_h and D_{4h} symmetry, illustrating the naming convention for surface copper atoms

All calculations used one processor of the SGI Power Challenge, to allow accurate measurement of the computation time without parallelization effects.

5.1.2. Results

In O_h symmetry, the optimized bond lengths were 2.256 Å (equivalent to an atomic radius of 112.8 pm). Although less than the atomic radius in the bulk of 1.278 Å, this is still considerably larger than any of the ionic radii, ranging from 0.77 Å for copper I to 0.54 Å for copper III. The calculated bond length is consistent with those computed for smaller copper cluster species (Cu_{10}; 2.40–2.50 Å).[214] In that work, geometries were optimized at GGA level, applying counterpoise and zero-point corrections.

The energy obtained in the O_h optimization was taken as a reference for the relative stability of the Cu_{13} cluster in other symmetries. Differences of the symmetry conformers will be provided in kcal/mol. The computation time required for one geometry update was about 4 minutes.

Under symmetry reduction from O_h to D_{4h}, the Cu_{ce}-Cu_{ax} and Cu_{ce}-Cu_{eq} bond lengths become different, when accompanied by an energy gain. In the optimized geometry, the central atom to equatorial atom bonds, henceforth referred to as equatorial bonds, were elongated to 2.74 Å. The axial bond lengths decreased to 2.015 Å. The bond length from equatorial atom to axial atoms, 2.281 Å, remained relatively close to the original bond length of 2.256 Å , see Table 5. The cluster in D_{4h} geometry was more stable than in O_h by 35.9 kcal/mol. The computation time needed for one geometry update was ca. 7 min or an increase of almost 100% relative to O_h symmetry.

All Cu_{13} cluster conformers found until then were "flat", i.e. the ratio of x(y) and z axis was larger than 1. Studies of the respective gold species indicated the existence of conformer with a more globular shape.[215] However, such an conformer was only accessible at computational parameters that ensure a higher accuracy at considerably higher computational costs (increased grid quality, inclusion of relativistic effects). This structure was not stable in a single point calculation with the standard parameter set. It could not even reach SCF convergence. The relative total energy, (see Table 5) was at least 22 kcal/mol less stable than the flat conformer, and is mentioned as an example for a different conformer, which becomes stable in a ligand shell situation (see Chapters 6.1, 6.2).

Table 5 Representative bond lengths, relative energies and atomization energies of Cu_{13} clusters with different symmetry constraints

symmetry	Cu_{ce} - Cu_{eq} [Å]	Cu_{ce} – Cu_{ax} [Å]	total energy †‡ [kcal/mol]	atom. energy per atom‡ [eV]
O_h	2.256	2.256	-	-2.334
D_{4h}	2.740	2.015	-22.4	-2.409
D_{4h} "round"	2.375	2.375	(10.4)	-
D_{2h}	2.740	2.015	-22.4	-2.409
C_{4v}	2.740	2.015	-22.4	-2.409

† Relative to the O_h conformer ($E_{tot,Oh}$ = -21201.34796 au)

‡ Single point GGA calculations using LDA optimized structures (E_{Cu} = -1633.91241 au)

Analysis of the corresponding one-electron spectra reveals the cause of the large distortion of the cuboctahedral cluster upon symmetry reduction. The partially occupied t_{2g} orbital in O_h symmetry correlates with the b_{2g} + e_g orbitals in D_{4h} (see Table 6).[216,217] In the present example however, the e_g orbital energy is increased by 0.6 eV while the b_{2g} orbital energy is decreased by 0.8 eV. In the O_h symmetry, the LUMO has e_g character, which splits into a_{1g} + b_{1g} in D_{4h}. These two orbitals now lie energetically lower than the e_g in D_{4h} and are subsequently occupied. The stabilization of the flat conformer is therefore not an effect of a Jahn-Teller distortion alone, but the result of a change to a different electronic configuration. As the HOMO in D_{4h} belongs to an one-dimensional irreducible representation (a_{1g}), an additional energy gain by Jahn-Teller distortion can not be expected.

Nevertheless, symmetry constraints were reduced to D_{2h} and C_{4v}. In the D_{2h} point group the axial atoms are separated into two sets, arbitrarily denoted axial for those located in the x-z-plane and axial' (prime) for those located in the y-z-plane. Although the calculation was set up with an appropriate difference of bond lengths of axial and axial' atoms, they were virtually identical in the converged geometry to the D_{4h} geometry. The axial and equatorial bond lengths remained the same as in the D_{4h} optimization ($\Delta r_i \leq 10^{-5}$ Å). This geometry was also –22.4 kcal/mol more stable than the O_h geometry, or virtually identical to the D_{4h} geometry. The time for one geometry point increased to about 19 min.

Table 6 Electronic configurations of Cu_{13} clusters in different symmetries, the HOMO designates the highest occupied molecular spin orbital, ↑ and ↓ denote majority and minority spin respectively, the last column shows the HOMO energies in eV

symmetry	configuration	HOMO (spin orbital)			Energy [eV]
O_h	$a_{1u}^2\ t_{2g}^5$	13	t_{2g}^2	↓	-4.467
D_{4h}	$a_{1g}^2\ b_{1g}^1$	23	a_{1g}^1	↑	-4.267
D_{4h} "round"	$b_{2g}^1\ e_g^4$	20	e_g^2	↑	-4.459
D_{2h}	$a_g^2\ a_g^1$	37	a_g^1	↑	-4.267
C_{4v}	$a_1^2\ b_1^1$	39	a_1^1	↑	-4.267

A change of symmetry constraints to C_{4v} did not result in a energy gain with respect to D_{2h} or D_{4h}. In fact, the total energy was again virtually identical ($\Delta E_{tot} < 10^{-3}$ kcal/mol)

to the D_{4h} conformer, or –22.4 kcal/mol with respect to the O_h symmetry optimization. The axial and equatorial bond lengths stayed at their familiar values of 2.015 Å and 2.740 Å respectively. The time for one geometry point decreased to 14 min/cycle, a reduction of 5 minutes relative to the D_{2h} optimization.

The atomization energies of the O_h cluster (E_B = 2.33 eV) and D_{4h} cluster (E_B = 2.41 eV) were compared reasonably to an estimated value derived from the calculations of Jug et al.[214] of E_B ~2.5 eV, which were carried out using the PW functional[185] and employed counterpoise correction. Similarly, the vertical ionization potential according to Janak's theorem (D_{4h} ; IP_1 = -4.267 eV) compared reasonably with an experimental estimate by Winter et al., where an upper bound of the IP of 5.58 eV was inferred from excitation thresholds.[218]

From these calculations, the D_{4h} symmetry was chosen as a suitable compromise between computational accuracy and computation time. This symmetry constraint allows addition of a flexible arrangement of 8 ligands, while keeping the computational effort moderate.

5.2. Model Ligand Coordination: $Cu_{13}(SH)_8$

To qualitatively assess the effects of ligands, their binding site and orientation preference on clusters, is common to replace bulky ligands by small model species. As the electronic interaction of the ligand head group is usually the strongest, this strategy is useful, even though electronic and steric effects of the tail groups are neglected. The potential energy surface of such a model system would provide qualitative insight into the thiolate coordination to copper clusters. In this way, useful starting geometries for the inspection of more realistic ligands can be obtained and it is also possible to estimate the binding energy of thiolate ligands to copper clusters. From similar computations on Au clusters, Nörtemann[215] concluded that the difference in binding energy between an on top and a threefold hollow site is about 0.3 eV or 6.9 kcal/mol. The gold and copper clusters differ in structure: the copper clusters investigated were flat. Thus, the circumscribing ellipsoid features two long and one short main axes. Only one of the Au clusters examined had a similar shape.[215] The three other $Au_{13}(SH)_8$ conformers exhibited two short and one long main axes (upright ellipsoidal). Genest found only upright ellipsoidal conformers.[219] Also, the bridge-hollow position of the sulfanyl ligands turned out to be energetically preferred over the on-top position.[219] On the other hand, energy differences were rather similar to those in the previous study. Ligands in bridge-hollow binding site were confirmed to be 0.3 eV stronger bound than the on-top position.

5.2.1. Model and Setup

The Cu_{13} cluster in D_{4h} symmetry as derived in the previous chapter served as reference structure of the model system. Here, as well in other cases, one can consider the assumption of a highly symmetric structure of the cluster as a model assumption.[56,58,204,220] To assess the properties of ligand orientations, four models were set up. In the first two, the ligands occupied threefold-hollow to bridge-hollow position above the 111 facet, each made up by two Cu_{ax} and one Cu_{eq} centers. The ligands were free to move on the plane bisecting this facet. In the other two conformers, the 8 ligands were placed in a on-top position above the Cu_{ax} centers. In each group, the ligands were oriented in the x-y-plane (out) and perpendicular to this plane (up) in one model respectively. All four conformations were optimized in D_{4h} symmetry. At the beginning, the ligands were positioned according to their adsorption sites with a copper to sulfur distance of 2.15 Å to the respective nearest atom(s).

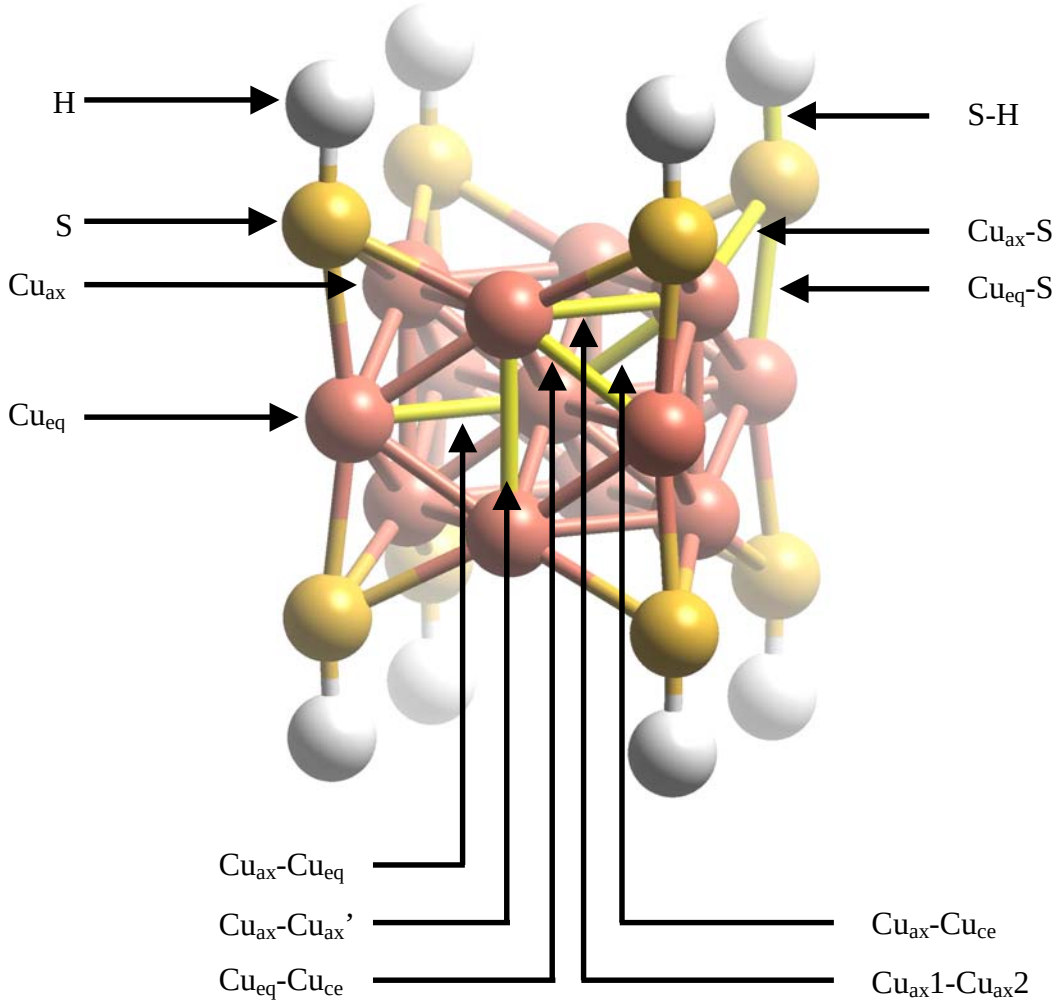

Figure 18 Nomenclature to describe $Cu_{13}(SH)_8$ model clusters. The example is in bridge-hollow coordination, ligands are oriented upwards

5.2.2. Total Energies and Binding Energies

The total energy of the optimized structures of $Cu_{13}(SH)_8$ varied with conformation and ligand orientation. First, structures with ligands at threefold-hollow sites rearranged to bridge-hollow sites during the optimization; also they were more stable than structures with ligands in on-top positions. The total energy of the clusters varied in a range of 7.5 eV with the bridge-hollow (up) conformation being the most stable and on-top (out) being the least stable.

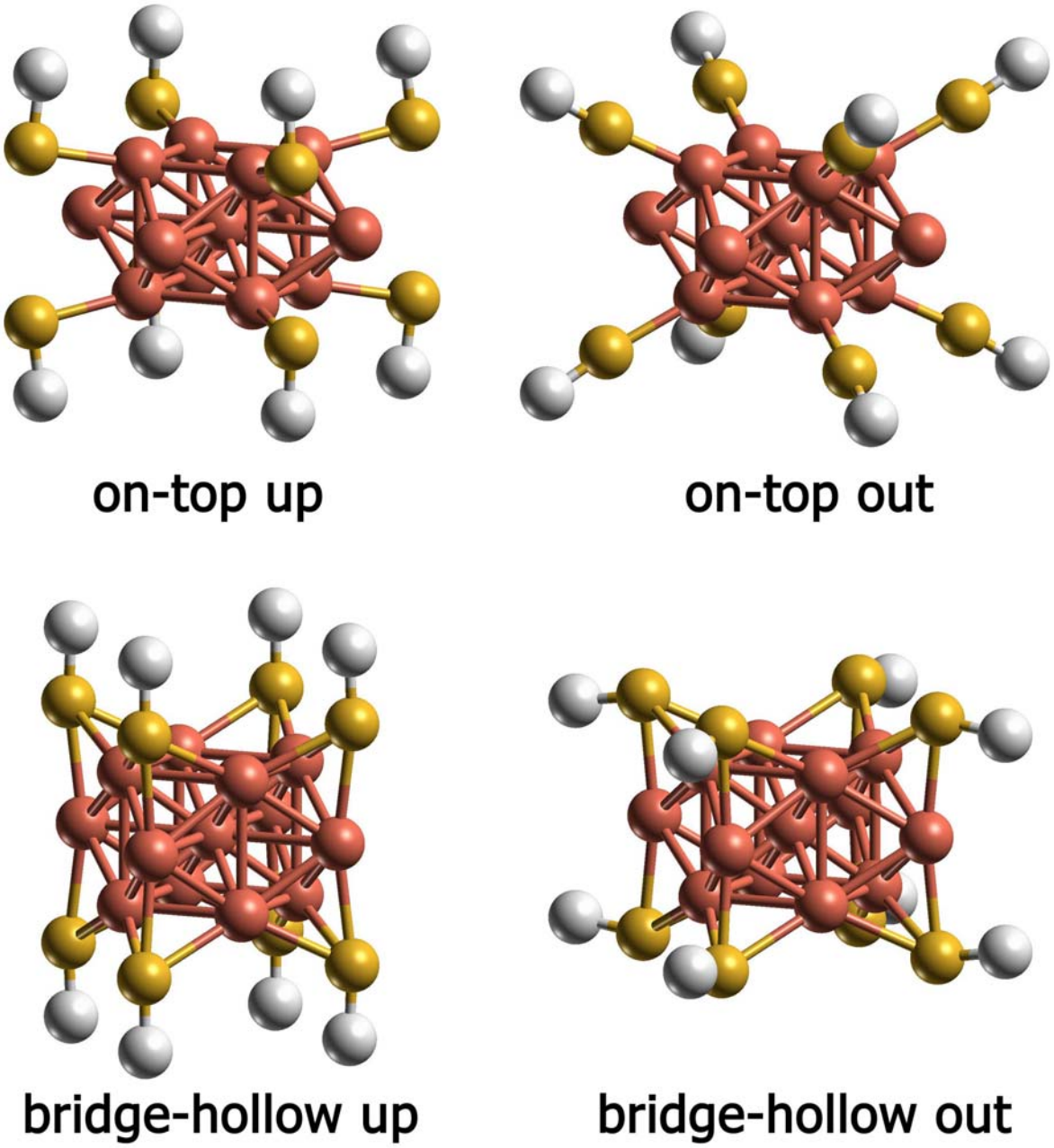

Figure 19 Optimized geometries of the 4 conformers of $Cu_{13}(SH)_8$

This finding agrees with the results of Genest for sulfanylated gold clusters. However the energy differences appear to be broader than for the Au clusters. Therefore, the different conformers vary in abundance. The structure of the on-top (out) conformer and its energy difference to the other conformers may look strange at first sight. The ligands do not show the typical Cu-S-H angle of ~110˚. It is still included in this study for reference purposes. Careful investigation confirmed, that the optimization was indeed

genuinely converged. Likewise, the electronic spectrum does not exhibit any anomalies. Thus it was concluded, that this structure is a genuine, if awkward looking minimum of the potential energy hypersurface of the model system $Cu_{13}(SH)_8$.

Table 7 Energy difference[a] relative to the bridge-hollow (up) structure and binding energies of various conformers (GGA single point calculations at LDA optimized geometries) energies in eV

ligand binding site	ligand orientation	relative total energy [eV]	binding energy per ligand [eV]
bridge-hollow	up	0.000	-3.12
bridge-hollow	out	0.942	-3.24
on top	up	1.696	-3.02
on top	out	7.470	-2.30

[a] See Appendix B for absolute total energies

Clearly, the binding energies follow the same trends as the total energies regarding the adsorption site and the orientation of the ligand. They range from 3.24 eV for the case of bridge-hollow (up) to nearly an 1 eV less for the case of on-top (out). The large energy difference of 0.7 eV between the two on-top conformers of as compared to the small energy spacing of 0.1 V between the two bridge-hollow conformers can be rationalized by the relative instability of the on-top (out) conformation. In summary one concludes, that all of the axial and equatorial conformers would have to be calculated also for larger species, as the differences may change depending on the immediate surrounding of the ligands, and additional steric interactions within other ligands. Note that the calculated binding energies are about 0.6 eV larger than in comparable surface adsorption calculations,[221] where Akinaga et al. computed surface adsorption energies of methyl thiolate on the copper (111) surface. Allowing relaxation of the adsorption site and ligand geometry, they obtained a (non-relativistic) binding energy of 2.63 eV per adsorbate. As a side remark it is noted, that in that study relativistic corrections of the binding energy were estimated to 0.0004 eV only. That result supports the strategy of the present study, namely to employ only non-relativistic models.

A LDA study of Cu_4SX clusters, (X being H and CH_3, respectively) by Kerdcharoen et al.[183] found significantly higher binding energies, ranging from 4.2 to 3.8 eV. However, these binding energies become comparable to those obtained in this

thesis, if one applies an ad-hoc-correction of about 1 eV to account for the overbinding of the LDA functional.

5.2.3. Cluster Core Geometry

The presence of ligands can obviously change pertinent bond distances of the underlying cluster core. This is demonstrated by Table 8, which presents a comparison between suitable geometrical properties of the D_{4h} symmetry "bare" cluster and the species with ligands. The Cu_{ce}-Cu_{eq} and Cu_{ce}-Cu_{ax} distances are referred to as first order bonds in the discussion to distinguish them from the second order bonds, which are $Cu_{ax}1$-$Cu_{ax}2$, between two axial copper atoms in the horizontal plane of the cluster, $Cu_{ax}1$-$Cu_{ax}1'$, between one axial copper atom and its image at the negative z coordinate and Cu_{eq}-Cu_{ax}, the distance between equatorial and axial atoms.

Table 8 Pertinent Cu-Cu distances of $Cu_{13}(SH)_8$, in Å

ligand binding site	ligand orientation	Cu_{ce} - Cu_{eq} [Å]	Cu_{ce}-Cu_{ax} [Å]	$Cu_{ax}1$-$Cu_{ax}2$ [Å]	$Cu_{ax}1$-$Cu_{ax}1'$ [Å]	Cu_{eq}-Cu_{ax} [Å]
bridge-holl.	up	2.57	2.09	2.37	2.48	2.20
bridge-holl.	out	2.74	2.04	2.33	2.41	2.30
on-top	up	2.68	2.01	2.29	2.40	2.26
on-top	out	2.71	2.01	2.32	2.34	2.26
Cu_{13} bare		2.74	2.01	2.32	2.33	2.28

Both first order bond lengths, Cu_{ce}-Cu_{eq} and Cu_{ce}-Cu_{ax}, are only weakly influenced by the presence of the ligands in the three least stable conformations. Only in the bridge-hollow (up) conformation the Cu_{ce}-Cu_{eq} bond length decreases by 17 pm. The shortening of this bond is accompanied by a concomitant increase of the bond lengths Cu_{ce}-Cu_{ax}, $Cu_{ax}1$-$Cu_{ax}2$ and $Cu_{ax}1$-$Cu_{ax}1'$. For all other conformers, similar to the Cu_{ce}-Cu_{eq} bond the changes in the Cu_{ce}-Cu_{ax} bond length are not strong. As can be seen, the changes in these "second order" bond lengths are fairly small, of the order of 1 pm; the largest increase of $Cu_{ax}1$-$Cu_{ax}1'$ again for the bridge-hollow (up) conformation, is 15 pm. This most strongly bound species is obviously undergoing the strongest stress on the cluster core. The overall trend shows that the Cu-Cu bonds change concurrently,

deforming the cluster into more round shape, rather than contracting the whole cluster with the flat shape left intact.

5.2.4. Ligand Geometry

As can be seen in Table 9, sulfur-copper bond lengths do not vary significantly in the bridge-hollow conformations. Shifting the ligands into equatorial positions moves the ligand head group only minimally in the direction of equatorial copper atoms (by 4 pm). This "downward" movement is accompanied by an elongation of the Cu_{ax}–S bond by 9 pm.

Table 9 Sulfur related bond lengths in $Cu_{13}(SH)_8$ clusters of different conformations; in Å

ligand binding site	ligand orientation	Cu_{eq} – S [Å]	Cu_{ax} – S [Å]	S – H [Å]
bridge-hollow	up	2.26	2.28	1.37
bridge-hollow	out	2.22	2.37	1.38
on-top	up	3.08	2.13	1.37
on-top	out	3.23	2.05	1.35

The situation was entirely different in the case of the on-top located ligands. The changes for both bond lengths are more drastic and as already seen in the evenly drastic changes in binding energy (Table 9). Bond length changes of 15 pm for Cu_{eq}–S and 8 pm for Cu_{ax}–S indicate considerable changes in the bonding situation when switching from an axial to an equatorial ligand orientation. Here, the curious ligand orientation in the on-top (out) case is mentioned again. The Cu_{ax}-S-H angle of 180° makes the assumption plausible, that this conformation is caused by the symmetry restriction to D_{4h}, which prohibit a ligand reorientation into a energetically favorable position. The sulfur-hydrogen bonds, on the other hand, do not change significantly for different ligand surroundings. Taking the value of 1.37 Å as reference, deviations of at most 2 pm seem nearly negligible considering the computational approach used. In summary, the calculations of $Cu_{13}(SH)_8$ showed that its properties will sometimes change in drastic ways dependent on the ligand binding site and orientation. Although the binding energies for on-top adsorption sites suggest that these binding site conformers are less

stable regardless of the ligand species, further investigations should not exclude them a priori. Inter-ligand interaction can contribute considerably to the binding energy of larger, more realistic ligands.

5.2.5. Conclusions

It can be concluded, that sulfanyl model ligands bind to copper clusters with a strong chemical bond. Comparison with previous calculations showed, that the binding energy of sulfanyl ligands is computed higher than that of alkyl thiole species. However, one can expect, that alkyl thioles will be bound to copper clusters with considerable binding energies as well. The bridge-hollow binding site was identified as energetically preferred. Without interaction between ligands, the sulfanyl ligands adopt a nearly perfect threefold-hollow ligand binding configuration. The higher the binding energy, the more the cluster is deformed into a round shape. However, this deformation into a round shape is not as pronounced as in the case of the bare cluster D_{4h} "round" mentioned in Chapter 5.1.2. In the case of the on-top (out) positioned ligands, the cluster-ligand interaction led to a less intuitive conformation of the cluster. It is anticipated that the steric interaction between bulkier ligands will exhibit a much stronger directing influence on ligand binding site as well as on the ligand orientation and the cluster shape.

6. Comparing QM and QM/MM Calculations of $Cu_{13}(SCH_2CH_3)_8$

A central goal of the present work is the application of the QM/MM method to copper thiolate clusters with a realistic ligand shell. To test the performance of the QM/MM approach, the results are compared with pure QM calculations. Structural properties like the conformation of the ligands and inter-ligand distances are investigated as well as energetic properties like total and binding energies of the individual clusters. Ground state structures of various conformers were determined, rather than only the most stable structure.

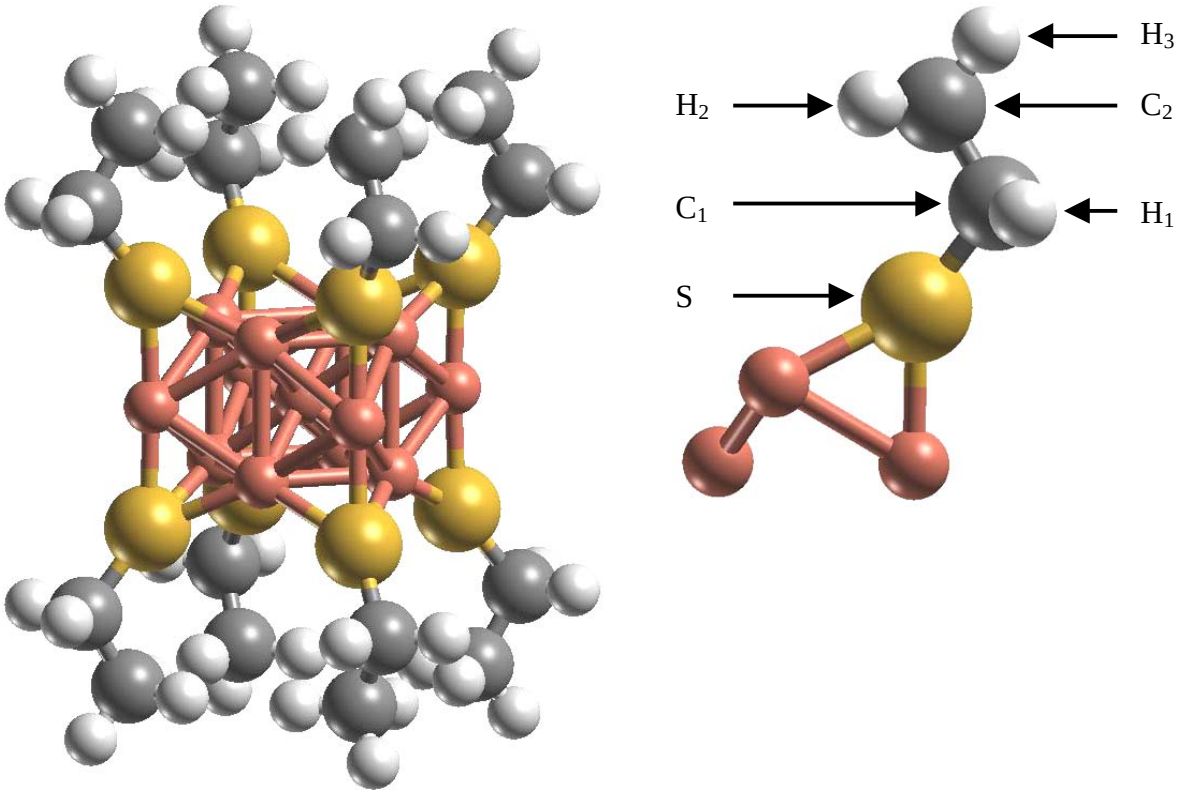

Figure 20 Example structure of the cluster $Cu_{13}(SCH_2CH_3)_8$ and the set of symmetry inequivalent atoms under D_{4h} symmetry; labeling of various atoms

Thus trends and preferences can be readily identified, which will be helpful not only in the evaluation of the hybrid method approach to ligand covered cluster system, but in the investigation of these systems themselves. In the following, the first in depth analysis of a metal cluster compound is presented, which will discuss in detail the results of pure quantum chemical and hybrid method computations. This will allow one to interpret these results with respect to the restriction of each model as a result of the underlying physics. The quantum mechanical reference results are discussed in Chapter

6.1; the hybrid method results will be presented and discussed in conjunction with their QM counterparts later. (Chaps. 6.2)

6.1. QM Calculations of $Cu_{13}(SCH_2CH_3)_8$ with Different Ligand Conformations

The density functional calculations of the ethylthiolized Cu_{13} clusters are not only considered as reference calculations for the hybrid method. Rather, they also exemplify strengths and shortcomings of this approach when applied to complex, composite metallic and organic systems.

6.1.1. Computational Setup of the Calculations

To constrain the number of conformers and to reduce the computational effort, the $Cu_{13}(SCH_2CH_3)_8$ cluster was treated in D_{4h} symmetry. This necessitated to distribute of the ethyl thiolate ligands in the same way as in the model $Cu_{13}(SH)_8$. The respective cluster core geometry was copied in straightforward fashion. As in the model $Cu_{13}(SH)_8$, the bridge-hollow and the on-top adsorption sites were examined. Similarly, the SCH_2CH_3 ligands were attached in such a way that the S-C_1-C_2 backbone lies in a mirror plane. The Cu_{ax}-S-C_1 angle and the S-C_1-C_2 angle of a ligand in the positive z half-space may be opened either towards the positive z-axis or away from it, respectively. Taking into account H atoms, the only further freedom to construct conformers is the staggered or eclipsed conformation of the CH_3 end group. Thus it is possible to construct 8 conformers per binding site with the SCH_2CH_3 ligand. To simplify the references to the resulting 16 conformers, four designators (of one letter each) were assigned to them, depending on the state of their conformation. The abbreviations and explanations refer to a ligand in the positive z half-space.

1. Binding site (**b** or **t**)

Two possible binding sites were examined. The respective conformations were labeled b for bridge-hollow or t for on-top.

2. S – C_1 bond orientation (**u** or **d**)

As the angle Cu_{ax}-S-C is typically around 105º, two major orientations of the ligand with respect to the cluster may be assumed. If the Cu-S-C angle of a ligand is opened toward the positive z-axis, the designation is upwards, **u**. If it is opened in the general direction of the negative z-axis, the designation is downwards, **d**.

3. Orientation of the C – C bond (**i** or **o**)

The S-C-C angle can either be opened in the direction of the positive z-axis or in the direction of the negative z-axis (or horizontal mirror plane). The former was termed "inward" or **i**, while the latter "outward" or **o**.

4. Ethyl conformation (**s** or **e**)

An ethyl group may occur in two different rotamers. The staggered form will be designated a **s** while the eclipsed form will be denoted an **e**.

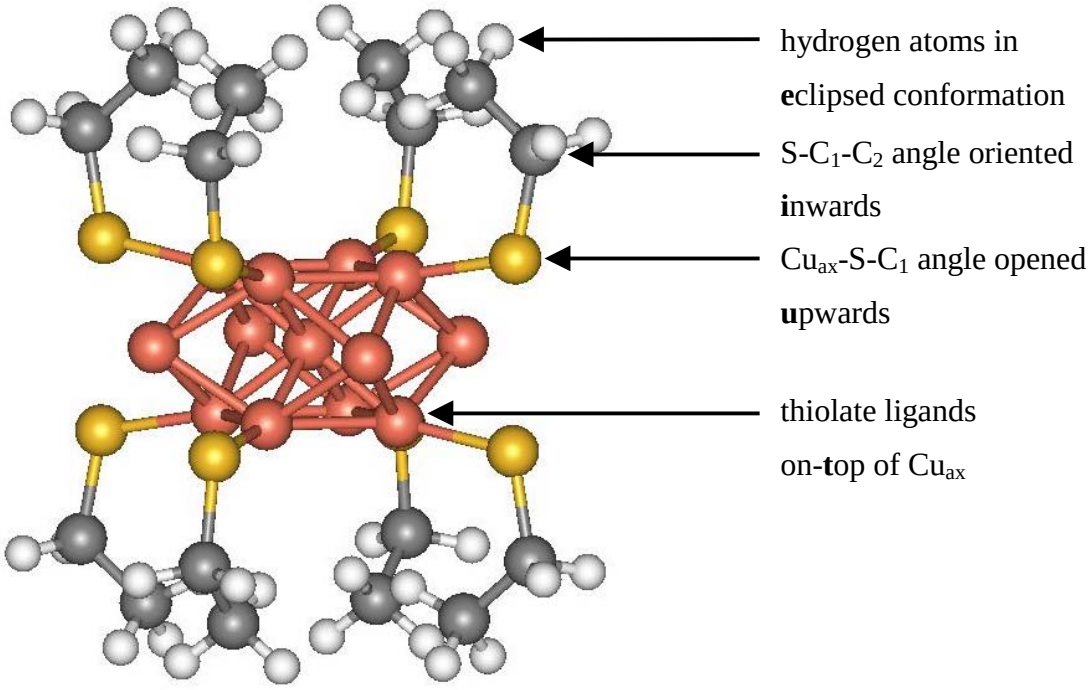

Figure 21 $Cu_{13}(SCH_2CH_3)_8$ in conformation **tuie** as an example for the conformation nomenclature

Ethyl thiolate ligands pre-optimized in C_s symmetry were attached in different conformations to the various binding sites of the D_{4h} geometry of Cu_{13} of the cluster discussed in Chapter 5.2. In the starting geometry, the distance Cu_{ax}-S was chosen to be 2.09 Å.

The quantum chemical computations were performed with the program PARAGAUSS using the parameters as discussed in Chapter 4. In the fashion established earlier, geometry optimizations were performed using the LDA functional. Subsequently, the total energy of the structure was determined in a single point GGA calculation. (for details, see Chapter 4) The z-matrix was constructed to restrict the movement of atoms to D_{4h} symmetry, using 17 internal degrees of freedom. The

maximum step length allowed was set to 0.3 au, corresponding to ~0.01 Å per bond length or ~1° per angle or dihedral angle.

Most calculations needed approximately 30 steps to reach geometric convergence. In a four processor parallel run on a SGI Power Challenge, for 30 steps at 2.5 hours per step this corresponds to 75 hours of computation time per conformation.

6.1.2. Overview of the Conformers

The following section intends to familiarize the reader with the results in a pictorial form, before details of the individual optimized structures will be discussed.

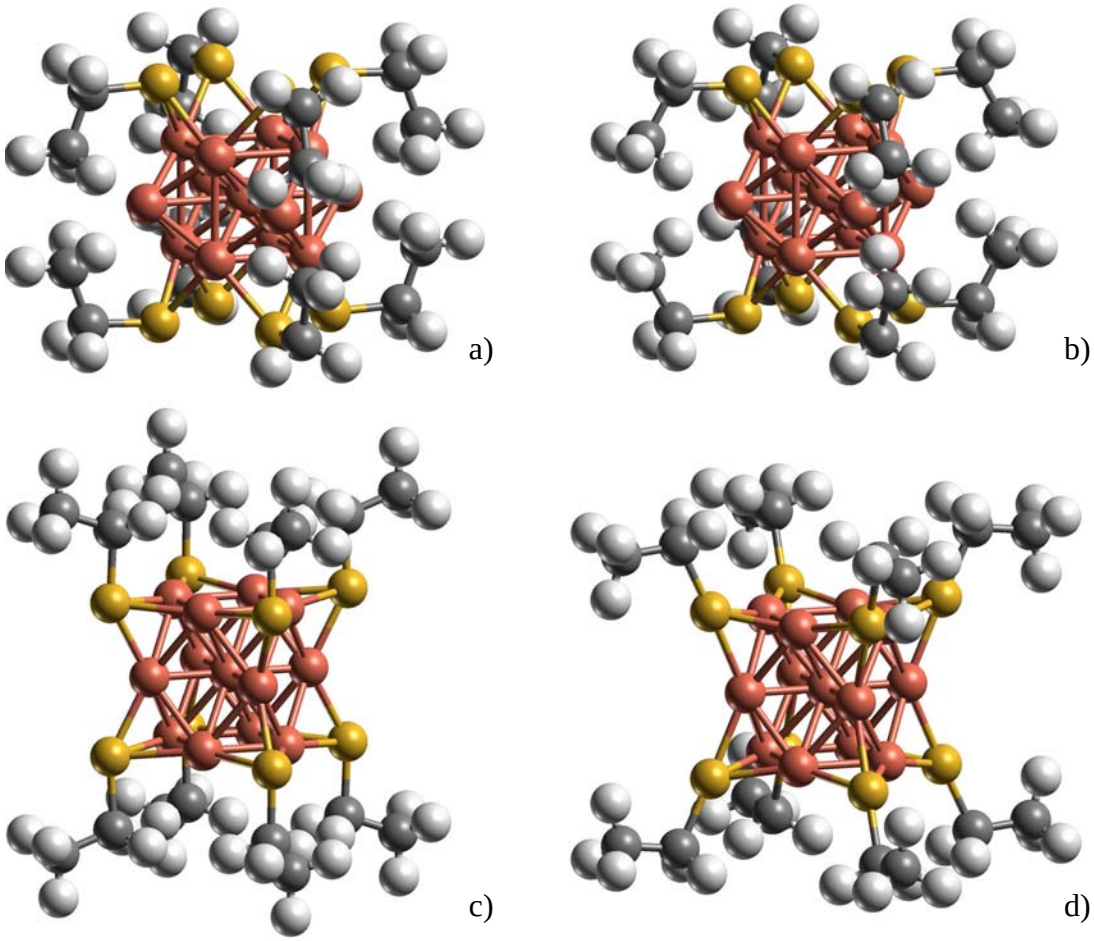

Figure 22 Structures of four bridge hollow coordinated conformers:
a) **bdos** b) **bdoe** c) **buos** d) **buoe**

The rotamer pair **bdos**-**bdoe** (a and b in Figure 22) are nearly indistinguishable at first glance. The ligands wrap the flat ellipsoidal cluster core. The bridging binding site is due to inter-ligand repulsion between the end group hydrogen atoms H_3-H_3'. In addition, the interaction between ligand end group and cluster core (H_3 – Cu_{eq}) might affect the

adsorption site. The conformers **buos** and **buoe** (Figure 22 c and d) behave rather differently. Their ligands leave the cluster core exposed. This comparison indicates, that the angles Cu_{ax}–S–C_1 and S–C_1–C_2 depend both on the fact whether ligand are in staggered or eclipsed form. The cluster core exhibits a more round form, instead of the common flat form and the ligands are located at almost ideal threefold-hollow positions.

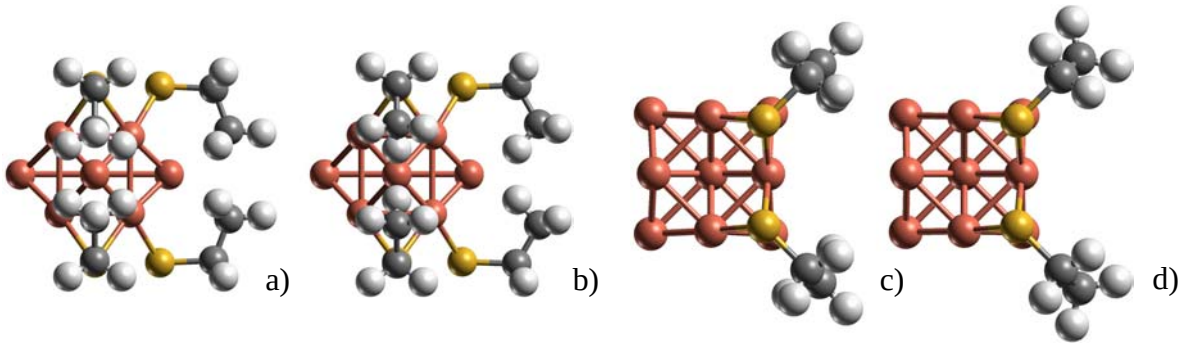

Figure 23 Side view of the conformers **bdos** (a) and **bdoe** (b) conformers; on top views of **bdos** (c) and **bdoe** (d); only four ligands are shown for ease of viewing

The side view of the conformers **bdos** and **bdoe** (Figure 23) reveals the peculiarities of the conformations. The hydrogen atoms of the methyl end groups are located in immediate vicinity of each other. In the conformer **bdoe**, the atoms H_3 exhibit a remarkably short distance to the atoms Cu_{eq}; as a result, the ligand wrap around the cluster core. Such a behavior was proposed by Luedtke and Landman for gold clusters passivated by alkyl thiolates as a result of MD simulations.[16] Later studies proposed similar behavior of hexadecylamine ligands on ruthenium particles as a function of the amine concentration.[222] The interaction between ligands in one z plane is comparably negligible (Figure 23 c), d).

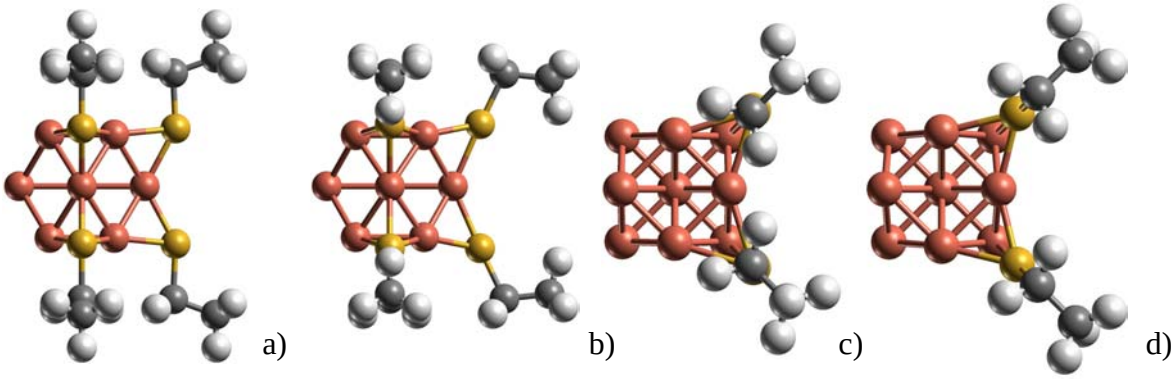

Figure 24 Side view of conformers **buos** (a) and **buoe** (b) conformers; on top views of **buos** (c) and **buoe** (d); only four ligands are shown for ease of viewing

The geometry directing importance of the various types of interaction is essentially reversed in the conformers **buos** and **buoe** as evidenced in Figure 24 (a)-(d). No short Cu_{eq}-H or H–H distances between methyl end groups are visible. Instead, short distances between H_1 atoms of ligands within the z plane deform the ligand chain orientation at the staggered–eclipsed conformer transition. Note the outward displacement of the alkyl chain by comparing Figure 24 (a) to (b) and (c) to (d). The negligible repulsion of the ligands admits an adsorption site that represents nearly perfect threefold-hollow coordination.

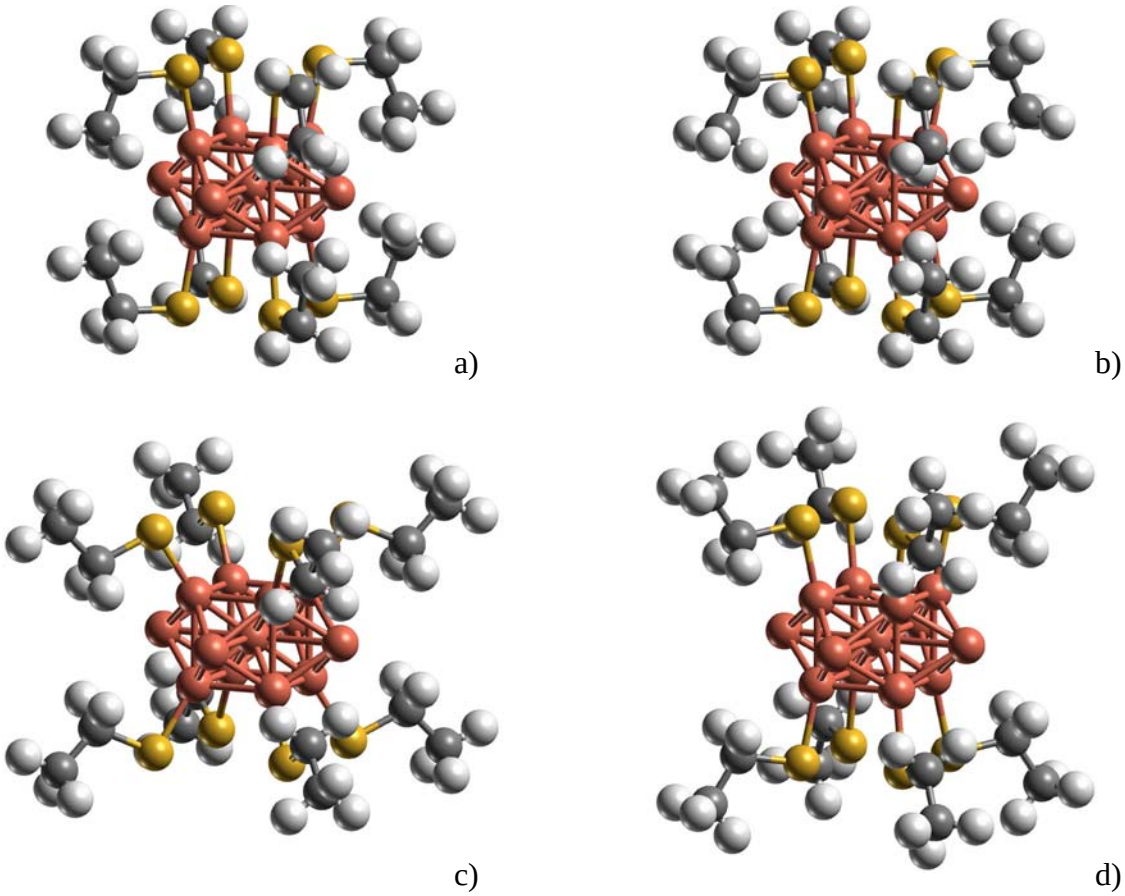

Figure 25 Examples of on-top coordinated structures of $Cu_{13}(SCH_2CH_3)_8$:
a) **tdos** b) **tdoe** c) **tdis** d) **tdie**

Figure 25 shows some close relations of the bridge-hollow and on-top conformers. The upper two conformations, **tdos** and **tdoe**, are virtually identical. The ligands, whose head groups are displaced to high z coordinates, wrap around the cluster core. Due to the binding site, the interaction between ligand end groups and cluster core is greatly reduced, although the atoms H_2 and H_3 still exhibit short distances to the atoms Cu_{eq}. The rotation of the CH_3 end group causes almost no change in the ligand backbone

geometry. All four conformers depicted in Figure 25 exhibit a flat ellipsoidal shape of the cluster core.

The ligand chains of the conformers **tdis** and **tdie** behave differently than the conformers **tdos**-**tdoe**. The distance of hydrogen atoms to the cluster core and to hydrogen atoms in other ligands is large enough to the possibility of a repulsive interaction. The change of the methyl end group conformation from staggered to eclipsed alone causes the considerable change in the ligand orientation with respect to the cluster. The sulfur atoms are shifted outward in the conformer **tdis** relative to **tdie**. However, the staggered-eclipsed isomerism does not effect the ligand backbone configuration in a noticeable way. A straightforward explanation is, that in these on-top cluster conformations the total energy is quite insensitive to the ligand orientation.

6.1.3. Relative Total Energies

The conformer **bdos** turned out to be the most stable of the 16 conformers under consideration. Its total energy shall be taken as a reference for the following comparisons. For the relative total energy data collected in Table 10, three trends are noticeable. First, clusters with on-top situated ligands tend to be less stable on average than bridge-hollow coordinated clusters. The conformers **buie**, **buos** and **bdoe** are exceptions. They are less stable by a few kcal/mol than the most stable on-top conformers **tuis** and **tuos**. Secondly, with only one exception, bridge-hollow conformers are more stable than their on-top counterparts of corresponding ligand orientation; once again the conformer **buos** forms the exception. Finally, staggered conformers are more stable than their eclipsed counterparts. Again, the pair **buos**-**buoe** with a reversed order forms an exception. Inspection of the **buos** geometry revealed a very short H_2-H_2' distance between methyl end groups of different ligands. The role of inter-atomic distances on the relative stability of conformations will be discussed later on, in Section 6.2. In most cases, the energy difference per ligand between staggered and eclipsed conformers is in the expected range, from ~3.5-4.0 kcal/mol.[223] Here, the conformation pairs **bdos**-**bdoe** and **tdos**-**tdoe** constitute exceptions. Both exhibit total energy differences in excess of 50 kcal/mol. Obviously, other influences than the staggered-eclipsed isomerism affect their energy differences considerably. For the pair **bdos**-**bdoe**, the high energy difference is especially baffling as the conformer **bdos** is the most stable one and the conformations under discussion are visually similar (Figure 22 a and b).

Table 10 Relative total energies[a] of conformers of $Cu_{13}(SCH_2CH_3)_8$ as well as energy differences between staggered and eclipsed conformers; all energies in kcal/mol; arbitrary ordering of the various conformers

conformation	relative total energy [kcal/mol]	difference staggered-eclipsed [kcal/mol]
buis	9.0	-30.8
buie	39.8	
buos	47.7	29.7
buoe	18.0	
bdis	1.4	-28.2
bdie	29.6	
bdos	0.0	-59.4
bdoe	59.4	
tuis	30.6	-28.6
tuie	59.2	
tuos	30.6	-26.3
tuoe	56.9	
tdis	82.7	-22.8
tdie	105.4	
tdos	63.2	-52.9
tdoe	116.1	

[a] Reference energy is -25062.580361036 au for the bdos conformer

The total energy varies by 116 kcal/mol; hence, all 16 conformers of the cluster under discussion are physically and chemically feasible. Therefore, in a given probe of copper clusters with ethyl thiolate ligands various conformations have to be expected. All bridge-hollow conformers are found within an energy range of ~60 kcal/mol or 7.4 kcal/(mol·ligand). Therefore, rotational isomerism represents the main influence on the energy differences, although other interaction mechanisms may also contribute.

6.1.4. Ligand Binding Energies

Isolated staggered and eclipsed ligand fragments were optimized for the computation of binding energies (Table 11); these reference energies have been collected in Appendix C. The resulting ligand binding energies range between -77 kcal/mol for **buoe** to -66 kcal/mol for **tdoe**. This relatively narrow energy range of just ~12 kcal/mol suggests a good binding situation for both binding sites and the 8 different conformations. Bridge-hollow coordinated structures tend to be stronger bound than on-top coordinated ones. Nevertheless, the conformers **tuis**, **tuie**, **tuos** and **tuoe** exhibit a larger binding energy than the conformer **buos**; recall that the conformer buos was already established as an exception in the total energy analysis (see Section 6.1.3).

Bridge-hollow conformers are always stronger bound than their on-top counterparts, by 2-4 kcal/mol in the case of "up" oriented conformers or even 7-10 kcal/mol in the case of "down" orientation. As the reference energies for the computation of ligand binding energies were computed separately for staggered and eclipsed conformers, the ligand binding energies of bridge-hollow and on-top coordinated are very similar. In most cases, the eclipsed conformers are actually slightly stronger bound than their staggered counterparts. Because differences between rotamers are usually below 1 kcal/mol, this discrepancy likely does not reflect a difference in the bonding mechanism, but rather reflects ligand-ligand and ligand-cluster interactions.

A comparison with $Cu_{13}(SH)_8$ in terms of binding energy shows that sulfanyl and ethyl thiolate bind to the copper cluster with comparable binding energies. The fairly low binding energy of the on-top (out) conformer of $Cu_{13}(SH)_8$ (Chapter 5.2.2) could not be reproduced. This finding emphasizes, that results of smaller model species may not always be transferable; it underlines the importance of computing as much of the conformer spectrum of a given compound as possible when a conformation dependent minimum search is conducted, even if previous findings may differ. Even to such a small copper cluster with 13 atoms, ethyl thiolate is binds in bridge-hollow and on-top coordination with sufficiently large binding energies; bridge-hollow coordinated species are usually preferred in terms of total energy as well as ligand binding energy.

Table 11 binding energies per ligand (in kcal/mol) of the 16 conformers of $Cu_{13}(SCH_2CH_3)_8$

conformation	binding energy per ligand [kcal/mol]	difference staggered-eclipsed [kcal/mol]
buis	-74.5	0.0
buie	-74.5	
buos	-69.7	-7.5
buoe	-77.2	
bdis	-75.5	-0.3
bdie	-75.8	
bdos	-75.7	3.6
bdoe	-72.1	
tuis	-71.8	-0.3
tuie	-72.1	
tuos	-71.8	-0.5
tuoe	-72.4	
tdis	-65.3	-1.0
tdie	-66.3	
tdos	-67.8	2.8
tdoe	-65.0	

6.1.5. Geometric Properties of $Cu_{13}(SCH_2CH_3)_8$: Cluster Core

A very important question is certainly whether the presence ethyl thiolate ligands affects the shape of the cluster in a notable fashion. Criteria to judge the shape under D_{4h} symmetry are the distances Cu_{ce}-Cu_{eq} and Cu_{ce}-Cu_{ax}. The bond distances Cu_{ce}-Cu_{eq} of both the bridge-hollow and on-top conformers are very similar as the corresponding reference values of $Cu_{13}(SH)_8$, although it is only in extreme cases (**buis**-**buie**) similar to the bare cluster. In the bridge-hollow coordinated conformers, the Cu_{ce}-Cu_{eq} bond

length varies between 2.747 Å for the **buis** conformer and 2.088 Å for the **buos** conformer with an average of 2.422 Å. When the obvious exceptions **buos** and **buoe** are excluded (see Figure 22 c and d), then the average of the Cu_{ce}-Cu_{eq} bond distance is 2.531 Å around values of 2.424 Å to 2.747 Å. Still, the variation of this bond length is high, considering it is caused by the change of conformation of the ligands alone. As the **buos**-**buoe** conformer pair is arguably the one with the weakest interaction between ligands and cluster core, one has to conclude that the elusive round shape of the cluster core is stabilized by ligands that interact only with their head groups, while tail groups of ligands interacting with the cluster core occur simultaneously the usual flat shape.

The consistency of the Cu_{ce}-Cu_{eq} bonds of the on-top conformers is remarkable, exhibiting bond lengths of ~2.66 Å throughout with very little variation, by only 4 pm. It was concluded that this consistency in bond lengths is achieved by the fact that the ligands are bound to the axial atoms alone. The ligand tail group interaction with the cluster core should lead to at least one of the bonds considerably deformed by transferred steric stress in the case of strong ligand cluster interaction (see Figure 25).

The relatively large variation between the two conformers **tdis** and **tdie** is interesting; it amounts to 4 pm in contrast to the rather low between other conformer pairs (e.g. 2 pm for **tuis**-**tuie**). Whether the deformation of the cluster core by the presence of alkyl thiolate ligands is reproducible has to be confirmed by further comparisons of other cluster core bond lengths.

A quite similar picture as obtained for the Cu_{ce}-Cu_{eq} bond is found for the Cu_{ce}-Cu_{ax} bond lengths. Average values fall into the range from 2.05 Å to 2.14 Å for the bridge-hollow conformers and from 2.01 Å to 2.05 Å for the on-top conformers. Obviously, the conformers **buos** and **buoe** constitute an exception; they will thus be referenced as the irregular pair in the following discussion. In the regular bridge-hollow conformers, the contraction of the Cu_{ce}-Cu_{eq} bond is accompanied by an expansion of the Cu_{ce}-Cu_{ax} bond. The changes in the bond lengths can be viewed as a reconstruction of the cluster surface, caused by the ligands. This conclusion is further supported by the two irregular cases, where the surface reconstruction leads to a totally new conformer of the cluster core. In the on-top conformers, the Cu_{ce}-Cu_{ax} bond remains virtually unchanged as compared to the $Cu_{13}(SH)_8$ geometry, mirroring the findings for the Cu_{ce}-Cu_{eq} bond lengths.

Table 12 Characteristic Cu-Cu bond lengths of the 16 conformers of $Cu_{13}(SCH_2CH_3)_8$ as well as reference values of previous calculations: Cu_{13} (D_{4h}), $Cu_{13}(SH)_8$ in bridge-hollow (up) and on-top (up) conformations, all values in Å

conformation	Cu_{ce} - Cu_{eq}	Cu_{ce} - Cu_{ax}	Cu_{ax} - Cu_{eq}	$Cu_{ax}1$ – $Cu_{ax}2$
buis	2.747	2.049	2.305	2.340
buie	2.650	2.068	2.251	2.352
buos	2.088	2.300	2.272	2.149
buoe	2.098	2.339	2.261	2.270
bdis	2.424	2.140	2.156	2.394
bdie	2.443	2.133	2.164	2.387
bdos	2.498	2.113	2.185	2.375
bdoe	2.426	2.134	2.159	2.382
tuis	2.686	2.014	2.263	2.289
tuie	2.667	2.020	2.253	2.295
tuos	2.686	2.014	2.263	2.289
tuoe	2.689	2.013	2.264	2.290
tdis	2.608	2.031	2.217	2.305
tdie	2.686	2.022	2.240	2.340
tdos	2.639	2.046	2.235	2.331
tdoe	2.650	2.031	2.230	2.330
Cu_{13} D_{4h}	2.741	2.015	2.281	2.323
$Cu_{13}(SH)_8$ bridge-hollow	2.574	2.092	2.201	2.371
$Cu_{13}(SH)_8$ on-top	2.679	2.014	2.263	2.336

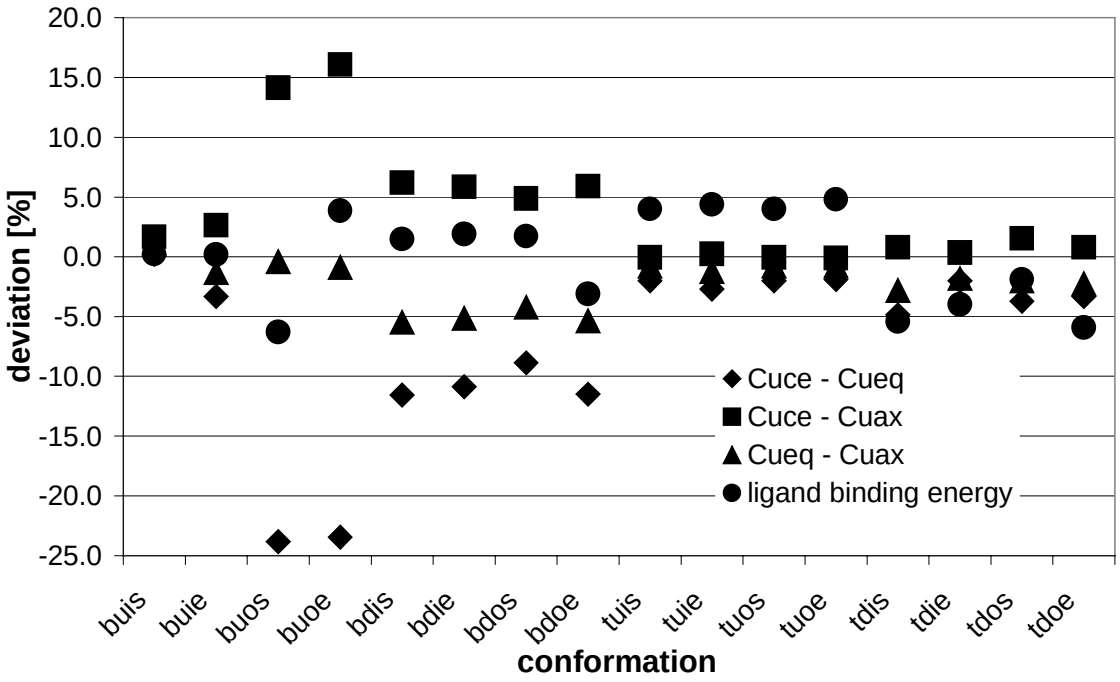

Figure 26 Fractional difference of binding energies and defining bond lengths (in percent) from their reference values to illustrate correlation. Reference values are:

a) average binding energies of bridge-hollow and on-top conformers, respectively, and b) the corresponding bond lengths of Cu_{13} in D_{4h} symmetry (Chapter 5.1.2)

The distances Cu_{ax}-Cu_{eq} also represent bonds because their values consistently lie in the range of 2.156 Å to 2.305 Å. Figure 26 shows no strict correlation of the binding energies with the bond lengths. While the **bdoe** conformer exhibits a low binding energy, the changes in its bond lengths are of the same nature as in the other bridge-hollow (down) conformers. The irregular bridge-hollow conformers further emphasize the uncorrelated behavior. Although their binding energies differ, the change in the bond lengths is of the same magnitude and direction. The on-top conformers show a correlation between binding energy and the change in bond lengths. All on-top (up) conformers exhibit larger than average binding energies, and slightly shorter Cu_{ce}-Cu_{eq} bond lengths as compared to Cu_{13}. The Cu_{ce}-Cu_{ax} bond is the least affected in the on-top (down) cases, where the strongest influence was to be expected, as the ligands bind to these atoms only. The on-top (down) cases exhibit smaller than average binding energies. The Cu_{ce}-Cu_{eq} and the Cu_{eq}-Cu_{ax} bond decrease in favor of the Cu_{ce}-Cu_{ax} bond which increases (by up to 2 percent). The increased exposure of the cluster core to the ligand chain (see Figure 25 a and b) does not lead to increased binding.

The Cu_{ax}- Cu_{eq} bond and the two outer shell inter-atomic distances $Cu_{ax}1$-$Cu_{ax}1$' and $Cu_{ax}1$-$Cu_{ax}2$ can be considered equally indicative of the binding situation of the cluster as the inter-shell bond lengths Cu_{ce}-Cu_{eq} and Cu_{ce}-Cu_{ax}. In the case of on-top coordination, this is understandable because the Cu_{eq} atoms do not participate in cluster-ligand bonds. The cluster core was shown to be susceptible to changes in the ligand bonding, adjusting its shape accordingly. However, both inter shell and intra-shell bond lengths for the second shell stay in the same range of a possible Cu-Cu bond in clusters (~2.10 Å-2.75 Å for various bonds).[204-206]

Analysis of the Cu-Cu bonds confirmed that in every case a valid cluster compound resulted. In no case, inter-atomic distances differed so drastically from the reference conformer as to assume a broken Cu-Cu bond. Rather, the computational method as well as the model proved stable enough to allow even a change of the cluster shape without a breakdown of the system, as evidenced by the conformers **buos** and **buoe**. It can be concluded already at this point that copper clusters of 13 atoms form stable compounds when covered by alkyl thiolate ligands.

6.1.6. Geometric Properties of $Cu_{13}(SCH_2CH_3)_8$: Ligand-Cluster Interface

The ligand-cluster interface consist of one bond in the on-top coordinated structures and two to three bonds in the case of bridge-hollow coordinated ligands. (Chapter 2.3) In the latter case, two of the Cu_{ax}-S bonds are equal in length because a D_{4h} symmetry restriction was imposed. In the bridge-hollow conformers the nature of the binding site is determined by the lengths of the Cu_{eq}-S and the Cu_{ax}-S bonds. Conformations with a Cu_{eq}-S bond shorter or equal to the Cu_{ax}-S bond, namely the bridge-hollow (up) cases, constitute nearly perfect threefold-hollow coordinations. In the bridge-hollow (down) cases, Cu_{eq}-S distances are so long that a considerable binding contribution of this interaction is unlikely. They can thus be addressed as bridge coordinated. The calculated Cu_{ax}-S bonds varied between 2.21 Å and 2.32 Å, while the Cu_{eq}-S bonds varied between 2.07 Å and 2.97 Å.

Cu-S bonds vary within the staggered-eclipsed pairs of the bridge-hollow coordinated clusters. In the pair **buis-buie** it is very weak, as only its Cu_{ax}-S bond dilates by 0.4 pm when changing from the staggered to the eclipsed conformer. In the **buos-buoe** pair, however, it is quite noticeable as the Cu_{ax}-S bond contracts by 10 pm while the Cu_{eq}-S bond dilates by 7 pm. The simple change from staggered to eclipsed conformation of the ligand thus causes a noticeable change in the ligand binding site- a clear sign of strong differences in the ligand-ligand interactions.

Table 13 Cu – S bond lengths detailing the binding situation of the ligands to the cluster

conformation	Cu_{eq} - S [Å]	Cu_{ax} - S [Å]
buis	2.073	2.206
buie	2.073	2.210
buos	2.184	2.317
buoe	2.258	2.213
bdis	2.582	2.247
bdie	2.604	2.248
bdos	2.975	2.286
bdoe	2.935	2.247
tuis	3.049	2.105
tuie	3.028	2.123
tuos	3.049	2.105
tuoe	3.050	2.105
tdis	3.635	2.111
tdie	3.781	2.147
tdos	3.834	2.170
tdoe	3.812	2.167
$Cu_{13}(SH)_8$ b.-h. (up)	2.258	2.281
$Cu_{13}(SH)_8$ on-top (up)	3.337	2.021

Similar Cu-S bond lengths as in this work have been found in DF calculations by Akinaga et al. who studied methyl thiolate adsorption on a copper (111) model surface employing the BLYP functional.[221] They found a Cu-S distance of 2.32 Å for the bridging adsorption site and a distance of 2.24 Å for the on-top site.[221] It is not surprising that these bonds lengths are consistently 0.1 Å longer than the ones obtained in the present study. Akinaga et al. fixed the methyl thiolate molecules to the perfect on-top and bridging adsorption sites, allowing only a movement perpendicular to the

surface; this restriction leads naturally to longer bonds. The known tendency of GGA functionals to overestimate bind lengths might contribute as well.[96]

In the on-top adsorption cases, only the Cu_{ax}-S distance is of immediate interest. Inter-atomic distances Cu_{eq}-S are consistently longer than 3 Å, ruling out directly bonding interactions. The Cu_{ax}-S distances measure 2.105 Å in the cases of **tuis**, **tuos** and **tuoe** and are only up to 7 pm longer in the **tdos** case. The two cases with the longest Cu_{ax}-S bond are those with the lowest binding energy. Other than that, no correlation was found between binding energies and Cu-S bond distances. The relatively large variation within the **tdis**-**tdie** pair was already noticed in the discussion of the cluster structures in Chapter 6.1.2. Rotation of the methyl end group to eclipsed conformation introduced widespread changes in the ligand backbone structure (Figure 25 c and d).

The angles Cu_{ax}–S–C_1 and Cu_{eq}–S–C_1 make up the cluster interface of the bridge-hollow conformations; only the angle $Cu_{ax} - S - C_1$ is pertinent in the case of the on-top ligands. Due to the differences in the appearance of the structures, a listed comparison as in the case of the bond lengths was not deemed meaningful; values are tabulated in Appendix C. Angles follow the ligand orientation. When the ligands are located in bridging adsorption sites (**bdis**, **bdie**, **bdos**, **bdoe**), the $Cu_{ax} - S - C_1$ angle assumes values around 105-110º while the $Cu_{eq} - S - C_1$ angle remains low at 60-80º. In the case of the threefold-hollow (buos-buoe) and bridge-hollow (**buis**-**buie**) coordinated ligands, both angles are more similar, with values around 120º.

6.1.7. Geometric Properties of $Cu_{13}(SCH_2CH_3)_8$: Ligand Geometry

The ligand chains seem to be almost unperturbed by the binding situation, exhibiting little or no variation between the conformations. This is especially true of the bonds farther away from the head group. With the introduction of additional CH_2-groups, the variation of the bond lengths are expected to vanish completely. The S-C_1 bond varies the most with differences between conformers of up to 5 pm. Most of the conformers, however, fall within a range of 1.83 ± 0.02 Å. Only the **buoe** conformer exhibits a deviating S-C_1 bond length of 1.87 Å.

Table 14 Ligand specific bond lengths in $Cu_{13}(SCH_2CH_3)_8$, values in Å

conformation	S - C_1	C_1 – C_2	C_1 - H_1	C_2 - H_2	C_2 - H_3
buis	1.821	1.503	1.103	1.104	1.105
buie	1.828	1.512	1.101	1.103	1.105
buos	1.851	1.505	1.105	1.104	1.105
buoe	1.873	1.512	1.100	1.103	1.106
bdis	1.848	1.508	1.115	1.104	1.105
bdie	1.847	1.523	1.114	1.103	1.104
bdos	1.811	1.496	1.105	1.120	1.107
bdoe	1.831	1.504	1.104	1.103	1.116
tuis	1.825	1.509	1.104	1.104	1.105
tuie	1.820	1.518	1.104	1.102	1.116
tuos	1.825	1.509	1.104	1.104	1.105
tuoe	1.825	1.524	1.103	1.103	1.105
tdis	1.825	1.502	1.104	1.105	1.105
tdie	1.823	1.519	1.109	1.102	1.104
tdos	1.815	1.507	1.105	1.112	1.107
tdoe	1.820	1.520	1.104	1.104	1.118

The S-C bonds of the present investigation are 1-7 pm shorter than those in the work of Akinaga et al.. Kerdcharoen et al. found S-C bond lengths of at least 1.85 Å when studying different alkyl thiolate chain lengths on Cu atoms and smaller clusters.[183] It can be concluded that the current work includes some stronger binding influence in the calculation of the bond lengths stemming from the larger cluster model, as in the work of Kerdcharoen et al. the S-C bond length deceased with increasing cluster size and the calculations of Akinaga et al. were conducted using a 18 atom cluster model of the surface. The three symmetry-inequivalent carbon-hydrogen bonds show small variations of at most 0.5 pm.

A detailed comparison of the bond angles between certain atom groups was not considered meaningful at this point. However in Chapter 6.2 they will be compared with

their counterparts from QM/MM calculations; see the fundamental data in Appendix C. For most cases, the angle $S - C_1 - C_2$ remains in the range 108-114º. Only in the case of **bdoe** a larger value of 118º is obtained. From Figure 23 b and d it can be seen, that this is the conformer with easily the strongest $H_3 - Cu_{eq}$ interaction. Obviously, this interaction exerts enough strain on the ligand to deform the ligand backbone structure. Thus far, not many similarities between bridge-hollow and on-top conformers could be found. It is interesting, though, that the **tdoe** conformer exhibits a large $S–C_1–C_2$ angle of the on-top conformations as well; even though the ligand-cluster core interaction is considered to be generally smaller in on-top conformers (see results of ligand binding energy), it is enough to deform the backbone angle to the second largest value in all on-top conformers at 114º. The largest $S–C_1–C_2$ angle can be found in the **tuie** conformer with 115º. The rest of the ligand angles remains very near their equilibrium values as computed in a separate MM calculation. The deviations in the order of 1-2º were considered too small to draw meaningful conclusions. Interested readers will find the angles tabulated in Appendix C.

In the discussion of energetic as well as geometric properties of the $Cu_{13}(SCH_2CH_3)_8$ cluster as calculated with a density functional approach, not much attention was paid to the causes of the noted special cases. The discussion of the reasons will turn out to much simpler when the QM/MM results for the same system will be available in the next section.

6.2. QM/MM Calculations of $Cu_{13}(SCH_2CH_3)_8$

The calculations of $Cu_{13}(SCH_2CH_3)_8$ in various conformations with the QM/MM technique are primarily thought as a detailed and sensitive test of the method. If the results of these computations are similar to the pure QM calculations, the QM/MM method can be considered a valid method for the computational treatment of coinage metal clusters with alkyl thiolate ligands. Once method and implementation has been proven valid for this class of metal organic compounds, they will surely be also applicable to other cluster compounds. Thus, a number of questions had to be answered by this set of calculations. Is the method able to reproduce the energetic and geometric properties of these complicated systems with satisfactory accuracy? Does it result in a adequate reduction of computation time? Is it a valid assumption that the QM part is described exclusively by the QM method? What differences between QM and QM/MM results are reasonable, or even desired? To be able to answer these questions, the results of the QM/MM calculations will be discussed in conjunction with their QM counterparts as well as models and concepts explaining them. Although the basic data like relative total energies, ligand binding energies and the geometric data will be presented in the order established by the previous section, the discussion will focus on causes of differences and similarities between QM and QM//MM calculations.

6.2.1. Computational Setup of the Calculations

The computational model of the cluster was reused in this set of calculations. Symmetry and degrees of freedom were retained. Starting geometries of the optimizations were identical to the starting geometries in the QM optimizations. Thus it was guaranteed to find the same local minima as in the QM optimizations only if they are accessible by both methods. This implies, that some parts of the energy hypersurface were examined indirectly as well. Only if the energy hypersurfaces of both methods run sufficiently parallel, it is guaranteed to find the same local minima in both methods when starting from the same geometry. Being able to reproduce geometric results of one method by a simplified method is a prerequisite for a reliable examination of local geometric minima with that method. Computational parameters for QM and MM computations were used as detailed in Chapter 4. The geometries were computed using the VWN functional, while the total energies were determined with the BP88 functional in single point calculations in the fashion explained in Chapter 4.

6. Comparing QM and QM/MM Calculations of $Cu_{13}(SCH_2CH_3)_8$

For the MM calculations, the MM3 force field as implemented in the TINKER program was used. This force field was specifically designed for an accurate description of organic molecules. Thus, the van der Waals interaction parameters for copper were missing in the standard implementation. Kerdcharoen et al. proposed and tested additional parameters suitable for copper thiolate species.[183]

The bonds between C_1 and C_2 were chosen as boundary between QM and MM parts. Thus, the QM model was reduced to $Cu_{13}(SCH_3)_8$. The capping H atoms for bond saturation were treated in the constant bond lengths ratio approach as described in Chapter 3.4.2 was used. The bond length ratio *g* was set to 0.709 as proposed by Morokuma.[174] The computation time decreased to about 2 to 2.2 hours per geometry update, as compared to 2.5–3 hours per geometry update in the QM calculations. With about 30 geometry update steps per optimization, this translated to 60 to 70 hours for a full optimization. On average, the QM/MM calculations required 10 optimization steps more than the respective QM calculations. The reason for this is not apparent from the outset.

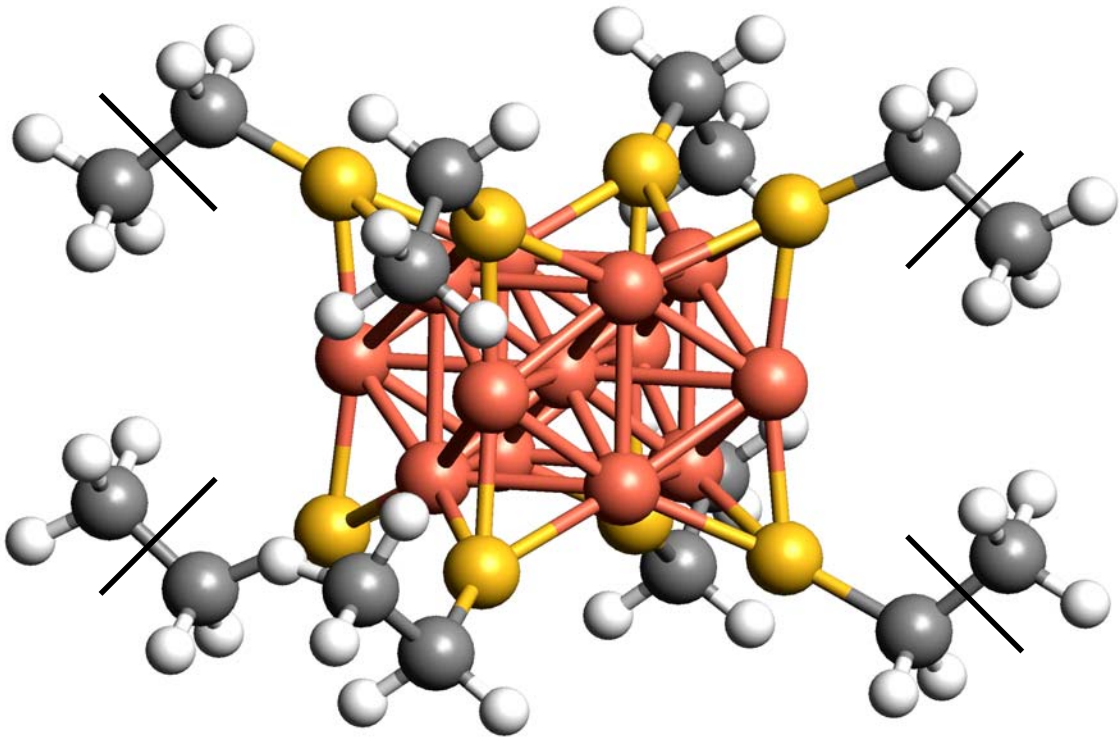

Figure 27 $Cu_{13}(SCH_2CH_3)_8$ in the bdos conformation; QM/MM boundary indicated by lines on 4 of the 8 ligands, the methyl end groups form the MM region, the $Cu_{13}(SCH_3)_8$ in the middle is the QM part; link atoms not drawn

6.2.2. Overview of the Differences between QM and QM/MM Results

The points of the potentially highest geometric differences between QM and QM/MM calculations are the cluster core and the cluster-ligand interface. The cluster core shows bond length changes of lower than 1 pm in all conformers except **bdos**, **bdoe**, **tuie** and **tdis**. The difference in QM and QM/MM description of the cluster ligand interface differs more. But even there, bond length changes of 1 pm and less can be observed for the **bdis**, **tuos** and **tdie** conformers. The **buis**, **buie**, **buoe**, **bdie**, **tuis** and **tuoe** conformers showed bond length differences between QM and QM/MM larger than 1 pm only in the $Cu_{eq} - S$ bond. The QM results are thus reproduced with good agreement for most conformers. The causes for the differences observed will be discussed using the following figures. The corresponding subsection 6.1.2 focused on the peculiarities of the QM optimized results. Some of the most obvious differences of QM and QM/MM optimized structures shall be discussed in the following.

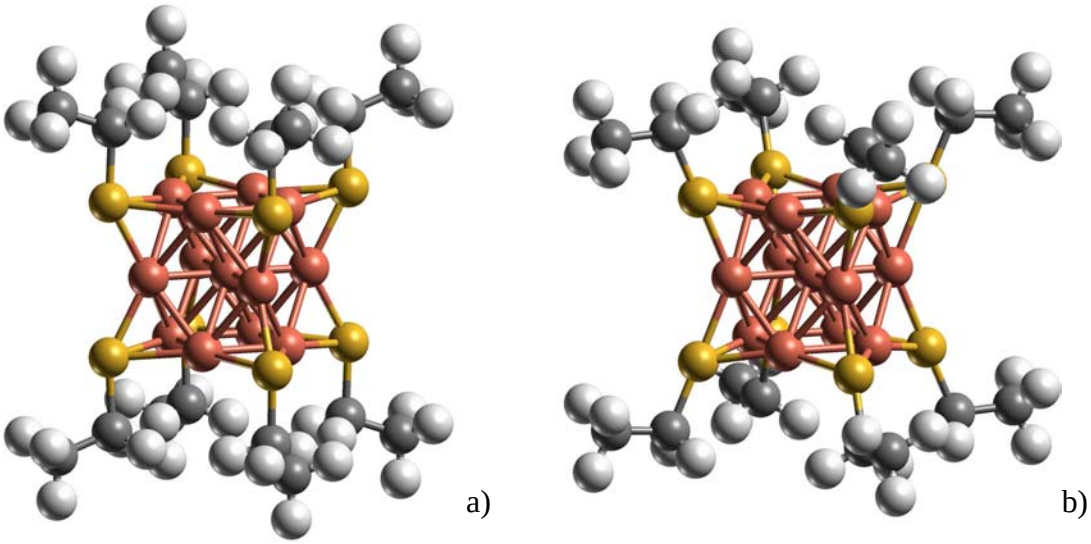

Figure 28 QM (a) and QM/MM (b) optimized geometries of the conformer **buos** of $Cu_{13}(SCH_2CH_3)_8$

Some differences can be spotted best when similarities are highlighted. The structures of **buos** optimized in QM and QM/MM are virtually identical except in one geometric feature, the cluster-ligand interface. Differences in cluster core bond lengths and ligand only bond lengths are less than 1 pm. Only the $Cu - S$ bonds differ by up to 4 pm. Likewise, bond angle differences are below 3° except in the $Cu_{ax} - S - C_1$ angle, where the difference is 27°. What causes this substantial difference between QM and QM/MM description?

The answer can be found with the help of Figure 29. Only the $H_1 - H_1'$ inter-atomic distance between adjacent ligands in one z plane is short enough to contribute significantly to the inter-ligand repulsion. From Figure 29 c and d it is obvious, that no other influences than the inter-ligand repulsion contribute to the structural differences. The symmetry restriction to D_{4h} allows only outward movement of the ligand chain to increase the distance H_1–H_1' from 2.23 Å in the QM geometry to 3.5 Å in the QM/MM geometry. Thus, the inter-ligand repulsion must be more pronounced in the QM/MM description. This difference in the **buos** conformer came as a surprise, as its cause resides completely in the QM part of the model ($H_1 - H_1'$ distance between ligand in a z plane). It was assumed before, that the MM contribution is completely cancelled for these atoms. The above example proves otherwise.

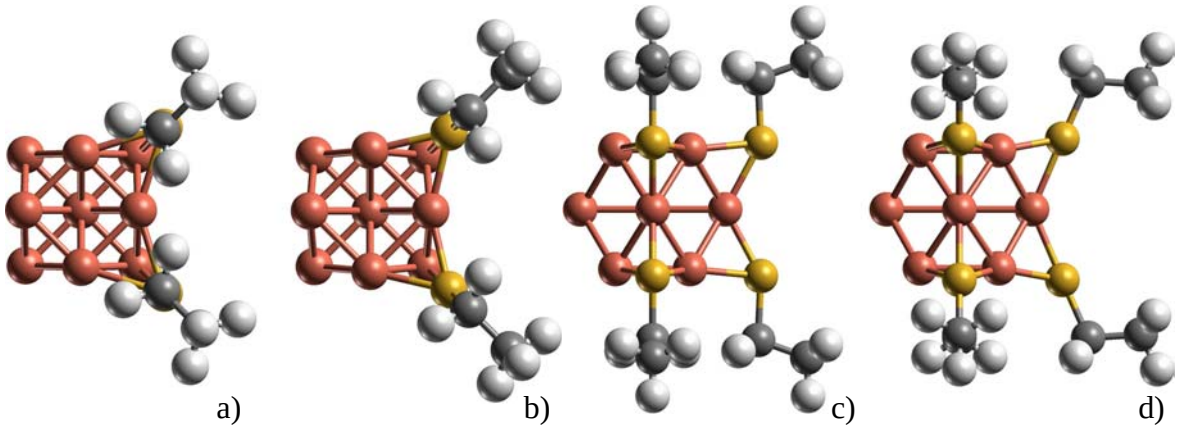

Figure 29 On-top views of the QM (a) and QM/MM (b) structures of the buos conformer; side views of QM (c) and QM/MM (d) structures; four ligands omitted to increase clarity

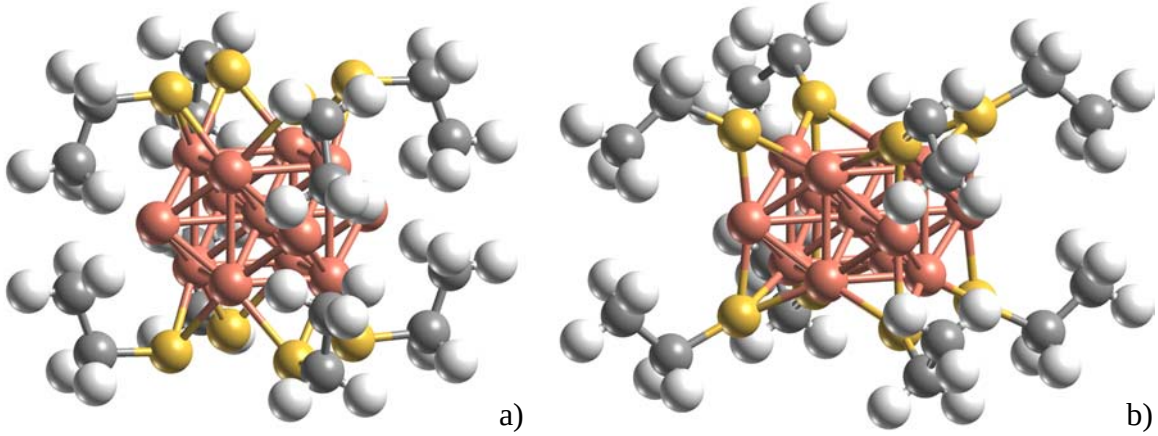

Figure 30 QM (a) and QM/MM (b) optimized structures of the **bdos** conformer of $Cu_{13}(SCH_2CH_3)_8$

Figure 30 shows the **bdos** conformation, where QM and QM/MM optimized structures differ seriously. The cluster core is visibly more flat in the QM/MM geometry. The ligand binding moved from an obvious bridge site in the QM structure to an almost threefold-hollow site in the QM/MM geometry. The $S - C_1 - C_2$ angle increased, spreading the ligand chains outwards. Thus, the short $Cu - H_2$ distances in the QM geometry of only 2.12 Å are corrected in the QM/MM geometry to a much more reasonable value of 3.39 Å. Despite this change, the basic feature of this conformation is retained. The ligand chains wrap around the cluster core. The $H_2 - H_2$" distance between hydrogen atoms of ligands above and below the x-y-plane also increased, from 1.92 Å in the QM to 2.57 Å in the QM/MM optimization of **bdos**. By this repulsion, the ligand chains are directed into a stretched conformation; this is mainly due to the D_{4h} symmetry restriction of the optimization.

The analysis confirms that the QM and QM/MM description differ mostly by their treatment of the non-bonded interaction.[96] The dispersion interaction of these non-bound atoms, also referred to as London forces, is a long-range attractive interaction decaying with the inverse sixth power of the interatomic distance. Dispersion describes induced dipole-dipole interactions, caused by electron-electron correlation effects between atoms with non-overlapping electron densities. Thus, it is completely non-local in nature and can not be described correctly by LDA functionals which contain only local contributions.[96] The occurrence of actual minima in LDA optimizations of non-bonded systems has been attributed to overlapping electron densities, which decay exponentially in r, and not to a physically correct description of true dispersion interactions dominated by the long-range fluctuating dipole term ($1/r^6$).[224] Test calculations showed the strong overbinding of the LDA functional with minima located at too short distances.[225] Thus, the QM calculations with the VWN exchange-correlation functional should result in underestimated Cu – H and H – H distances.

The QM/MM calculations treat these non-bonding interactions completely with the MM method. The functional form and its parameters have been calibrated to fit experimentally available data (see also Chapter 3.2 and ref. 125 and references therein). It is thus reasonable to assume that the treatment of the non-bonded interaction in the MM method is more reliable than in the QM method currently employed.

6.2.3. Total Energies

The total energy differences of the QM/MM calculations deviate from those calculated at the QM level in some aspects. In the QM as well as QM/MM calculations, energies of staggered and eclipsed conformers differ by ~30 kcal/mol or 3.75 kcal/(mol·ligand). But, the staggered-eclipsed conformer total energy difference is more uniform in QM/MM calculations. Only the rotamer difference of the **tdis**-**tdie** and **tdos**-**tdoe** pairs is 10 kcal/mol smaller or larger, respectively.

Table 15 Relative total energies[a] in the QM/MM approach and their pairwise staggered-eclipsed energy difference; difference to QM total energies of 16 conformers of $Cu_{13}(SCH_2CH_3)_8$

conformation	relative total energy [kcal/mol]	difference staggered-eclipsed [kcal/mol]	difference QM-QM/MM [kcal/mol]
buis	0.0	-27.5	9.0
buie	27.5		12.3
buos	8.3	-30.6	39.5
buoe	38.9		-20.8
bdis	3.2	-31.2	-1.8
bdie	34.4		-4.8
bdos	6.6	-33.3	-6.6
bdoe	39.9		19.5
tuis	42.0	-32.7	-11.4
tuie	74.7		-15.5
tuos	29.3	-30.4	1.3
tuoe	59.7		-2.8
tdis	85.6	-24.5	-2.9
tdie	110.1		-4.7
tdos	111.7	-40.6	-48.5
tdoe	152.3		-36.2

[a] relative to the total energy of the buis conformer of -24747.9441 au

The QM/MM calculations gave the **buis** conformer as the most stable (bdos in QM). The range of the QM/MM total energies is larger by ~40 kcal/mol, with largest value of 152 kcal/mol for the **tdoe** conformer. Also, the energy ordering of the conformers changed. As the staggered-eclipsed isomerism introduces additional ordering effects, the on-top and bridge hollow conformers shall be compared separately at first. Among the bridge-hollow coordinated conformers, the **bdos** conformer, which was the most stable one in the QM calculations switches its place with the **buis**, which was third. The **bdis** conformer retains its second most stable place. The anomaly of the **buos**-**buoe** pair, where the eclipsed conformer was more stable than the staggered one in the QM calculations, does not occur. This is due to the orientation and interaction of the ligands (see Figure 28). The other bridge-hollow eclipsed conformers follow in less ordered fashion. In the QM/MM calculations all bridge-hollow staggered conformations are more stable than their eclipsed counterparts. Additionally, any eclipsed conformer is less stable than all staggered ones.

The on-top structures show differences in their behavior as well. The **tuis** and **tuos** structures switch first and second place. However, this change is not significant because the QM energies of these conformers are almost degenerate, within few hundredths of a kcal/mol. However, in the QM/MM calculations **tuos** is more stable by 13 kcal/mol than **tuis**. The corresponding eclipsed rotamers follow in the same order as in the QM calculations, with an energy spacing of ~30 kcal/mol. All four on-top (down) conformers were computed less stable than the on-top (up), unlike in the QM calculations. But, as the conformer **tdie** in QM/MM has almost the same energy as the conformer **tdos**, (separated by only 1.6 kcal/mol,) the total energy sequence of the QM calculations is essentially retained.

Thus, from the total energies, three conformer pairs can be already identified as interesting cases: (i) the **buos**-**buoe** pair, in which the expected energy sequence staggered-eclipsed is reversed (see Figure 22,Figure 24,Figure 28,Figure 29); (ii) the conformers **bdos** and **buis** which switch their places as the most stable conformers (see Figure 30); and last, but not least (iii) the bdos-bdoe pair which exhibits the largest rotamer energy difference in the QM calculations with almost 60 kcal/mol, but a normal one of ~30 kcal/mol in the QM/MM calculations (see Figure 30). Although the on-top coordinated conformers have their own peculiarities, they are attributed less importance because they are less stable.

6.2.4. Ligand Binding Energies

The binding energies per ligand as calculated in the QM/MM approach stay within the same range as in the QM calculations (-77 to -70 kcal/mol for bridge-hollow coordination, -72 to -60 kcal/mol for on-top coordination). The difference between QM and the corresponding QM/MM calculation exhibits following trends; see Table 16. Staggered conformers show a by -5 to 0 kcal/mol slightly increased binding energy, in cases, where QM and QM/MM calculations differ mainly by the treatment of H-H interaction between ligands(**buis**, **buos**, **bdis**, **tdis**). When the cause of the difference is a short Cu-H distance in the QM geometry, a slight decrease in binding energy is calculated (**bdos**, **tdos**). Eclipsed geometries are weaker bound by 2-9 kcal/mol than in the QM calculations.

Table 16 Binding energies per ligand and differences to the corresponding QM values; in kcal/mol

conformation	binding energy per ligand [kcal/mol]	difference staggered-eclipsed [kcal/mol]	difference QM/MM – QM [kcal/mol]
buis	-75.9	-3.9	-1.4
buie	-72.0		2.5
buos	-74.9	-4.3	-5.2
buoe	-70.6		6.6
bdis	-75.5	-4.3	0.0
bdie	-71.2		4.6
bdos	-75.1	-4.6	0.6
bdoe	-70.5		1.6
tuis	-70.7	-4.5	1.2
tuie	-66.1		6.0
tuos	-72.3	-4.3	-0.4
tuoe	-68.0		4.4
tdis	-65.2	-3.5	0.1
tdie	-61.7		4.6
tdos	-62.0	-5.5	5.8
tdoe	-56.4		8.6

Whereas the staggered-eclipsed binding energy difference in the QM calculations follows no readily apparent rules, it is almost uniformly in the range of 4 kcal/mol in the QM/MM calculations. Two on-top coordinated species exhibit ligand binding energies larger than at least two bridge-hollow coordinated ones. Bridge-hollow conformations are more stable; every on-top conformation has a smaller binding energy than its bridge-hollow counterpart. An interesting finding appeared when the QM/MM ligand binding energies were reviewed together with the total energies of the conformers. Apart from the conformers **buoe** and **bdoe**, the order of total energies and ligand binding energies is the same. The QM calculations did not show such trend. As both **buoe** and **bdoe** were already noted as exceptions in the analysis of the total energies, they should be put under additional scrutiny in the following discussion.

6.2.5. Geometric Properties of $Cu_{13}(SCH_2CH_3)_8$: Cluster Core

The basic features of the cluster shape remained unchanged in the majority of the conformers (Table 18). Bond length differences between QM and QM/MM optimizations are below 1 pm in the conformers **buis**, **buos**, **buoe**, **bdis**, **tuis**, **tuos**, **tuoe** and **tdie**. Thus, the cluster core geometry remains unchanged when the QM description of the ligands does not considerably differ from the QM/MM description. Even in the case of the conformers **buos** and **buoe**, the more spheric shape of the cluster core is retained. There, the Cu_{ce} - Cu_{ax} bond is longer than the Cu_{ce} - Cu_{eq} bond, as opposed to the "normal case", where the Cu_{ce} - Cu_{ax} bond is shorter than the Cu_{ce} - Cu_{eq} bond. In the established fashion, the values of bridge-hollow and on-top coordinated conformers shall be discussed separately.

The Cu_{ce} - Cu_{eq} bonds of the bridge-hollow conformers vary between 2.09 Å for the **buos** and **buoe** conformers and 2.74 Å for **buis** with an average of 2.46 Å. Thus, longest and shortest Cu_{ce} – Cu_{eq} bond lengths are found in the same conformers as in the QM calculations. Again, excluding the exceptions **buos** and **buoe**, the average value is 2.58 Å, 5 pm longer than the corresponding QM value. This difference is due to the conformers **bdos** and **bdoe** which exhibit 0.1 Å and 0.2 Å longer Cu_{ce} – Cu_{eq} bonds than their QM counterparts. Their cluster core is considerably deformed with respect to the QM calculations. Leaving aside the two exceptional cases, the Cu_{ce} - Cu_{ax} bond lengths range between 2.01 Å and 2.15 Å with an average of 2.05 Å. The QM calculations exhibited a similar distribution, where the maximum value was only 0.01 Å larger. Thus, the bond lengths lie within the same plausible range, even though no QM to QM/MM comparison of the individual conformers was made yet. In Chapter 6.1, the

length of the Cu_{ax}-Cu_{eq} bond was identified as a indicative of the cluster shape. While the QM optimizations determined values between 2.16 Å and 2.30 Å, the QM/MM calculations yielded Cu_{eq}–Cu_{ax} bonds on average 0.1 Å shorter between 2.15 and 2.29 Å

Table 17 Characteristic Cu – Cu bond lengths (in Å) of the 16 conformers of $Cu_{13}(SCH_2CH_3)_8$ in the QM/MM calculations

conformation	$Cu_{ce} – Cu_{eq}$	Cu_{ce} - Cu_{ax}	$Cu_{ax} – Cu_{eq}$	$Cu_{ax}1– Cu_{ax}2$
buis	2.735	2.048	2.291	2.349
buie	2.728	2.050	2.289	2.347
buos	2.094	2.344	2.261	2.276
buoe	2.094	2.345	2.262	2.276
bdis	2.412	2.146	2.152	2.400
bdie	2.410	2.147	2.152	2.400
bdos	2.607	2.070	2.220	2.359
bdoe	2.608	2.072	2.214	2.375
tuis	2.691	2.016	2.268	2.290
tuie	2.692	2.010	2.265	2.287
tuos	2.688	2.014	2.265	2.288
tuoe	2.688	2.014	2.265	2.288
tdis	2.686	2.021	2.240	2.339
tdie	2.686	2.021	2.240	2.339
tdos	2.662	2.020	2.231	2.326
tdoe	2.665	2.019	2.232	2.327

The Cu–Cu bonds of the on-top conformers exhibit an astounding property: the corresponding bonds of a pair of rotamers at most by 0.6 pm. Whereas the staggered or eclipsed state of the methyl end group had considerable influence on the cluster geometry in the QM calculations, it is negligible in the QM/MM calculation. On one hand, this is to be expected, as the QM part of the QM/MM model does not contain the end group and should be indifferent to its conformation. On the other hand, the

interaction between the methyl group in the MM part and the cluster core is considerable as evidenced by the geometric change in the case of the bdos in Figure 30 and, although to a lesser extent, even the buos conformer in Figure 28. This subject was discussed in Chapter 6.2.2 in more detail. The perturbing electronic interaction between ligand end group and cluster is replaced by the more qualitative van der Waals interaction in the QM/MM model which acts on the ligand geometry stronger than on the cluster core.

Table 18 Cu_{ce}–Cu_{eq} and Cu_{ce}-Cu_{ax} bond lengths from QM/MM calculations and changes relative to their corresponding QM values; in Å

conformation	$Cu_{ce} – Cu_{eq}$	difference QM/MM-QM	Cu_{ce} - Cu_{ax}	difference QM/MM-QM
buis	2.735	-0.012	2.048	-0.001
buie	2.728	0.077	2.050	-0.018
buos	2.094	0.007	2.344	0.044
buoe	2.094	-0.004	2.345	0.006
bdis	2.412	-0.012	2.146	0.006
bdie	2.410	-0.033	2.147	0.014
bdos	2.607	0.109	2.070	-0.044
bdoe	2.608	0.182	2.072	-0.062
tuis	2.691	0.005	2.016	0.002
tuie	2.692	0.024	2.010	-0.010
tuos	2.688	0.002	2.014	-0.000
tuoe	2.688	-0.001	2.014	-0.000
tdis	2.686	0.079	2.021	-0.010
tdie	2.686	0.001	2.021	-0.001
tdos	2.662	0.023	2.020	-0.025
tdoe	2.665	0.015	2.019	-0.012

In the cases where $Cu_{ce} – Cu_{eq}$ bonds change by more than 1 pm QM/MM values are longer than their QM counterparts. Only the conformer **bdie** constitutes an exception.

The Cu_{ce} - Cu_{ax} bonds are shorter by 1-6 pm in the same conformers. In consideration of the wide range of Cu – Cu bond lengths realized in the given compound, these variations seem negligible.

Although the MM contribution to the description of the cluster core is minor, the defining bond lengths of the cluster reflect the different method clearly. Whereas qualitative features of the cluster compound under study are retained, the cluster core adapts to the ligand conformation. In the on-top cases, where the cluster-ligand interaction is limited to one atom type only, the differences between QM and QM/MM treatment are small. The bridge-hollow cases exhibit larger changes of the core geometry. The stronger core-ligand interaction, as evidenced by larger ligand binding energies, enables the proliferation of geometry directing ligand interactions.

6.2.6. Geometric Properties of $Cu_{13}(SCH_2CH_3)_8$: Cluster – Ligand Interface

Reviewing the Cu – S bond lengths of the bridge conformers alone, the directing influence of the QM/MM description becomes apparent again. The ligands of the **buis** and **buie** conformers assume a position closer to a threefold-hollow coordination by increasing the Cu_{eq} – S bond length. The ligand binding site of **buos** and **buoe** become nearly identical by shifting Cu – S bonds in opposite directions. The conformers **bdos** and **bdoe** experience the largest shifts as they change the binding site from clearly bridge to threefold-hollow (see also Figure 30). The changes are less drastic in the on-top conformers. In most cases, the differences between QM and QM/MM geometry are up to about 3 pm. Only the **tdis** conformer stands out with a Cu_{ax} – S bond length change of 5 pm. The Cu_{eq} – S inter-atomic distance will not be considered for the on-top conformers.

It is evident from Table 19 that the directing influence of the QM/MM method extends to the bond angles of the cluster-ligand interface. The values of staggered and eclipsed conformers pair up nicely. In conformations where the inter-ligand repulsion is comparably small, the values of staggered and eclipsed conformers are virtually identical, e.g. in the **buos**-**buoe** and **bdis**-**bdie** pairs. The similar distances of the **bdos**-**bdoe** pair show that inter-ligand repulsion does not need to be negligible, but only similar in strength. The difference in the **buis**-**buie** pair is acceptable, when the commonly accepted accuracy of bond angles of a few degree is taken into account. The rightmost column of Table 19 illustrates the extent of the directing influence.

Table 19 Cu-S bond lengths and $Cu_{ax} – S – C_1$ angles detailing ligand bonding in the QM/MM calculations of $Cu_{13}(SCH_2CH_3)_{8;}$ the difference between QM/MM and QM calculations is also given; bond lengths and their differences in Å, angles and their differences in degrees

conf.	bond Cu_{eq}-S	difference QM/MM-QM	bond Cu_{ax}-S	difference QM/MM-QM	angle Cu_{ax}-S-C_1	difference QM/MM-QM
buis	2.110	0.036	2.206	0.000	141.7	4.4
buie	2.110	0.038	2.202	-0.008	137.7	7.2
buos	2.219	0.035	2.181	-0.136	118.7	26.0
buoe	2.218	-0.041	2.180	-0.033	118.8	-2.3
bdis	2.575	-0.007	2.254	0.007	106.8	1.6
bdie	2.576	-0.028	2.254	0.006	106.8	3.0
bdos	2.137	-0.838	2.222	-0.064	147.9	33.9
bdoe	2.132	-0.804	2.219	-0.028	147.4	29.1
tuis	3.028	-0.020	2.105	-0.001	112.3	14.8
tuie	3.044	0.016	2.096	-0.027	111.3	10.7
tuos	3.059	0.010	2.116	0.010	94.5	-3.0
tuoe	3.058	0.008	2.116	0.011	94.6	-3.9
tdis	3.791	0.156	2.160	0.049	91.6	-6.3
tdie	3.791	0.011	2.160	0.012	91.6	-0.9
tdos	3.770	-0.064	2.142	-0.028	109.6	10.6
tdoe	3.767	-0.046	2.138	-0.029	112.5	12.8

In the analysis, an equalizing trend was observed geometric parameters. This means that each rotamer pair exhibited (nearly) equal values of a geometric parameter which can be different from those in other rotamer pairs. It will be noted where appropriate in the discussion. The Cu_{ax}–S–C_1 angles of the conformers **buos**, **bdos** and **bdoe** are bent considerably to the corresponding equalized values of 118° for **buos** (and **buoe**) and 147° for **bdos**-**bdoe**. The angles tend to open as compared to the QM calculations, reflecting an increased cluster-ligand repulsion which is propagated to the interface

angle. Only in the **buoe** conformer, the Cu_{ax}–S–C_1 angle decreases noteworthy in the QM/MM calculation relative to the QM calculation.

As the cluster-ligand and inter-ligand interactions are weaker in the on-top conformers, QM-to-QM/MM differences are consequentially smaller. For the same reason, differences between rotamers are smaller. The pairing effect, clearly observable in the QM/MM values, is less pronounced in the QM results as evidenced in the differences between them. Being bound only to one Cu_{ax} atom, the Cu_{ax}-S-C_1 angle takes values smaller than in the bridge-hollow conformers (~100º for the conformers **tuos**, **tuoe**, **tdis** and **tdie**; ~110º for other conformers).

The Cu – S bond lengths of bridge-hollow and on-top conformers are comparable (by absolute value) to the QM calculated results. Thus, they reproduce the findings of the QM values, in that they differ from to the reference values in the literature. The pairing of bond lengths and bond angles between staggered and eclipsed conformations (equalizing) indicates the reduced importance of the rotamer state in the QM/MM method. The cluster-ligand interface is governed by the ligand conformation as a whole rather than the end group geometry.

The discussion of the ligand interface allows some inferences on the total energy of the conformers. Different relative total energies in QM and QM/MM calculations can be traced back to the equalizing trend in the cluster geometry due to the ligand interface interaction. In the conformer pair **bdos**-**bdoe**, the changes in the cluster as well as the cluster-ligand interface geometry are most drastic. The cluster core shows a much flatter shape, where the interface changes from bridge to threefold-hollow coordination. As the ligand end group no longer contributes to the ligand-cluster interaction, the structure is destabilized as a whole. This energy loss is compensated in part by the increased stability of the threefold-hollow binding site, but not completely, as evidenced in the QM to QM/MM total energy difference of the **bdos** conformer. Thus, the reversed order of total energies between **bdos** and **buis** conformers can be attributed to the reduced stability of the **bdos** conformer in the QM/MM method.

6.2.7. Geometric Properties of $Cu_{13}(SCH_2CH_3)_8$: Ligand Geometry

In the discussion of the ligand geometry, special consideration is given the C_1-C_2 bond as it is the link bond, treated simultaneously in the QM and QM/MM approach. The S-C_1 bond be affected by a ligand structure change. Mechanical stress on individual bonds in alkyl chains is seldom strong enough to induce bond distortions worth

discussing. The backbone angle S–C_1–C_2 and even the individual C–H containing angles can be distorted by ligand-ligand and cluster-ligand interaction.

Inspection of Table 20 shows that distortion of S–C_1 and C_1–C_2 bonds are small for most conformers. The decrease (by 4 pm) of the S – C_1 bond of the conformer **buoe** in the QM/MM geometry is the largest one calculated for the bridge-hollow conformers. Other conformers feature deviations from 0.5 and 2 pm between QM and QM/MM calculations. The S – C_1 bond is shorter in the QM/MM calculation than in the QM results for all, but the conformers **bdis**, **bdie** and **bdos**. The values in the corresponding conformers pair nicely, except in the **bdos**-**bdoe** rotamer pair, where they differ by almost 1 pm. It is noticeable that four distinct values of the S–C_1 bond are realized in the conformers under consideration. As the long S – C bonds of the QM calculations could not be reproduced, the QM/MM values are even shorter than the values determined by Akinaga et al.[221] for the adsorption of methyl thiolate on copper surfaces. This shorter bond (by 5-7 pm), is likely caused by the considerably larger bond strength of the ligands to the cluster. This conclusion is corroborated by a comparison with the bond length results of Kerdcharoen et al. where a shortening of the S – C bond was found when the cluster size was increased.[183]

Table 20 Ligand backbone bond lengths S – C_1 and C_1 – C_2 as well as QM-QM/MM differences of the 16 conformers of $Cu_{13}(SCH_2CH_3)_8$; all values in Å

conformation	S - C_1	diff. QM/MM-QM	C_1 - C_2	diff. QM/MM-QM
buis	1.816	-0.005	1.523	0.020
buie	1.816	-0.012	1.538	0.026
buos	1.830	-0.021	1.524	0.019
buoe	1.830	-0.043	1.538	0.026
bdis	1.853	0.006	1.529	0.021
bdie	1.853	0.006	1.544	0.021
bdos	1.827	0.016	1.523	0.027
bdoe	1.820	-0.011	1.538	0.034
tuis	1.817	-0.008	1.522	0.012
tuie	1.819	-0.001	1.541	0.023
tuos	1.826	-0.000	1.525	0.016
tuoe	1.825	0.000	1.539	0.016
tdis	1.816	-0.009	1.537	0.035
tdie	1.816	-0.006	1.537	0.018
tdos	1.816	-0.000	1.524	0.018
tdoe	1.813	-0.006	1.540	0.020

The S–C_1 bonds of the on-top coordinated conformers mirror the behavior of the bridge-hollow coordinated ones. However, they exhibit only two distinct values. The QM/MM calculated bond lengths are slightly shorter or at most equal to the corresponding QM calculated distances. Although the S–C_1 bond is close to the QM-MM system boundary, the change of method does not introduce considerable distortions; the average absolute deviation was less than 1 pm. This finding lends further credibility to the results of the bridge-hollow conformers, where shorter bonds than in the literature were found.

Table 21 Ligand specific bond lengths of the 16 conformers in the QM/MM calculations; also shown are the differences to the corresponding QM values; all values in Å

conf.	C_1 - H_1	difference QM/MM-QM	C_2 - H_2	difference QM/MM-QM	C_2 - H_3	difference QM/MM-QM
buis	1.104	0.001	1.112	0.008	1.113	0.008
buie	1.104	0.002	1.113	0.010	1.112	0.007
buos	1.103	-0.002	1.113	0.010	1.113	0.008
buoe	1.103	0.003	1.113	0.010	1.112	0.007
bdis	1.115	-0.001	1.113	0.009	1.113	0.008
bdie	1.115	0.000	1.113	0.010	1.112	0.008
bdos	1.104	-0.001	1.113	-0.007	1.113	0.007
bdoe	1.104	0.000	1.113	0.010	1.111	-0.005
tuis	1.106	0.002	1.109	0.006	1.113	0.008
tuie	1.106	0.002	1.113	0.011	1.108	-0.009
tuos	1.105	0.001	1.113	0.009	1.113	0.008
tuoe	1.105	0.002	1.113	0.011	1.112	0.008
tdis	1.109	0.005	1.113	0.008	1.112	0.007
tdie	1.109	-0.000	1.113	0.011	1.112	0.009
tdos	1.108	0.002	1.112	0.001	1.113	0.006
tdoe	1.108	0.003	1.113	0.009	1.107	-0.011

The C_1-C_2 bond is the link bond, and thus not entirely dependent on the QM or MM model alone. Recalling Eq. (3.12) of Chapter 3.4.2., the forces acting on the C_2 atom are a mixture of both QM and MM parts of the model via the link bond. The ratio of the frontier bond to link bond is set to a constant value, *g*, which is parameterized for models of alkan chains (C-C bonds at both sides of the bond under consideration). As the system boundary of the current model is neighboring a S–C instead of a C–C bond, the chemical environment is different in the MM description than intended. This different chemical environment causes the C_1–C_2 bonds found in the QM/MM calculations to be ~2 pm longer than in the QM calculations. This way, they show a

better agreement with most experiments, which find C–C bonds in alkyl thiolates of about 1.53 Å.[127-130] The frontier bond length is mainly determined by the MM parameter set in the QM/MM calculations.

Table 22 The ligand backbone angle S – C_1 – C_2 of the 16 conformers of $Cu_{13}(SCH_2CH_3)_8$ and differences to the corresponding QM values; all values in degrees

conformation	S - C_1 – C_2	difference QM/MM-QM
buis	110.3	1.6
buie	111.2	0.4
buos	110.1	2.8
buoe	111.2	1.6
bdis	108.7	0.2
bdie	109.9	-0.5
bdos	113.4	0.8
bdoe	113.8	-3.9
tuis	117.3	9.0
tuie	119.8	5.0
tuos	110.4	2.0
tuoe	111.4	1.7
tdis	113.5	3.8
tdie	113.5	-0.1
tdos	117.1	4.4
tdoe	119.3	4.9

It is interesting, that the $C_1 – C_2$ bonds of the bridge-hollow conformers in staggered conformations are consistently 1.5 pm shorter than their eclipsed counterparts. This perfectly illustrates the bond weakening and thereby lengthening effect of the staggered-eclipsed isomerism. Whereas this lengthening was also found in the QM calculations as well, it was not as consistent as in the QM/MM calculations. The on-top conformers

feature very similar properties, with the exception of the **tdis**-**tdie** conformer pair. Here, staggered and eclipsed conformers exhibit $C_1 - C_2$ bonds of equal length.

Table 23 Selected ligand angles of the QM/MM calculations of $Cu_{13}(SCH_2CH_3)_8$; also given are the differences to the QM values; all values in degrees

conf.	S - C_1 - H_1	difference QM/MM-QM	C_1 - C_2 - H_2	difference QM/MM-QM	C_1 - C_2 - H_3	difference QM/MM-QM
buis	109.7	2.5	111.8	1.7	111.3	-0.4
buie	109.3	3.9	111.4	-0.5	112.9	3.9
buos	109.4	1.3	111.8	1.5	111.2	0.3
buoe	109.1	3.9	111.4	-0.4	112.9	2.4
bdis	111.9	2.1	111.8	2.1	111.2	-0.1
bdie	111.7	2.6	111.4	-0.7	113.0	3.5
bdos	108.0	1.6	111.8	3.2	111.3	-4.0
bdoe	108.2	4.5	111.5	-2.1	113.0	3.7
tuis	107.5	-0.5	111.7	1.7	111.4	-0.2
tuie	107.0	1.5	111.3	-1.0	114.2	3.6
tuos	110.2	2.1	111.8	1.8	111.3	-0.3
tuoe	110.0	2.7	111.4	-0.7	112.9	3.1
tdis	108.4	1.1	111.4	1.0	112.6	1.0
tdie	108.4	3.4	111.4	-0.1	112.6	2.5
tdos	107.7	1.6	112.2	3.0	111.0	-1.0
tdoe	107.2	1.8	111.3	-1.5	114.2	4.6

Differences in the QM/MM values of C_1–H_1 bond lengths are small for both types of conformers, bridge-hollow and on-top; also, this bond is very similar in staggered-eclipsed. None of the conformers differs from its QM calculated counterpart by more than 0.5 pm. As the C_1–H_1 bond is almost completely described by the QM part of the model, this small difference is understandable. The $C_2 - H_2$ and $C_2 - H_3$ bonds, however, change by up to 1 pm. In most of the conformers, they increase by 1 pm. The C_2–H_2 bond of the conformer **bdos** and the C_2–H_3 bond of the conformers **bdoe**, **tuie**

and **tdoe** constitute exceptions as they are shorter by 1 pm in the QM/MM calculations than in the corresponding QM calculations. These special cases were characterized by comparably long bonds in the QM calculations, which in the QM/MM calculations adjusted to the length given by the C – H bond length parameter of the MM3 force field (1.112 Å).

It is reasonable that the $S - C_1 - C_2$ angle exhibits differences between QM and QM/MM calculations, as it defines the ligand conformation to a large extent. If the descriptions of the cluster differ considerably, this angle changes as well. In most of the conformers, the angle is larger in the QM/MM calculations as compared to the QM calculations. For most of the conformers the angle differs by at most 1.5 degree; thus, the ligand angle description by both methods is rather similar. Other conformations, where the $S–C_1–C_2$ angle difference is more pronounced, exhibit a unclear pattern. In the conformation **buos**, where the cluster-interface angle $Cu_{ax}–S–C_1$ changes by 26º, the backbone angle difference is large, 2.6º. The conformer **bdos** features the largest cluster-interface angle difference, 34º; there, the backbone angle is changed by only 0.8º. This and similar observations on other conformer once more lead back to the pairing effect of staggered and eclipsed conformers as the driving force behind the differences between QM and QM/MM calculations. No other causes of these backbone angle changes of differing extent are readily apparent. The values of staggered and eclipsed conformers differ at most by 3º; this value is obtained only in the case of the conformer pair **tuis**-**tuie**.

All three intra-ligand angles under consideration lie within two degrees of their corresponding reference values of the MM3 force field. The $S\text{-}C_1\text{-}H_1$ angles stay at their QM values in the conformations with small inter-ligand repulsion (**buos**), and open by a 2-4º in conformations with a stronger ligand interaction (**bdos**, **bdoe**). Where the inter-ligand repulsion is strong in both QM and QM/MM calculations, as in the conformers **tuis** and **tuie**, the angles differ little as well. With only few exceptions, the $C_1–C_2–H_2$ angle of the staggered conformations assumed a value of 112º, whereas the eclipsed conformers showed angles of 111º.

The $C_1–C_2–H_3$ angle assumes distinct values of 111º and 113º in staggered and eclipsed conformations, respectively. Only three exceptions are noticeable. The conformers **tuie** and **tdoe** show a slightly larger $C_1 – C_2 – H_3$ angle of 114º. In these two cases, the cluster-hydrogen (**tdoe**) and inter-ligand hydrogen repulsion (**tuie**) induces an opening of this particular angle as any other interaction is absent (see e.g. Figure 25 (b)). The rotamer pair **tdis**-**tdie** constitutes an exception as it exhibits an average value

of 112.6º. The extreme similarity of these two rotamers, likely due to the flat interaction profile rather than any particular cause, was already noted.

The methyl end group geometry is determined by inter-ligand and cluster-ligand interactions. The ligand bond lengths of bridge-hollow and on-top conformers do not change significantly between the two methods. The similarity between staggered and eclipsed conformations (pairing effect), observed in other geometric parameters is less pronounced in the ligand bond lengths. The angles defining the ligand geometry, however, show definite pairing effects with distinct values for rotamer pairs. The influence of the methyl end group conformation (staggered or eclipsed) is visible in the C–C–H angles where staggered and eclipsed conformers express distinct sets of values, but less so in the S–C_1–H_1 angle, which depends mostly on the chemical surrounding of the ligand.

6.2.8. Conclusion

QM and QM/MM results have been compared for the 16 isomers of $Cu_{13}(SCH_2CH_3)_8$ and good agreement was found for ten conformations. In the remaining conformers, structure changes between QM and QM/MM calculations are due to differences in interactions: short distances between hydrogen atoms of neighboring ligands in a plane perpendicular to the z axis (H_2-H_2' **buis**, **tuis**; H_3–H_3' **buie**, **tuie**) or through the x-y-plane (H_2–H_2'' **tdoe**; H_3-H_3'' **tdos**) or short distances between hydrogen atoms of the methyl end group and the Cu_{eq} atoms of the cluster core (Cu_{eq}–H_2 **bdos**; Cu_{eq}–H_3 **bdoe**). Small differences in the conformers **buis** and **tuis** (H_2-H_2'), **buie**, **tuie** (H_3–H_3') as well as in the conformers **buos**, **buoe**, **tuos** and **tuoe** (H_1–H_1') have similar origin. The interactions between these (non-bonded) groups of atoms are treated differently in the QM and QM/MM methods (see Chapter 6.2.2). Cluster geometries could be reproduced with the QM/MM method with an accuracy of 1 pm and better in non-perturbed conformers, although the cluster geometry of Cu_{13} was shown to crucially depend on the ligand configuration around it (Chapters 5.1, 5.2 and 6.1). Equally good agreement was achieved in the description of the cluster interface made up by one to three Cu – S bonds. Ligand bond lengths (S–C, C–C, C–H) were reproduced equally accurate, with differences between QM to QM/MM results higher than 1 pm only in the link bond (C_1 – C_2). The empirical C-C bond length parameter in the MM3 force field introduced by the model was identified as the source for the larger disagreement (2 pm) between the corresponding QM and QM/MM results.

6. Comparing QM and QM/MM Calculations of $Cu_{13}(SCH_2CH_3)_8$

While total energies of QM/MM and QM methods differ naturally, the spectrum of conformers derived by the relative total energies showed a predictable and sensible behavior. Differences in this spectrum could be traced back to meaningful changes in the description of non-bonded interactions. The ligand binding energies determined by both methods agreed within chemical accuracy (~2 kcal/mol).

From the comparison of QM and QM/MM results presented in this chapter one concludes that the QM/MM method is indeed applicable to this class of systems, reproducing the conformations with adequate accuracy, while delivering satisfactory energetic results. In cases where non-bonded interactions within the molecule are to be expected, the QM/MM method proved actually superior to a pure QM calculation at LDA level. The QM/MM method is computational less demanding as the system size increases and thus it is a promising approach for metal cluster systems with complex ligand shells.

7. Computations of Periodic Two-Dimensional Arrays of Copper Thiolate Clusters

The previous chapters showed the application of QM and QM/MM method to solitary clusters. However, properties of clusters often change in the presence of a chemical matrix (see Section 2.5). To study the interaction of clusters in ordered array which constitute one type of a chemical matrix, the QM/MM method was extended to periodic boundary conditions as detailed in Chapter 3.3 and 3.4. In this chapter, the interaction between ligand chains of neighboring clusters will be examined as one of the sources of cluster layer stabilization. Other stabilizing effects, such as surface template effects, solvent stabilization and direct magnetic cluster-cluster interaction will be neglected for the moment. Two clusters were chosen for investigation: $Cu_{13}(SCH_2CH_3)_8$ and its homologue $Cu_{13}(CH_2CH_2CH_3)_8$. A methylene group was introduced in the ligand model, increasing the potential for inter-ligand interaction and allowing to study the effects of different ligand chain lengths. To keep the investigation focused, only one suitable conformation of each compound was chosen. The properties were computed in a two-dimensional infinite lattice of clusters in an end-on and an interlocked orientation of the respective clusters. The distance between cluster centers was varied via the lattice constant. The minimum energy geometries at different lattice constants were obtained by optimizing the geometry of the individual cluster in the field of an infinite layer. The optimal lattice constant was determined via the minimum of the total energy with respect to the inter-cluster distance.

7.1. Computational Details

Computations of cluster layers were performed using the QM/MM implementation with the MM program DL_POLY_2 as discussed in Sections 3.4.2 and 3.4.3. The extended MM3 force field was used as in the previous QM/MM calculations. For the QM part of the calculations, the DF program PARAGAUSS was employed. No GGA single point calculations were performed as only optimized geometries and their relative total energies were required. The computational parameters were the same as discussed in Chapter 4.

The computational models were the ethylthiolate cluster $Cu_{13}(SCH_2CH_3)_8$ and its homologue $Cu_{13}(SCH_2CH_2CH_3)_8$. The ligand were set up in all-trans conformation, corresponding to the conformer **bdos** in the case of the ethylthiolate cluster. Because of the large conformation space of both cluster compounds, a thorough examination as in the case of $Cu_{13}(SCH_2CH_3)_8$ was considered unfeasible. The core parts of the cluster

consisting of the models $Cu_{13}(SCH_3)_8$ (R(central), see Figure 27) were restricted to D_{4h} symmetry. The corresponding end groups were optimized without symmetry restriction.

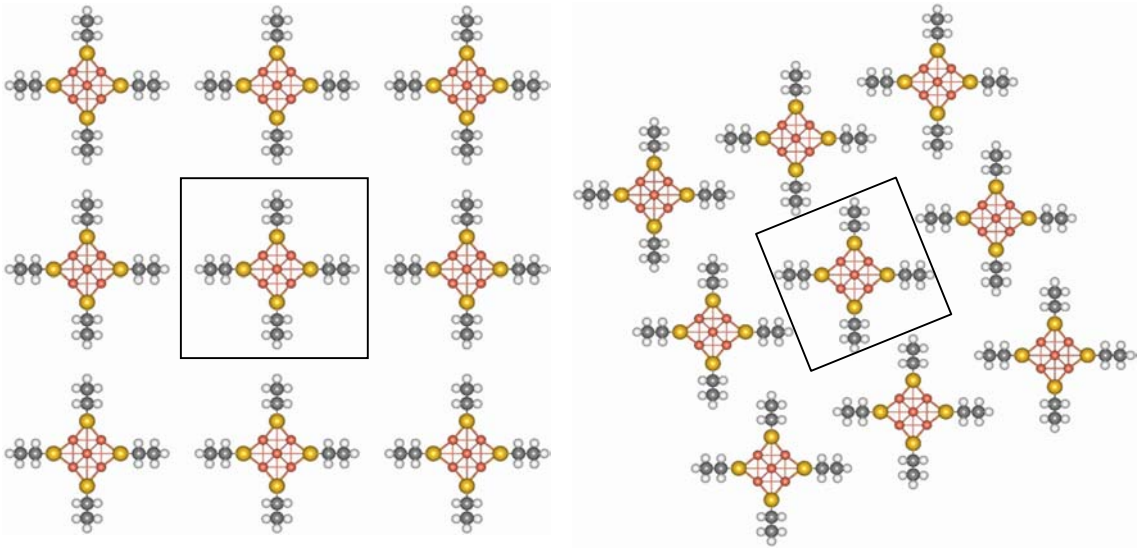

Figure 31 Top views of parts of lattices of $Cu_{13}(SCH_2CH_3)_8$ in end-on (left-hand panel) and interlocked (right-hand panel) orientations of the clusters. The boundaries of one tetragonal unit cell are marked; in the interlocked orientation, parts of one cluster may reach into neighboring unit cell; due to periodicity, this nevertheless results in one cluster per unit cell

The tetragonal unit cell contained a single cluster. A two-dimensional layer was simulated by choosing the unit cell vector $|\vec{C}|$ much larger than vectors $|\vec{A}|$ and $|\vec{B}|$ ($|\vec{A}| = |\vec{B}| \approx$ 10-20 Å; $|\vec{C}| =$ 100 Å). Thus, MM interaction between cluster cores was reduced. The lattice constant $|\vec{A}| = |\vec{B}|$ was optimized.

Four optimizations of cluster layers were conducted. In two series of calculations, (on layers of clusters with ethylthiolate and propylthiolate ligands, respectively,) the edges of the unit cell were aligned parallel to the ligands. Thus, the ligands of the cluster images in adjacent cells interacted end-on (see Figure 31 left). In a second series, the unit cell was tilted by 22.5° with the z axis as the rotation axis, for both types of ligands, respectively. This situation is depicted on the right side of Figure 31. At this angle, the ligands can interlock, increasing the number of possible non-bonding interactions which can contribute to the stabilization of the cluster layer. For brevity, the term “interlocked orientation” is used.

At each simulation cell size, the geometry of the cluster was optimized. The resultant QM/MM total energy according to Eq. 3.10 contains the stabilizing contribution by the non-bonded interaction of cluster images. The total energy of a reference "gas phase" cluster is subtracted where the simulation cell is quasi-infinite, i.e. all three cell vectors are set to a length of 100 Å. This relative total energy can be interpreted as the stabilization energy by non-bonded interaction reduced by a contribution due to conformational deformation of the cluster structure. Both contributions vary in magnitude and sign depending on the nearest-neighbor distance. The size of the optimized unit cells will depend on the orientation of the neighbors relative to each other, i.e. ultimately on the shape of the unit cell.

7.2. Results of the Calculations

First, the computational results for square arrays of $Cu_{13}(SCH_2CH_3)_8$ clusters in end-on cluster orientation (see Figure 31) will be presented and discussed. Here, the basic features of the calculations can be determined most clearly. The discussion of the cluster in interlocking orientation and the corresponding results for $Cu_{13}(SCH_2CH_2CH_3)_8$ will be presented in more compact form, based on the conclusions achieved here.

The variations of the total energies of the computations of $Cu_{13}(SCH_2CH_3)_8$ at different lattice constants were collected in Figure 32. Clearly, all relative total energies except at extremely short lattice constants are lower than the reference total energy of the isolated cluster. The van der Waals interaction between ligand chains stabilizes the cluster layer. At a lattice constant of 15.7 Å, the minimum of the relative total energy is achieved. There, the layer is stabilized by ~2 kcal/(mol·cluster). From 15.7 Å to shorter lattice constants, the total energy increases with decreasing lattice constant. At lattice constants shorter than ~15 Å the ligand conformation changes from **bdos** to **bdis** (see Figure 33). Further compression of the unit cell yields a slightly lower relative total energy again.

The increased inter-ligand distance accompanying the conformation change from **bdos** to **bdis** reduces the van der Waals interaction. The total energy of the achieved bdis conformation is thus lowered. By reducing the steric repulsion between ligand chains, the layer is stabilized. From the structure data in Appendix D, one can see that the deformation of the ligand structure prior to the conformation change is minimal.

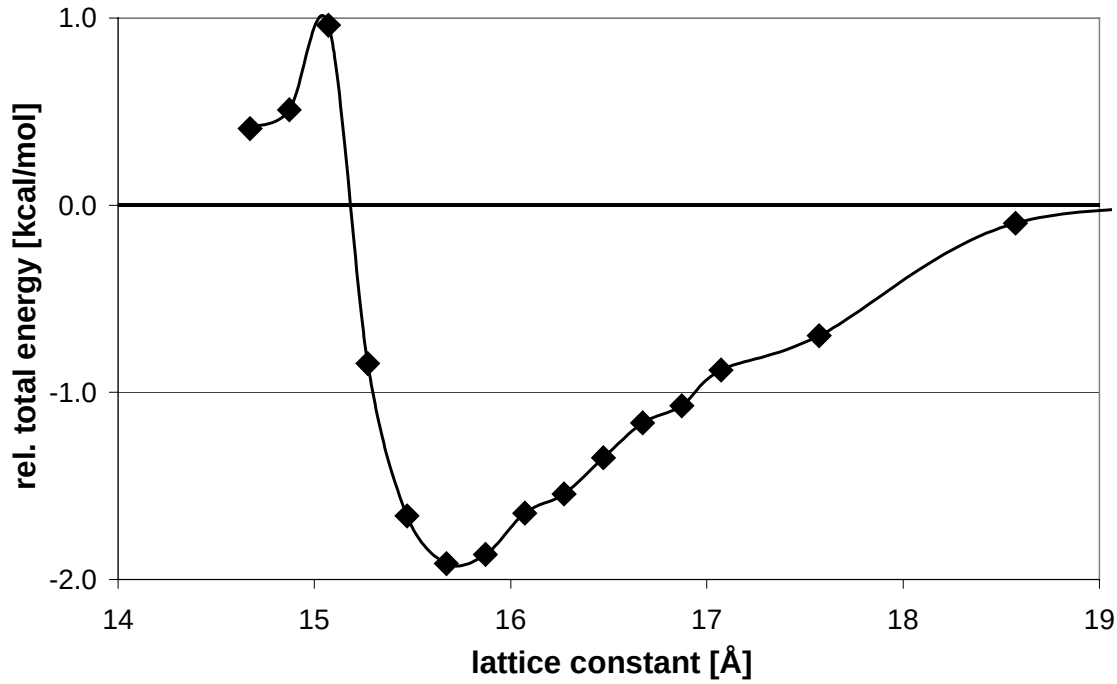

Figure 32 Relative total energy of optimized square layer of $Cu_{13}(SCH_2CH_3)_8$ clusters in end-on orientation of the periodic images; total energy of the isolated cluster E_{tot} = -24693.2347915799 au

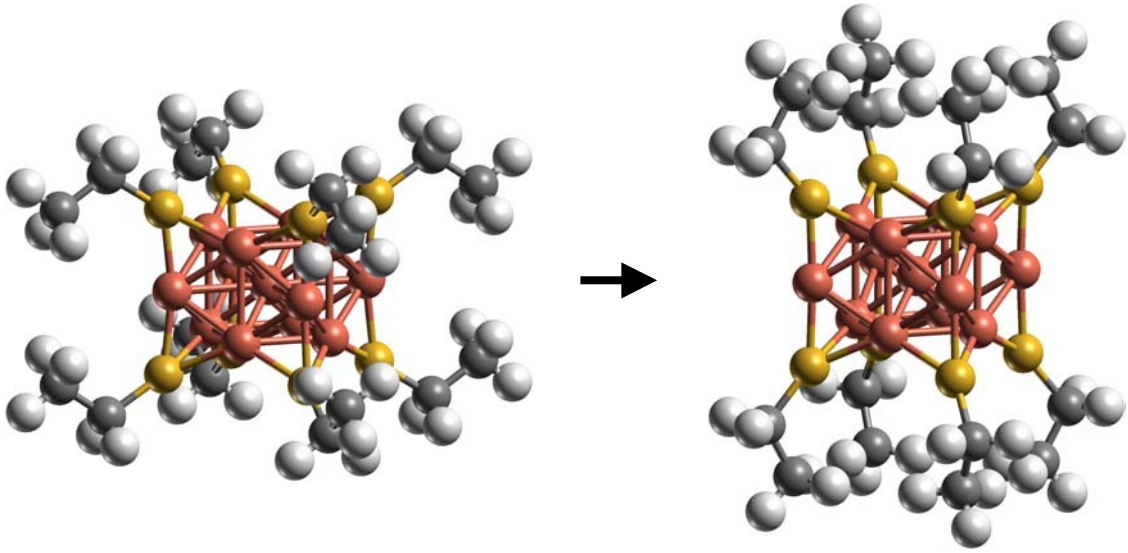

Figure 33 Structure of $Cu_{13}(SCH_2CH_3)_8$ in **bdos** conformation (left) used as starting geometry for the set of calculations; at lattice constants lower than 15 Å the **bdis** conformation is adopted (right)

Figure 34 enables one to analyze the energy contributions from the model parts. It can be seen that any deviations from the expected smooth curve of the QM/MM total energy are caused by variations in the MM partial energies only. The QM energy of the central part (R(central)) of the model remains nearly indifferent to the lattice constant. It slightly decreases (by at most 0.06 kcal/mol at a lattice constant of 15.5 Å) reflecting a deformation of the central part of the model into an energetically favorable geometry by the interaction of the outer part. Only at small lattice constants, the deformation becomes considerable as evidenced by the increase in the QM energy at lattice constants shorter than 15.3 Å.

Both MM partial energies of central part and total model (R(total)) vary in similar fashion. At large lattice constants, they indistinguishable from the corresponding energies of the isolated cluster. They decrease from lattice constants of 18.5 Å (R(total)) and 16.5 Å (R(central)) on to lower lattice constants, respectively. At 15.3 Å they exhibit a minimum of 10.2 kcal/mol and 11.1 kcal/mol for the central part and total model, respectively. At shorter lattice constants, both exhibit a sharp increase caused by the exponentially increasing van der Waals repulsion between ligand end groups of neighboring clusters. It is noteworthy, that the minima of the partial energies are located at a shorter lattice constant than that of the combined QM/MM total energy (15.7 Å). The energy combination scheme cancels part of the non-bonding interaction between neighboring molecules in the cluster core region (R(central)). This is largely caused by the small ligand model used in this study. The short distance between cluster cores renders the interaction between them too attractive. A realistic description is achieved only with the combined QM/MM total energy,. This becomes apparent when the current set of calculations is compared with the pentane calculation of Chapter 3.4.3. The ligand chain in the MM part is longer there. Consequently, the intermolecular hydrogen-hydrogen distance at minimum energy is determined completely by the interaction of the MM parts of adjacent periodic images of the molecule. The cancellation effect of the van der Waals interaction is less pronounced if the outer MM part is considerably larger than the central part, e.g. the ligand chains are longer.

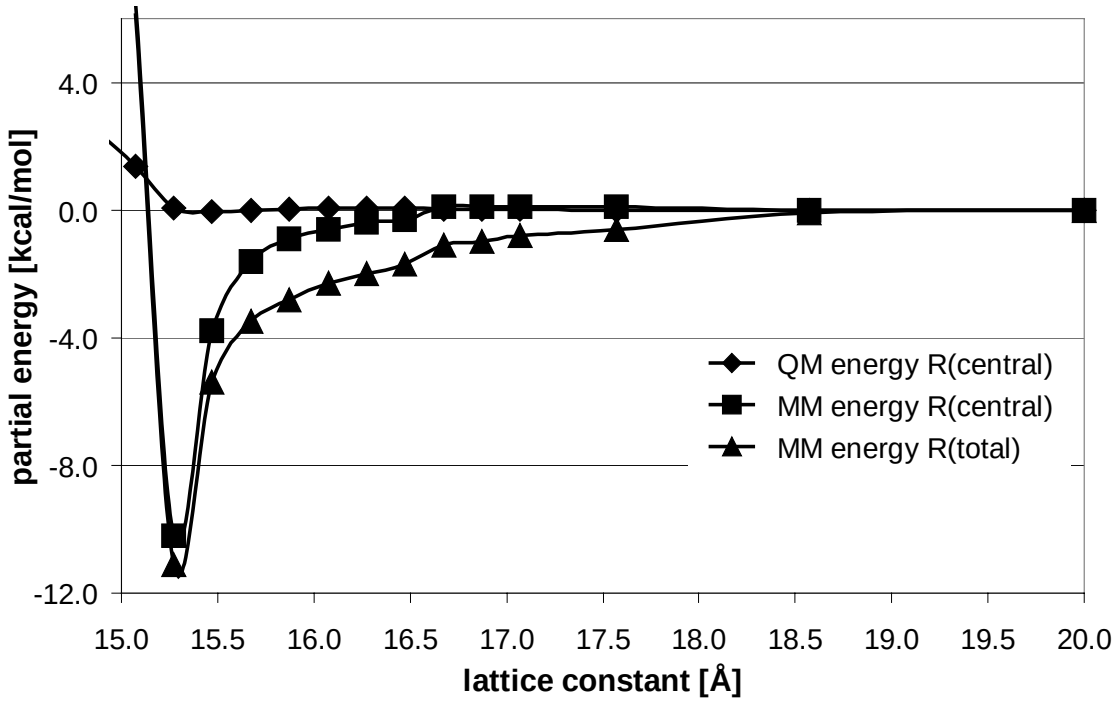

Figure 34 Partial energies of the QM/MM total energy of the $Cu_{13}(SCH_2CH_3)_8$ layer in end-on orientation at different lattice constants; data points at lattice constants less than 15 Å omitted for clarity; reference energies tabulated in Appendix D

The graph of the MM energy of the central part (MM energy R(central) in Figure 34) exhibits irregularities in the lattice constant range between 16 Å and 17.5 Å in the range of approx. 0.1 kcal/mol. The same holds true for the MM energy of the total model. The irregularities in both partial energies are caused by atoms moving across the van der Waals cutoff distance. Their respective contributions to the "appear" at a certain threshold.

In Figure 35 the results of the cluster with ethylthiolate ligands in end-on orientation are compared to those with interlocking orientation. The energy curves are rather different: they show the increased energy gain by the van der Waals interaction of the clusters, when the ligand chains are set up to interlock. The relative total energy of the cluster layer in interlocking orientation shows a stabilization energy of 21.7 kcal/mol, one order larger than for end-on orientation (1.9 kcal/mol). To a small part, this is due to the larger number of atoms in close contact to neighboring clusters. The atoms contribute considerably to the van der Waals interaction energy. The interlocking orientation allows at least three such contacts as opposed to the end-on orientation which allows only one. On the other hand, one of these H-H contacts can contribute at

most 0.2 kcal/mol to the stabilization energy (see Section 3.4.3). Thus the overwhelming contribution has to come from other interactions.

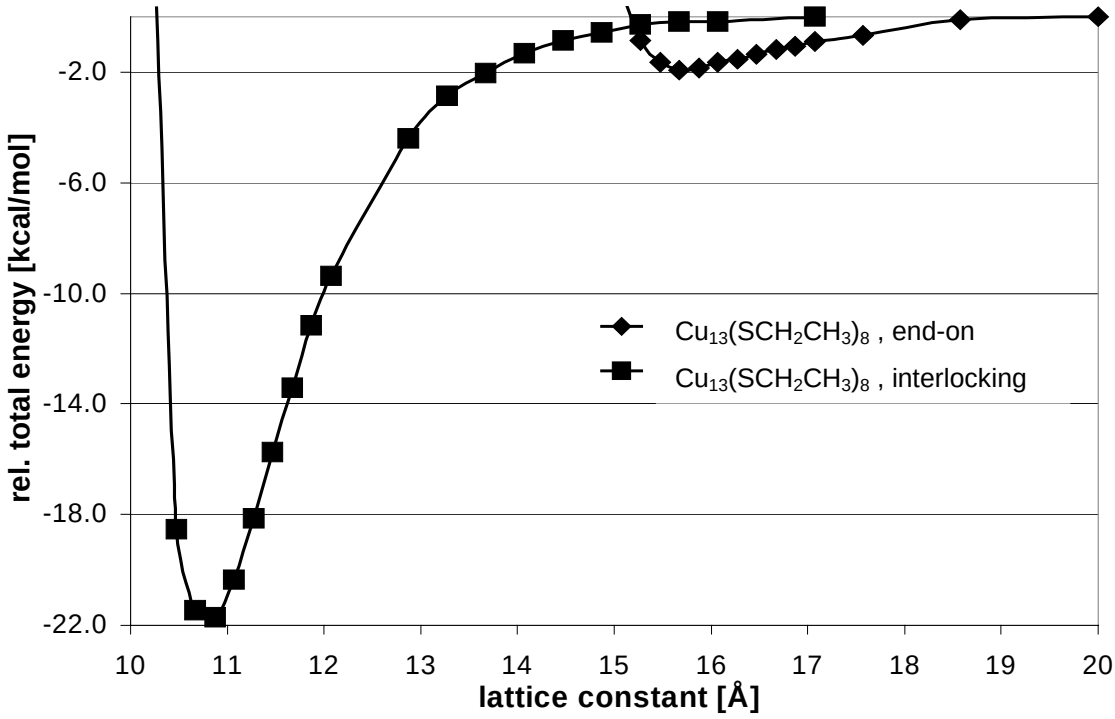

Figure 35 Relative total energies of two-dimensional square lattices of $Cu_{13}(SCH_2CH_3)_8$ clusters in end-on and interlocked relative orientation; E_{tot}(interlocked) = -24693.2356063536 au

The copper core atoms and the thiolate head groups are the only atoms that are inaccessible to interaction in the end-on orientation, but accessible in the interlocked. Furthermore, their possible contribution to the van der Waals energy is more than a tenfold of a H-H contribution at any given distance, according to their parameter set.[127-130] The stabilization energy of the layer in this model is thus mostly provided by the interaction between ligand head groups on one cluster and the cluster core as well as the cluster ligand interface on another one. The minimum of the relative total energy is displaced to shorter lattice constants as expected; it is located at a lattice constant of 10.8 Å.

This finding is underlined by the analysis of the partial energies (see). The MM energy of the total part causes the cluster layer stabilization almost exclusively.

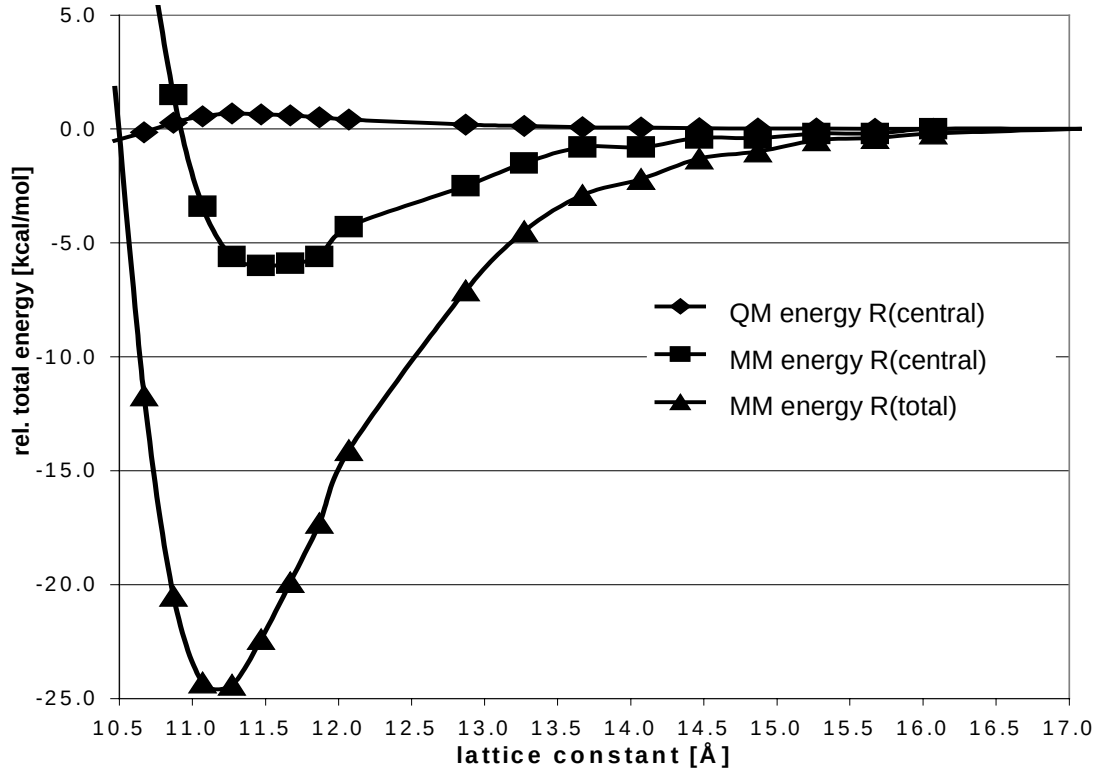

Figure 36 Partial energies of the QM/MM total energy of $Cu_{13}(SCH_2CH_3)_8$ in interlocking orientation for various lattice constants; unit cell rotated by 22.5° with respect to the cluster; data points at lattice constants less than 10.5 Å omitted for clarity; reference energies tabulated in Appendix D

As it can be seen from Figure 36, the irregularities of the partial energies increase with their absolute values. The steps at 12.1 Å in both MM partial energies are clearly discernible despite the wider energy scale of the figure. The cause is the clipping of non-bonded interaction contributions due to the varying van der Waals cutoff in the single calculations (see discussion of the end-on orientation, above). In the relative total energy these fluctuations vanish (see Figure 35). However, this error cancellation effect is accidental.

The methyl end groups in the outer part of the model provide the major contribution to the stabilization energy. The energy gain of the central part of the model, which is subtracted in the calculation of the total energy, is only one fourth of the outer part energy gain. All three partial energies reflect the findings for the corresponding partial energies of the end-on calculations.

Figure 37 gives an overview of the results of the calculations on $Cu_{13}(SCH_2CH_2CH_3)_8$ in comparison to the ethylthiolated clusters; the general trends are similar. The end-on oriented clusters yield arrays with larger lattice constants than the cluster with interlocked orientation. The longer ligands cause a shift of the minima of both end-on (18.3 Å) and interlocked orientation (11.7 Å) towards larger lattice constants as compared to 15.7 Å and 10.8 Å for the $Cu_{13}(SCH_2CH_3)_8$ cluster in end-on and interlocking orientation, respectively. The $Cu_{13}(SCH_2CH_2CH_3)_8$ clusters in end-on orientation are stabilized by 3 kcal/mol ($Cu_{13}(SCH_2CH_3)_8$, E_{st} = 2 kcal/mol). Thus, the main contribution of the stabilization energy is provided by interaction of the methyl end groups. The added methylene chain segments account for an additional stabilization of 0.14 kcal/mol per ligand. The propylthiolated cluster array in end-on orientation is thus 37 % more stable than the ethylthiolated one.

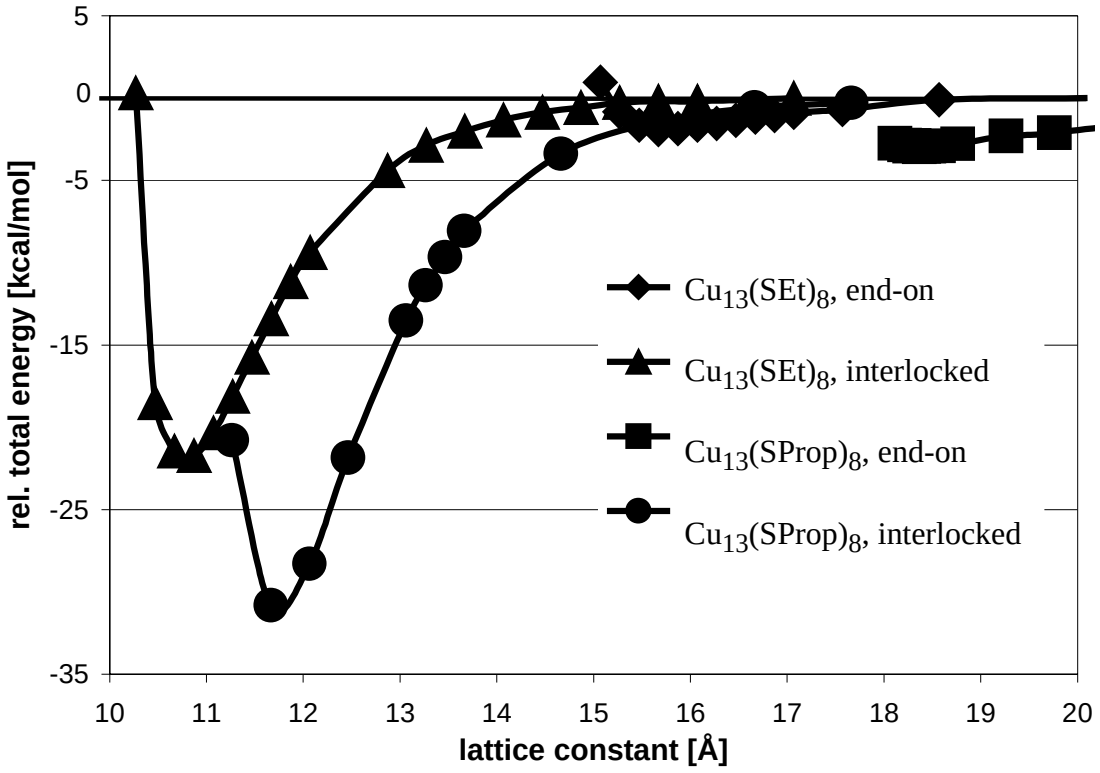

Figure 37 Relative total energies of $Cu_{13}(SCH_2CH_3)_8$ and $Cu_{13}(SCH_2CH_2CH_3)_8$ in end-on and interlocking orientations, respectively; reference energies tabulated in Appendix D

In the case of the interlocking orientation however, the longer ligand chain results in an increased stabilization of the layer by 9 kcal/mol per cluster. At a total stabilization energy of 31.8 kcal/mol, this represents an increase of 29 % as compared to the

ethylthiolated cluster. The stabilization energy is largely governed by the relative orientation of the ligand chains, and not only a simple function of the ligand chain length.

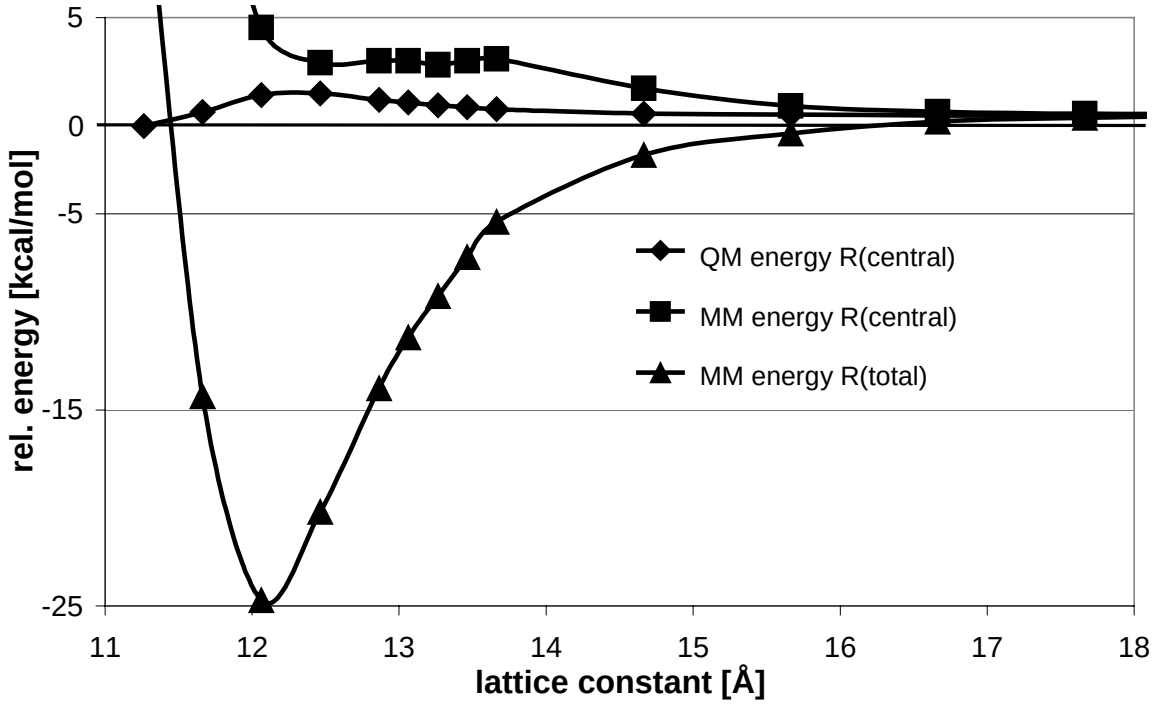

Figure 38 Partial energies contributing to the total energy for interlocking orientation of $Cu_{13}(SCH_2CH_2CH_3)_8$ at different lattice constants; data points at lattice constants less than 11 Å omitted for clarity; reference energies tabulated in Appendix D

The energy contributions for the $Cu_{13}(SCH_2CH_2CH_3)_8$ cluster in interlocking orientation show a curious pattern indeed (see Figure 38). The QM description of the central part implies a destabilization of the cluster, caused by a deformation of the geometry of the central part the stronger cluster-cluster interaction. The energy of the central part falls below its corresponding gas phase value only for lattice constants shorter than 11 Å. As any other interaction is absent by definition, the central part of the model must be accidentally distorted into a energetically favorable position by the directing influence of the outer part of the model. The MM partial energy of the central model part reflects likewise influences, being larger than the gas phase energy at all lattice constants. Only the MM energy of the total model behaves as expected, reflecting attractive van der Waals interaction.

The behavior of the energy contributions can be reasoned as follows. In the interlocked orientation of the clusters, attractive as well as repulsive interaction of ligands in neighboring clusters requires them to rotate around the C–C bonds to relieve

steric stress. In the central part of the model, this rotation is forbidden by the imposed D_{4h} symmetry as the ligand backbone lies in a mirror plane. Thus, the angles $S–C_1–H_{link}$ and $H_1–C_1–H_1$ are deformed from their optimal values in the gas phase. This change induces the observed increase in the QM and MM energies of the central part. In the MM energy of the total model, this effect is covered up by stronger van der Waals interaction.

In all four examples considered, the geometry of the cluster as well as of the ligands remained virtually unchanged when the unit cell was larger than a system specific threshold. The ligand chains were compressed in the end-on orientation according the dominating forces along the ligand backbones. As mentioned in the discussion of the relative total energies of the cluster $Cu_{13}(SCH_2CH_3)_8$, this behavior changed drastically below a certain threshold of the lattice constant. At values below 15 Å for the end-on and 10.3 Å for the interlocking orientation, the conformation switched "spontaneously" from **bdos** to **bdis**. In the end-on orientation, the whole ligand was compressed by 0.11 Å (difference between starting and final positions of the H_3 atoms) prior to the conformation change. In the interlocked cluster layer, the ligands were compressed by only 0.03 Å (atomic positions again). Although the spontaneous conformation change at strongly inter-ligand repulsions is desirable, no additional insight can be gained without further extensive study. Pertinent intra-molecular distances of both orientations of $Cu_{13}(SCH_2CH_2CH_3)_8$ systems examined changed less than 0.003 Å. They were not compressed until their conformations switched; however, it is likely that they might if the unit cell becomes sufficiently small. Even though the symmetry breaking lateral movement of the ligand chains within the x-y-plane was allowed in the $Cu_{13}(SCH_2CH_2CH_3)_8$ clusters, it did not occur in the current calculations.

7.3. Concluding Remarks

The above calculations on periodic two-dimensional cluster lattices show clearly the potential of the QM/MM method. The stabilization energy of cluster layers was determined for a model of van der Waals interaction only between ligand chains. Longer ligands were shown to stabilize cluster layers better. The stabilization energy per cluster increased by ~30 % when the model ligands were extended from ethylthiolate to propylthiolate. Cluster layers with interlocked ligand chains exhibit a considerably higher stabilization energy. The closer contact between ligand chains increases the stabilization energy by more than one order of magnitude. Concomitantly with this larger stabilization, the optimal lattice constant is reduced. In the

$Cu_{13}(SCH_2CH_3)_8$ model it decreases from 15.7 Å to 10.8 Å and in the $Cu_{13}(SCH_2CH_2CH_3)_8$ model from 18.3 Å to 11.7 Å. Geometry changes observed were small, except at very short lattice constants were the ligands changed their conformation.

8. Summary

The topic of this thesis was the application of the hybrid QM/MM method to ligand protected transition metal clusters and copper thiolate species have been chosen as examples. Three goals have been reached. The application of a QM/MM approach to transition metal clusters was validated by a detailed comparison with density functional calculations. A QM/MM method utilizing periodic boundary conditions was implemented. This implementation was then used to calculate the geometric and energetic properties of ordered arrays of ligand protected copper clusters.

In the first part, a consecutively refined cluster model was used to generate reference data for studying effects of ligand attachment to the cluster Cu_{13}. The bare cluster, a simplified sulfanyl (SH) ligand shell of 8 ligands and the ethylthiolate ligand were used to study the binding situation of the corresponding ligand model, the accuracy of the results and the computational feasibility. Then, the 16 conformers of $Cu_{13}(SCH_2CH_3)_8$ in D_{4h} symmetry were analyzed in detail at both the LDA level of density functional theory and with the corresponding hybrid QM/MM method. Energies were self-consistently calculated using the GGA BP86 functional at the LDA optimized structures.

The bare cluster Cu_{13} was shown to adopt a flat configuration with the parameter set used in this investigation. Successive reduction of symmetry constraints from O_h via D_{4h} to D_{2h} and C_{4v} revealed the relatively high D_{4h} symmetry as best tradeoff between accuracy of prediction versus computational expense. The total energy was shown not to change significantly under reduction of the symmetry constraints below D_{4h} (< 0.1 kcal/mol).

The ligand binding site investigation with sulfanyl model ligands in place of alkyl thiolates revealed the bridge-hollow binding site as energetically preferred compared to the on-top adsorption site. Binding energy and relaxation of the cluster geometry were affected by the binding site and the orientation of the ligand relative to the cluster. The sulfanyl model ligand showed a comparable binding energy to that of alkylthiolate ligands in the later calculations. However, the dependence of the binding energy on the adsorption site and the orientation was overestimated, as a comparison with other calculations and subsequently obtained results showed.

The calculations of the 16 conformers of $Cu_{13}(SCH_2CH_3)_8$ in D_{4h} symmetry using the LDA exchange-correlation functional illustrated strengths and weaknesses of that method. The bridge-hollow adsorption site was confirmed as most stable. However, due

to overestimated binding interaction between cluster core and ligand end groups, some on-top conformers were computed up to 40 kcal/mol more stable than the least stable bridge-hollow conformers. The ligand binding energies of on-top and bridge-hollow conformers were comparable in the range 65-77 kcal/mol. Structures with ligands adsorbed in bridge-hollow sites showed ligand binding energies larger or equal to on-top structures. The ligand-cluster interaction was strong enough to deform bond lengths in the cluster core by several 0.1 Å, depending on the conformation. In two of the bridge-hollow conformers the cluster core was even prolate (upright ellipsoidal, with two short main axes and one long one), in contrast to the other 14 conformers where the cluster core was oblate (flat ellipsoidal, with two long main axes and one short one) as in the ligand free state. The ligand chains wrapped around the cluster core in some conformers. In that way, atoms of the ligand end groups came into close contact with the cluster core. Whereas these contacts caused deformation of the cluster core relative to the bare cluster, they did not change the ligand geometry to a significant extent. However, the total or ligand binding energy was determined more by the binding site and the conformation of the ligands than by the cluster-ligand end group interaction. To illustrate this point, consider the conformer **bdos** (see Chapter 6.1.1 for the conformer nomenclature) which was found to be the most stable conformer, featuring the shortest H-Cu contacts and a large ligand binding energy of 76 kcal/mol. The conformer **buoe**, in contrast, is 18 kcal/mol less stable than the conformer **bdos**, it has no H-Cu contacts, but exhibits the highest ligand binding energy of 77 kcal/mol nevertheless.

The QM/MM calculations of the same system reproduced the QM results in most aspects. Here, a QM/MM implementation according the IMOMM method was applied, using TINKER as the MM program. The geometric structures of some conformers were nearly indistinguishable between QM and QM/MM calculations. However, the results differed where non-bonding interactions between atoms were involved. The density functional method at the LDA level describes non-bonding interaction between atoms generally as too attractive, resulting in too short distances between non-bonded atoms; the MM part of the QM/MM method describes these interactions as repulsive at such short distances, according to a parameterized potential. Thus, the short distances between the cluster core and ligands were enlarged in the corresponding conformers. This repulsion between atoms not sharing a common bond was identified as the cause of even small differences between QM and QM/MM geometries; examples are interactions between equatorial copper atoms of the cluster core and two not symmetry equivalent hydrogen atoms of the ligand end group (Cu_{eq}–H_2; Cu_{eq}–H_3) or hydrogen atoms of neighboring ligands in a plane perpendicular to the z axis (H_2-H_2'; H_3-H_3') or hydrogen

atoms interacting across the x-y-plane (H_2-H_2"; H_3-H_3"). In conformers, where the non-bonded interactions were negligible, most bond lengths were reproduced by the QM/MM method with an accuracy of 1 pm. The only exception was the C-C bond connecting QM and MM part of the model. This bond was consistently calculated 2 pm longer in the QM/MM approach, as a consequence of the empirical bond length parameter of the C-C bond in the MM3 force field, introduced by the QM/MM method. Bond angles were accurately reproduced in non-perturbed conformers, with deviations not exceeding 4°. The ordering of total and ligand binding energies reflected the changes in the conformer structures. QM/MM binding energies varied between 76 kcal/mol and 56 kcal/mol. They were smaller in most conformers than the corresponding QM binding energies. Only the conformers **buis** and the **buos** showed larger binding energies in the QM/MM calculations compared to the QM results (by 1.4 and 5.2 kcal/mol, respectively). The largest difference was found in the conformer **tdoe** with a ligand binding energy which was smaller in the QM/MM calculation by 8.6 kcal/mol. The energy ordering of conformers was similar, when conformers with strong non-bonding interactions were neglected.

These results demonstrated that the QM/MM method (in the form of the IMOMM strategy) is applicable to transition metal clusters with complex organic ligand shells. The ability of the MM approach to describe organic molecules at considerably lower computational costs complements the strength of the DF method to describe the complicated electronic structure of transition metal clusters. At the same time, the weaknesses of contemporary DF and MM methods are compensated. The electronic and geometric structure of transition metal clusters can not be described by the MM approach in a satisfactory fashion. Non-bonded interactions, which are described too attractive by the LDA functional, are replaced with an empirical force field utilizing a parameterized van der Waals term.

To allow the calculation of ordered structures of ligated transition metal clusters, the QM/MM implementation was extended to use the MM program DL_POLY_2, which provides the required capabilities. DL_POLY_2 can be augmented by further force field terms if necessary. The standard version of DL_POLY_2 was supplemented by specific interpolation functions and parameter sets required for the force field MM3. The QM/MM suite was adapted to the input and output format specific to DL_POLY_2. A functional test using a pentane model confirmed the accuracy of the QM/MM calculations (at the IMOMM level) using DL_POLY_2 as the MM program.

Application to a linear periodic arrangement of pentane molecules provided the functional test of the periodic capabilities of the implementation.

In the third part, the properties of two-dimensional layers of an alkylthiolated copper cluster were determined using the QM/MM implementation with periodic boundary conditions. Four different setups of layers were examined: two of the cluster $Cu_{13}(SCH_2CH_3)_8$ in the conformation **bdos**, and two for $Cu_{13}(SCH_2CH_2CH_3)_8$, featuring more extended propylthiolate ligands in the all-trans conformation of the ligands corresponding to **bdos**. For each cluster type, two arrangements were studied: with the ligand end groups oriented end-on or interlocking. The lattice constants were successively reduced to study the consequences for the stabilization energy of the layer. D_{4h} symmetry was imposed only on the central part of the models which contained $Cu_{13}(SCH_3)_8$, the ligand end groups experienced no symmetry restriction. The cluster layers in end-on ligand orientation showed stabilization energies by one order of magnitude smaller than in interlocking ligand orientation. The number of inter-cluster van der Waals contacts affected the stabilization. Thus, the stabilization energy is lower in the end-on ligand orientation models. For the same reason, the layers of clusters with ethylthiolate ligands showed ~30% smaller stabilization energies (2 kcal/mol, end-on; 22 kcal/mol, interlocking) than layers of clusters with propylthiolate ligands (3 kcal/mol, end-on; 32 kcal/mol, interlocking). In the model $Cu_{13}(SCH_2CH_3)_8$, the equilibrium lattice constant decreased from 15.7 Å (end-on) to 10.8 Å (interlocking) and in the model $Cu_{13}(SCH_2CH_2CH_3)_8$ from 18.3 Å (end-on) to 11.7 Å (interlocking). Thus, introduction of an additional methylene moiety into the ligand chain elongated the distance between clusters by 2.6 Å in the end-on, but only 0.9 Å in the interlocking orientation of clusters. The compression of the cluster layer beyond the equilibrium induced a change in the conformation of ligands from **bdos** to **bdis** for both models $Cu_{13}(SCH_2CH_3)_8$ at lattice constants of 15 Å in the end-on orientation of ligands and at 10.3 Å in the interlocked orientation. The increasingly repulsive van der Waals interaction between ligands at shorter lattice constants caused a sharp increase of the total energy of the clusters. The change of conformation reduced the van der Waals repulsion significantly.

This thesis showed the applicability of the QM/MM approach, in the form of the IMOMM method, to transition metal clusters with complex ligand shells. The QM/MM strategy opens the possibility for detailed investigations of these complex systems which, if treated by a first-principles method, would lie beyond the current computational feasibility.

Appendix A

Adaptation of the MM3 Force Field Parameters for Use in DL_POLY_2

Bonds

Because of the ease of computation, the bond oscillator function is often approximated using a polynomial fit. The MM3 implementation uses the fourth order approximation:

$$E_{bond} = 71.94\, k_s\, (r_{ij} - r_0)^2\, [1 - 2.55\, (r_{ij} - r_0) + (7/12) \bullet 2.55^2 \bullet (r_{ij} - r_0)^2] \,, \qquad (9.1)$$

where k_s is the energy constant pertaining to the atom pair, r_{ij} is the distance between the two atoms while r_0 is the equilibrium distance specific for the pair. This term is written as:

$$E_{bond} = \frac{1}{2} k_1 (r_{ij} - r_0)^2 + \frac{1}{3} k_2 (r_{ij} - r_0)^3 + \frac{1}{4} k_3 (r_{ij} - r_0)^4 \,, \qquad (9.2)$$

in the DL_POLY_2 implementation, where the k_i are independent constants, which may be converted by comparison with Eq. 9.1:

$$\begin{aligned} k_1 &= k_s \bullet 71.94 \bullet 2 \\ k_2 &= -k_s \bullet 71.94 \bullet 2.55 \bullet 3 \\ k_3 &= k_s \bullet 71.94 \bullet 2.55^2 \bullet 7/12 \bullet 4 \end{aligned} \qquad (9.3)$$

Note that the units are omitted for k_s and k_i, but are suitably chosen to result in an energy of the unit [kcal/mol].

Angles

The energy contribution of angular potentials are computed for any two atoms which are in turn bound to a third. The angle θ may assume values between 0° and 180°. The length of distances $\vec{r}_{ik}$ and $\vec{r}_{kj}$ do not enter this energy expression. There are however extended MM implementations, which take these items into account.[121]

The contribution of the bond angle potential to the total energy can be expressed in multiple ways. One of the most often used ones is the polynomial approximation, as used in the MM3 force field in a sixth order polynomial:

$$E_\theta = 0.021914 \bullet k_\theta \bullet (\theta - \theta_0)^2 \, [1-0.014(\theta - \theta_0) + 5.6 \bullet 10^{-5} (\theta - \theta_0)^2 - 7.0 \bullet 10^{-7} (\theta - \theta_0)^3 + 9.0 \bullet 10^{-10} (\theta - \theta_0)^4] \quad , \tag{9.4}$$

where k_θ is a suitably chosen (in value and unit) energy constant depending on the atom types of i, j and k.

The fifth and sixth order terms were introduced in the MM3 definition only in the latest revision of the MM2 force field. Again, the coefficients had to be adjusted to the corresponding DL_POLY_2 implementation:

$$E_\theta = \frac{1}{2} k_1 (\theta - \theta_0)^2 + \frac{1}{3} k_2 (\theta - \theta_0)^3 + \frac{1}{4} k_3 (\theta - \theta_0)^4 + \frac{1}{5} k_4 (\theta - \theta_0)^5 + k_5 \frac{1}{6} (\theta - \theta_0)^6 \quad , \tag{9.5}$$

where k_i are the independent coefficients converted by using the following equations:

$$\begin{aligned} k_1 &= k_\theta \bullet 2 \bullet 0.021914 \\ k_2 &= -k_\theta \bullet 3 \bullet 0.021914 \bullet 0.014 \\ k_3 &= k_\theta \bullet 4 \bullet 0.021914 \bullet 5.6 \bullet 10^{-5} \\ k_4 &= -k_\theta \bullet 5 \bullet 0.021914 \bullet 7.0 \bullet 10^{-7} \\ k_5 &= k_\theta \bullet 6 \bullet 0.021914 \bullet 9.0 \bullet 10^{-10} \end{aligned} \tag{9.6}$$

The units of the individual coefficients k_θ and k_i are suitably chosen to result in an energy of the unit [kcal/mol]. The MM3 force field proposes three values of the equilibrium angle, depending on whether there are 0, 1 or 2 hydrogen atoms bound to the central atom apart from the atoms participating in the angular interaction.

Dihedral angles

The dihedral angle is the angle between the two planes defined by the atom triples (i, k, l) and (k, l, j) respectively. This angle is dependent on the element and atom types of atoms i to k. The bond lengths $\vec{r}_{ik}$, $\vec{r}_{kl}$ and $\vec{r}_{lj}$ as well as the angles θ_{ikl} and θ_{klj} do not enter the equation. Note that there are force field types, that include some or all of these items into higher order terms.

The MM3 force field as well as the DL_POLY_2 implementation of included terms approximate the dihedral angle interaction as a Fourier series of three cosine terms:

$$E_\omega = (k_1/2) \bullet (1 + \cos\omega) + (k_2/2) \bullet (1 - \cos 2\omega) + (k_3/2) \bullet (1 + \cos 3\omega) \quad , \tag{9.7}$$

where the k_i are independent coefficients. The respective k_i have suitably chosen units to result in energies of the unit [kcal/mol].

van der Waals Interactions

Atoms, which are not bound to one another nevertheless polarize each other which can be approximately described by the picture of induced dipole moments. This induced dipole-dipole interaction results in an energy gain at a certain distance and respective forces acting on these atoms.

Elements possess an optimum distance at which the interaction between them results in a slight energy gain in the range of a few kcal/mol. To be able to describe the effect for all possible interactions, it would be necessary to include pair terms for every atom pair. This route was suggested in the DL_POLY_2 implementation, allowing definition of van der Waals interactions only as atom pair parameters regardless of their type or element. The MM3 force field suggests a more uniform approach, defining these parameters as atom type based. This means that all atoms of one atom type possess the same van der Waals (and other non-bonded) interaction behavior.

The elementary functional form used to describe the interaction was suggested by Lewis and is generally named Buckingham potential[226,227] and is equal in TINKER and DL_POLY2 implementations:

$$E_{vdW} = k_1 \left(\frac{r_0}{r_{ij}} \right)^6 + k_2 \exp\left\{ k_3 \frac{r_{ij}}{r_0} \right\} \tag{9.8}$$

In the MM3 implementation the coefficient k_i are combined, reducing the Eq. 9.8 to:

$$E_{vdW} = k_{vdW} \left[-2.25 \left(\frac{r_0}{r_{ij}} \right)^6 + 1.84 \bullet 10^5 \exp\left\{ 12 \bullet \frac{r_{ij}}{r_0} \right\} \right] \tag{9.9}$$

DL_POLY_2 uses the slightly different form noted below:

$$E_{vdW} = -k_1 \bullet \left(\frac{1}{r_{ij}} \right)^6 + k_2 \exp\left\{ -\frac{r_{ij}}{k_3} \right\} \tag{9.10}$$

The individual coefficients are converted using the following equations:

$$k_1 = k_{vdW} \bullet 2.25 \bullet r_0^6$$
$$k_2 = k_{vdW} \bullet 1.84 \bullet 10^5 \qquad (9.11)$$
$$k_3 = \frac{r_0}{12}$$

As atom type based coefficients are used in the MM3 implementation, these have to be converted to atom pair based values:

$$r_{0,\,vdW}[t(i),t(j)] = r_{0,\,vdW}[t(i)] + r_{0,\,vdW}[t(j)]$$
$$k_{vdW}[t(i),t(j)] = \frac{k_{vdw}[t(i)] + k_{vdW}[t(j)]}{2} \quad , \qquad (9.12)$$

where $r_{0,\,vdW}[t(i),t(j)]$ is the pair based van der Waals distance parameter (not the respective van der Waals radius) in DL_POLY_2 and $r_{0,\,vdW}[t(i)]$ and $r_{0,\,vdW}[t(j)]$ are the respective atom type based parameters in the MM3 force field definition. The parameter t(x) is a specifier for the MM3 atom type (and its DL_POLY_2 analogue).

The constants $k_{vdW}[t(i),t(j)]$, $k_{vdW}[t(i)]$ and $k_{vdW}[t(j)]$ specify the energy constants for the atom pair and the atom types, respectively. Note that some atom type pairs, i.e. C-H, possess special, pre-computed pair parameters for their van der Waals interaction, which can be converted straightforwardly in Eqs. (9.11).

Charges

In the current implementation of the QM/MM approach, the treatment of charges (atomic or otherwise) is not included. It is not always possible to assign a given amount of electronic density, i.e. charge, to an individual nucleus.[96] While the dipole moment of the whole molecule is experimentally accessible,[228-230] the contributions by individual atoms are not.

The problem all force field implementations face is the assignment of a charge distribution model for molecular fragments (mostly atoms). Nearly all force field implementations assign point charges to atom types reflecting partial charges or contributions to dipole moments, which are fitted to experimental data. The number of different atom types increases with this approach, as elements may exhibit different point charges in different chemical environments. The QM/MM approach aggravates this problem, as it adds an unphysical moiety to the equations whose particular charge is generally not known, although approximations, i.e. by Mullikan analysis, were tried.[231]

The implementation of accurate treatment of charges was thus left out in this work. The MM3 force field implementation differs from the general idea in that it assigns bond dipoles to atomic dimers. While not fundamentally different,[127,232,233] this approach complicates the adaptability to the approach used in DL_POLY_2 and the conversion of parameters.

Appendix B

Table 24 Total energies of $Cu_{13}(SH)_8$ in various conformations, see Section 5.2.2

ligand binding site	ligand orientation	total energy [au]
bridge-hollow	up	-24381.473820164
bridge-hollow	out	-24381.468292701
on-top	up	-24381.399306173
on-top	out	-24381.196774146

Appendix C

Table 25 Total energies (DF-BP86) of the conformers of $Cu_{13}(SCH_2CH_3)_8$

conformation	total energy [au]
buis	-25062.566046866
buie	-25062.516939880
buos	-25062.504308554
buoe	-25062.551598802
bdis	-25062.578130397
bdie	-25062.533167365
bdos	-25062.580361036
bdoe	-25062.485671940
tuis	-25062.531560298
tuie	-25062.485962958
tuos	-25062.531560298
tuoe	-25062.489636889
tdis	-25062.448607300
tdie	-25062.412338157
tdos	-25062.479704818
tdoe	-25062.395388363

Table 26 QM reference energies of $Cu_{13}(SCH_2CH_3)_8$ (DF-BP86)

reference system	total energy [au]
Cu_{13} D_{4h}	-21242.0120780013
SCH_2CH_3 C_s, staggered	-477.4504604819
SCH_2CH_3 C_s, eclipsed	-477.4443556465

Table 27 Angles of the cluster-ligand interface in QM calculations of the 16 conformers of $Cu_{13}(SCH_2CH_3)_8$

conformation	Cu_{ax}-S-C_1	Cu_{eq}-S-C_1
buis	137.3	149.7
buie	130.5	162.0
buos	92.8	149.4
buoe	121.1	177.8
bdis	105.2	64.1
bdie	103.9	62.5
bdos	114.0	81.6
bdoe	118.3	87.6
tuis	97.5	119.2
tuie	100.5	121.4
tuos	97.5	119.2
tuoe	98.5	119.8
tdis	97.8	83.5
tdie	92.4	84.8
tdos	99.0	91.3
tdoe	99.7	91.7

Table 28 Ligand angles of the 16 conformers in the QM calculations of $Cu_{13}(SCH_2CH_3)_8$

conf.	S-C_1-C_2	S-C_1-H_1	C_1-C_2-H_2	C_1-C_2-H_3	H_1-C_1-H_1	H_2-C_2-H_2	H_2-C_2-H_3
buis	108.7	107.1	110.1	111.7	109.6	106.7	109.0
buie	110.8	105.4	111.9	109.1	109.3	108.2	107.8
buos	107.3	108.1	110.3	110.9	108.1	107.8	108.7
buoe	109.6	105.2	111.8	110.5	109.2	108.2	107.2
bdis	108.5	109.9	109.7	111.3	110.2	107.9	109.0
bdie	110.3	109.1	112.1	109.5	110.3	107.8	107.5
bdos	112.6	106.4	108.6	115.3	109.1	111.3	106.5
bdoe	117.7	103.7	113.6	109.3	106.9	110.2	104.7
tuis	108.4	108.1	110.0	111.6	107.8	107.7	108.8
tuie	114.9	105.4	112.2	110.6	107.6	108.8	106.3
tuos	108.4	108.1	110.0	111.6	107.8	107.7	108.8
tuoe	109.7	107.3	112.1	109.8	107.2	108.0	107.3
tdis	109.8	107.3	110.4	111.6	108.0	107.2	108.5
tdie	113.7	105.0	111.6	110.0	106.3	108.2	107.7
tdos	112.7	106.2	109.2	112.0	108.8	108.5	109.0
tdoe	114.4	105.4	112.8	109.6	107.4	109.9	105.6

Appendix D

Table 29 Bond lengths of $Cu_{13}(SCH_2CH_3)_8$ at different lattice constants, in the gas phase geometry (100 Å), before (15.1 Å) and after (14.9 Å) the change of the conformation of the ligand from **bdos** to **bdis**, in Å

	lattice constant = 100 Å	lattice constant = 15.1 Å	lattice constant = 14.9 Å	**bdis** gas phase
	bdos	**bdos**	**bdis**	
Cu_{ce}-Cu_{eq}	2.604	2.624	2.732	2.412
Cu_{ce}-Cu_{ax}	2.073	2.067	2.048	2.146
Cu_{eq}-Cu_{ax}	2.212	2.222	2.289	2.152
Cu_{eq}-S	2.127	2.128	2.109	2.575
Cu_{ax}-S	2.219	2.206	2.206	2.254
S-C_1	1.828	1.819	1.823	1.853
C_1-C_2	1.527	1.524	1.526	1.529
C_1-H_1	1.103	1.103	1.102	1.115
C_2-H_2	1.114	1.115	1.113	1.113
C_2-H_3	1.113	1.109	1.113	1.113

Table 30 Partial energies of the QM/MM total energy of the $Cu_{13}(SCH_2CH_3)_8$ layer in end-on orientation at different lattice constants

lattice constant [Å]	QM energy central part [au]	MM energy central part [au]	MM energy total molecule [au]
20.0	-24693.2316043799	6.9063438	6.9031566
18.6	-24693.2315981924	6.9063438	6.9029972
17.6	-24693.2316000026	6.9065032	6.9022004
17.1	-24693.2315749741	6.9065032	6.9018817
16.9	-24693.2315592645	6.9065032	6.9015630
16.7	-24693.2315457207	6.9065032	6.9014036
16.5	-24693.2315237892	6.9058657	6.9004475
16.3	-24693.2315123424	6.9057064	6.8999694
16.1	-24693.2315180362	6.9053876	6.8994913
15.9	-24693.2315505436	6.9049096	6.8986945
15.7	-24693.2316288214	6.9037940	6.8975790
15.5	-24693.2317007830	6.9002881	6.8945512
15.3	-24693.2315170601	6.8900891	6.8854676
15.1	-24693.2294341055	6.9167022	6.9128776
14.9	-24693.2277645679	6.5444372	6.5382222
14.7	-24693.2277647174	6.5444372	6.5380628

Table 31 Partial energies of the QM/MM total energy of $Cu_{13}(SCH_2CH_3)_8$ in interlocking orientation for various lattice constants; unit cell rotated by 22.5˚ with respect to the cluster

lattice constant [Å]	QM energy central part [au]	MM energy central part [au]	MM energy total molecule [au]
17.1	-24693.2316223536	6.0985479	6.0945639
16.1	-24693.2316138951	6.0985479	6.0942452
15.7	-24693.2316082267	6.0982292	6.0939265
15.3	-24693.2315993114	6.0982292	6.0937671
14.9	-24693.2315861191	6.0979105	6.0929703
14.5	-24693.2315744699	6.0979105	6.0924923
14.1	-24693.2315311188	6.0972731	6.0910580
13.7	-24693.2315060394	6.0972731	6.0899425
13.3	-24693.2314243501	6.0961575	6.0873927
12.9	-24693.2313189809	6.0945639	6.0832494
12.1	-24693.2309691386	6.0916955	6.0720942
11.9	-24693.2308154271	6.0896238	6.0669947
11.7	-24693.2306870839	6.0891457	6.0628513
11.5	-24693.2305988822	6.0889863	6.0588673
11.3	-24693.2305485779	6.0896238	6.0556801
11.1	-24693.2307411262	6.0931297	6.0558395
10.9	-24693.2311977460	6.1009383	6.0618951
10.7	-24693.2318620808	6.1138465	6.0759188
10.5	-24693.2324450764	6.1301012	6.0974324
10.3	-24693.2274698949	5.7369601	5.7293108

Table 32 QM/MM total energy of gas phase structures used in the calculation of the QM/MM relative total energies of $Cu_{13}(SCH_2CH_3)_8$ and $Cu_{13}(SCH_2CH_2CH_3)_8$ layers in end-on and interlocking orientations, respectively

cluster system		total energy [au]
$Cu_{13}(SCH_2CH_3)_8$	end-on	-24693.2347915799
$Cu_{13}(SCH_2CH_3)_8$	interlocking	-24693.2356102000
$Cu_{13}(SCH_2CH_2CH_3)_8$	end-on	-24693.2315022938
$Cu_{13}(SCH_2CH_2CH_3)_8$	interlocking	-24693.2307599000

Table 33 Partial energies contributing to the QM/MM total energy for interlocking orientation of $Cu_{13}(SCH_2CH_2CH_3)_8$ at different lattice constants

lattice constant [Å]	QM energy central part [au]	MM energy central part [au]	MM energy total molecule [au]
18.7	-24693.2312356632	6.1077908	6.1079502
17.7	-24693.2312129392	6.1077908	6.1077908
16.7	-24693.2311973382	6.1079502	6.1074721
15.7	-24693.2311447389	6.1084283	6.1065159
14.7	-24693.2310422220	6.1098625	6.1047630
13.7	-24693.2307051879	6.1122529	6.0993447
13.5	-24693.2305473168	6.1120935	6.0964763
13.3	-24693.2303882132	6.1117748	6.0932891
13.1	-24693.2301576076	6.1120935	6.0899425
12.9	-24693.2299393899	6.1120935	6.0857991
12.5	-24693.2294088392	6.1119342	6.0757595
12.1	-24693.2295401360	6.1148027	6.0685883
11.7	-24693.2309364808	6.1340852	6.0851617
11.3	-24693.2320698455	6.1608577	6.1288263

Appendix E

Basis Sets

Hydrogen (Z = 1) (6s, 1p) basis set

Reference: [188]

Contraction : (6s, 1p) $\rightarrow$ [4s, 1p]

	s	p
α_1	0.089891	1.000000
α_2	0.258053	
α_3	0.797670	
α_4	2.823854	
α_5	12.409558	
α_6	82.636374	

Carbon (Z = 6) (9s, 5p, 1d) basis set

Reference: [188]

Contraction: (9s, 5p, 1d) $\rightarrow$ [5s, 4p, 1d]

	s	p	d
α_1	0.156590	0.12194	0.60000
α_2	0.511900	0.38554	
α_3	2.418049	1.20671	
α_4	6.175776	4.15924	
α_5	16.823562	18.84180	
α_6	50.815942		
α_7	178.350830		
α_8	782.204795		
α_9	5240.635258		

Sulfur (Z = 16) (12s, 9p, 2d) basis set

Reference: [188]

Contraction: (12s, 9p, 2d) $\rightarrow$ [6s, 5p,2d]

	s	p	d
α_1	0.157093	0.102867	0.183000
α_2	0.434389	0.291781	0.658000
α_3	2.142870	0.773628	
α_4	5.570960	2.242910	
α_5	18.116800	5.502670	
α_6	43.157900	13.893800	
α_7	108.669000	37.496000	
α_8	296.954000	116.981000	
α_9	901.843000	494.274000	
α_{10}	3168.040000		
α_{11}	13921.800000		
α_{12}	94181.100000		

Copper (Z = 29) (15s, 11p, 6d) basis set

Reference: [188]

Contraction: (15s, 11p, 6d) $\rightarrow$ [6s, 4p, 3d]

	s	p	d
α_1	0.040791	0.099100	0.149100
α_2	0.113303	0.265000	0.414875
α_3	0.330500	0.711445	1.473290
α_4	0.964080	1.906670	4.516280
α_5	2.578480	4.693820	13.549000
α_6	9.393570	11.743500	48.543900
α_7	22.298300	27.055100	
α_8	67.359100	65.323900	
α_9	158.399000	172.195000	
α_{10}	395.099000	532.106000	
α_{11}	1071.970000	2245.290000	
α_{12}	3239.820000		
α_{13}	11373.400000		
α_{14}	50072.900000		
α_{15}	337200.000000		

Bibliography

[1] Lu, D.-L.; Tanaka, K. J. *Phys. Chem. B* **1997**, 101, 4030

[2] Hohenberg, P.; Kohn, W. *Phys. Rev. B* **1964**, 136, 864

[3] Kohn, W.; Sham, L.J. *Phys. Rev A.* **1965**, 140, 1133

[4] Warshel, A.; Karplus, M. *J. Am. Chem. Soc.* **1972**, 94, 5612

[5] Maseras, F.; Morokuma, K. *J. Comput. Chem.* **1995**, 16, 1170

[6] Matsubara, T.; Maseras, F.; Koga, N; Morokuma, K. *J. Phys. Chem.* **1996**, 100, 2573-2580

[7] Whetten, R.L.; Khoury, J.T.; Alvarez, M.; Murthy, S.; Vezmar, I.; Wang, Z.L.; Stephens, P.W.; Cleveland, C.L.; Luedtke, W.D.; Landmann, U. *Adv. Mater.* **1996**, 8, 428

[8] Sarathy, K.V.; Thomas, P.J.; Kulkarni, G.U.; Rao, C.N.R. *J. Phys. Chem. B* **1999**, 103, 399

[9] Brust, M.; Walker, M.; Bethell, D.; Schiffrin, D.; Whyman, R. *J. Chem. Soc., Chem. Commun.* **1994**, 801-802

[10] Nuzzo, R.G.; Allara, D.L. *J. Am. Chem. Soc.* **1983**, 105, 4481

[11] Poirier, G.E. *Chem. Rev.* **1997**, 97, 1117

[12] Rohwerder, M.; Stratmann, M. *MRS Bull.* **1999**, 24, 43

[13] Boal, A.K.; Rotello, V.M. *J. Am. Chem. Soc.* **2000**, 122, 734

[14] Holmlin, R.E.; Haag, R.; Chabiyc, M.L.; Ismagilov, R.F.; Cohen, A.E.; Terfort, A.; Rampi, M. Whitesides, G. M. *J. Am. Chem. Soc.* **2001**, 123, 5075

[15] Finklea, H.O. in Bard, A.J.; Rubinstein, I., Eds. Electroanalytical Chemistry 1996, 19, 109

[16] Luedtke, W.D.; Landmann, U. *J. Phys. Chem.* **1996**, 100, 32, 13323

[17] Whetten, R.L. et al. In *Chemical Physics of Fullerenes 5 and 10 Years later*, Andreoni, W. Ed. Kluwer, Dordrecht, **1996**, 475

[18] Hornayak, G.L.; Kröll, M.; Pugin, R.; Sanitowski, T.; Schmid, G.; Bovin, J.-O.; Karrson, G.; Hofmeister, H.; Hopfe, S. *Chem. Eur. J.* **1997**, 3, 1951

[19] Brust, M.; Walker, M.; Bethell, D.; Schiffrin, J.D.; Whyman, R. *J. Chem. Soc., Chem. Comm.* **1994**, 801

[20] Brust, M.; Bethell, D.; Kiely, J.D.; Schiffrin, J.D. *Langmuir* **1998**, 14, 5425

[21] Sarathy, K.V.; Thomas, P.J.; Kulkarni, G.U.; Rao, C.N.R. *J. Phys. Chem. B* **1999**, 103, 399

[22] Alivisatos, A.P.; Johnsson, K.P.; Peng, X., Wilson, T.E.; Loweth, C.J.; Burchez, M.P. Jr.; Schulz, P.G. *Nature*, **1996**, 382, 609
[23] Sarathy, K.V.; Kulkarni, G.U.; Rao, C.N.R. *Chem. Commun.* **1997**, 537
[24] Sarathy, K.V.; Raina, G.; Yadav, R.T.; Kulkarni, G.U.; Rao, C.N.R. *J. Phys. Chem. B* **1997**, 101, 9876
[25] Kiely, C.J.; Fink, J.; Brust, M.; Bethell, D.; Schiffrin, J.D. *Nature* **1998**, 396, 444
[26] Whetten, R.L.; Khoury, J.T.; Alvarez, M.M.; Murthy, S.; Vezmar, I.; Wang, Z.; Stephens, P.W.; Clevend, Ch.L.; Luedtke, W.D.; Landman, U. *Adv. Mater.* **1996**, 8, 428
[27] Harfenist, S.A.; Wang, Z.L.; Whetten, R.L.; Vezmar, I.; Alvarez, M.M. *Adv. Mater.* **1997**, 9, 817
[28] Chi, L.F.; Rakers, S.; Drechsler, T.; Hartig, M.; Fuchs, H.; Schmid, G. *Thin Solid Films* **1998**, 329, 520
[29] Dorogi, M.; Gomez, J.; Osifchin, R.G.; Andres, R.P.; Reifenberger, R. *Phys. Rev. B* **1995**, 52, 9071
[30] Dubois, J.G.A.; Gerrittsen, J.W.; Shafranjuk, S.E.; Boon, E.F.G.; Schmid, G.; van Kempen, H *Europhys. Lett.* **1996**, 33, 279
[31] Schön, G.; Simon, U. *Colloid. Polym. Sci.* **1995**, 273, 101
[32] Collier, C.P.; Saykally, R.J.; Shiang, J.J.; Henrichs, S.E.; Heath, J.R. *Science* **1997**, 277, 1978
[33] Turton, R. *The Quantum Dot: A Journey into the Future of Microelectronics*; Oxford University Press: New York, **1995**
[34] Valden, M.; Lai, X.; Goodman, D.W. *Science*, **1998**, 281, 1647
[35] Chen, S.; Sommers, J.M. *J. Phys. Chem. B* **2001**, 105, 8816-8820
[36] Engler, E.M.; Andose, J.D.; Schleyer, P.v.R. *J. Am. Chem. Soc.* **1973**, 95, 8005
[37] Altona, C.L.; Faber, D.H. Top. *Curr.Chem.* **1974**, 45, 1
[38] Dunitz, J.D.; Burgi, H.B. MTP International Reviews of Science, Series ; *Chemical Crystallography*, Robertson, J.M.R., Ed.; Buttersworths: London, **1975**; p 81
[39] Allinger, N.L. *Adv. Phys. Org. Chem.* **1976**, 13, 1
[40] Singh, U.C.; Kollman, P.A. *J. Comput. Chem.* **1986**, 7, 718
[41] Wood, W. W.; Parker, F.R. *J. Chem. Phys.* **1957**, 27, 720
[42] Theodorou, D. N.; Suter, U. W. *J. Chem. Phys.* **1985**, 82, 2, 955

[43] Ponder, J.W.; et al. *TINKER Software Tools for Molecular Design*, **1990-1999**
[44] Smith, W.; Forrester, T.R. *DL_POLY_2* , Daresbury Lab. **1998**
[45] Cotton, F.A. *Q. Rev. Chem. Soc.* **1966**, 416
[46] Atkins, P.; de Paula, J. *Atkins' Physical Chemistry*, Oxford University Press, Oxford, **2001**
[47] Aiyer, H.N.; Vijayakrishnan, V.; Subanna, G.N.; Rao, C.N.R. *Surf. Sci.* **1994**, 313, 393
[48] Johnson, D.C.; Benfield, R.E.; Edwards, P.P.; Nelson, W.J.H.; Vargas, M.D. *Nature*, **1985**, 314, 231
[49] Volotkin, Y.; Sinzig, J.; de Jong, L.J.; Schmid, G.; Vargaftik, M.N.; Moiseev, I.I. *Nature*, **1996**, 384, 624
[50] Vijayakrishnan, V; Chainani, A.; Sarma, D.D.; Rao, C.N.R. *J. Phys. Chem.* **1992**, 96, 8679
[51] Busani, R.; Folker, M.; Chesnovsky, O. *Phys. Rev. Lett.* **1998**, 81, 3836
[52] Rademann, K.; Rademann, O.D.; Schlauf, M.; Even, V. Hensel, F. *Phys. Rev. Lett.* **1992**, 69, 3208
[53] Fendler, J.H. Ed.; *Nanoparticles and Nanostructured Films*, Wiley-VCH, Weinheim, **1998**
[54] Brack, M. *Spec. d. Wiss.* **1998**, 32-37
[55] Buck, U. *Phys. Blätter* **1994**, 50, 11, 1052
[56] Krüger, S., Seemüller, T., Wörndle, Rösch, N., *Int. J. Quantum Chem.* **2000**, 80, 567
[57] Krüger, S.; Vent, S.; Rösch, N. *Ber. Bunsenges. Phys. Chem.* **1997**, 101, 1640
[58] Häberlen, O.D.; Chung, S.-C.; Stener, M.; Rösch, N. *J. Chem. Phys.* **1997**, 106, 5189
[59] Cotton, F.A.; Wilkinson, G. *Advanced Inorganic Chemistry*, Wiley, New York, **1998**
[60] Rademann, K.; Rademann, O.D.; Schlauf, M.; Even, V.; Hensel, F. *Phys. Rev. Lett.* **1992**, 96, 3208
[61] Teo, B.K.; Zhang, H.; Kean, Y.; Dang, H.; Shi, X. *J. Chem. Phys.* **1993**, 99, 4, 2929-2941
[62] Nuzzo, R.G.; Zegarski, B.R.; Dubois, L.H. *J. Am.Chem. Soc.* **1987**, 109, 733
[63] Grönbeck, H.; Curioni, A.; Andreoni, W. *Int. J. Quantum Chem.* **2000**, 80, 598
[64] Grönbeck, H.; Curioni, A.; Andreoni, W. *J. Am. Chem. Soc.* **2000**, 122, 3839

[65] Fenter, P.; Eberhardt, A.; Eisenberger, P. *Science* **1994**, 266, 1216
[66] Hostetler, M.J.; Templeton, A.C.; Murray, R.W. *Langmuir* **1999**, 15, 3782
[67] Hasan, M.; Bethell, D.; Brust, M. *J. Am. Chem. Soc.* **2002**, 124, 7, 1132
[68] Leff, D.V.; Ohara, P.C.; Heath, J.; Gelbart, W.M. *J. Phys. Chem.* **1995**, 99, 7036
[69] Edwards, P.P.; Johnston, R.L.; Rao, C.N.R.; *Metal Clusters in Chemistry* (Eds. Braunstein, P.; Oro, G.; Raithby, P.R.), Wiley-VCH, **1998**
[70] Simon, N.J.; Drexler, E.S.; Reed R.P. *NIST MN 177*
[71] Busani, R.; Folker, M.; Chesnovsky, O. *Phys. Rev. Lett.* **1998**, 81, 3836
[72] Heaton, B.T. *Phil. Trans. R. Soc.* London, **1982**, A308, 95
[73] Chung, S.-C.; Krüger, S.; Schmidbaur, H.; Rösch, N. *Inorg. Chem.* **1996**, 35, 5387
[74] Chatt, J.; Duncanson, L.A. *J. Chem. Soc.* **1953**, 2939
[75] Rao, C.N.R.; Kulkarni, G.U.; Thomas, P.J.; Edwards, P.P. *Chem. Eur. J.* **2002**, 8, 1, 29
[76] Rao, C.N.R.; Kulkarni, G.U.; Thomas, P.J.; Edwards, P.P. *Chem. Soc. Rev.* **2000**, 29, 27
[77] Shipway, A.N.; Katz, E.; Willmer, I. *Chem. Phys. Chem.* **2000**, 1, 18
[78] Schmid, G.; Chi, L.F. *Adv. Mater.* **1998**, 10, 515
[79] Wuelfing, W.P.; Zamborini, F.P.; Templeton, A.C.; Wen, X.; Yoon, H.; Murray, R.W. *Chem. Mater.* **2001**, 13, 87
[80] Pileni, M.P. *New J. Chem.* **1998**, 693
[81] Thomas, P.J.; Kulkarni, G.U.; Rao, C.N.R. *J. Phys. Chem. B* **2000**, 104, 8138
[82] Whetten, R.L.; Shafigullin, M.M.; Khoury, J.T.; Shaaf,T.G.; Vezmar, I.; Alvarez, M.M.; Wilkinson, A. *Acc. Chem. Res.* **1999**, 32, 397
[83] Ohara, P.C.; Leff, D.V.; Heath, J.R.; Gelbart, W.M. *Phys. Rev. Lett.* **1995**, 75, 3466
[84] Korgel, B.A.; Gullam, S.; Conolly, D.; Fitzmaurice, D. *J. Phys. Chem. B* **1998**, 102, 8379
[85] Russier, V.; Petit, C.; Legrand, C.; Pileni, M.P. *Phys. Rev. B* **2000**, 62, 3910
[86] Petit, C.; Pileni, M.P. *Appl. Surf. Sci.* **2000**, 162-163, 519
[87] Petit, C.; Taleb, A.; Pileni, M.P. *Adv. Mater.* **1998**,10, 259
[88] Sun, S.; Murray, C.B.; Weller, D.; Folks, L.; Maser, A. *Science* **2000**, 287, 1989
[89] Brust, M.; Bethell, D.; Shiffrin, D.J.; Kiely, C.J. *Adv. Mater.* **1995**, 7, 795

[90] Janes, D.B.; Kolagunta, V.R.; Osifchin, R.G.; Bielefeld, J.D.; Andres, R.P.; Henderson, J.I.; Kubiak, C.P. *Superlattices Microstruct.* **1995**, 18, 275
[91] Kagan, C.R.; Murray, C.B.; Bawendi, M.G. *Phys. Rev. B* **1996**, 54, 8633
[92] Snow, A.W.; Wohltjen, H. *Chem. Mater.* **1998**, 10, 947
[93] Liu, Y.; Wang, Y.; Claus, R.O. *Chem. Phys. Lett.* **1998**, 298, 315
[94] von Barth, U. in *Many Body Phenomena at Surfaces*: Langreth, D.; Suhl, H. Eds.; New York, Academic, **1984**, p. 3
[95] Dreizler, R.M.; da Providencia, J. *Density Functional Methods in Physics*, **1985**, New York, Plenum
[96] Holthausen, M.C.; Koch, W. *A Chemist's Guide to Density Functional Theory*, Wiley-VCH, **2000**
[97] Janak, J.F. *Phys. Rev. B* **1978**, 18, 7165
[98] Perdew, J.P.; Parr, R.G.; Levy, M.; Balduz, J.L. Jr. *Phys. Rev. Lett.* **1982**, 49, 1691
[99] Payne, M.C.; Teter, M.P.; Allan, D.C.; Arias, T.A.; Joannopoulos, J.D. *Rev. of Mod. Phys.* **1992**, 64, 4, 1045
[100] Hedin, L.; Lundqvist, B.I. *Phys. Rev. B* **1976**, 13, 4174
[101] Vosko, S.H.; Wilk, L.; Nusair, N. *Can. J. Phys.* **1980**, 58, 1200
[102] Becke, A.D. *Phys. Rev. A* **1988**, 38, 3098
[103] Burke, K.; Perdew, J.P.; Wang, Y. *Electronic Density Functional Theory*, Plenum Press, New York, **1998**
[104] Laming, G.J.; Termath, V.; Handy, N.C. *J. Chem. Phys.* **1993**, 99, 8765
[105] Becke, A.D. *J. Chem. Phys.* **1993**, 98, 1372
[106] Becke, A.D. *J. Chem. Phys.* **1993**, 98, 5648
[107] Stevens, P.J.; Devlin, J.F.; Chabalowski, C.F.; Frisch, M.J. *J. Phys. Chem.* **1994**, 98, 11623
[108] Engler, E.M.; Andose, J.D.; Schleyer, P.v.R. *J. Am. Chem. Soc.* **1973**, 95, 8005
[109] Rasmussen, K.; *Potential Energy Functions in Conformational Analysis*, Springer Verlag, Berlin **1985**
[110] Rappé, A.K.; Casewit, C.J. *Molecular Mechanics across Chemistry*, University Science Books, Sausalito, CA, **1997**
[111] Comba, P.; Hambley, T.W. *Molecular Modeling of Inorganic Compounds*, VCH, New York, **1995**
[112] Weiner et al. *J. Am. Chem. Soc.* **1983**, 106, 765

[113] Bartell, L.S. *J. Am. Soc.* **1977**, 99, 3279

[114] Allinger, N.L. *J .Am. Soc.* **1977**, 99, 8127

[115] Burkert, U.; Allinger, N.L. *Molecular Mechanics*; American Chemical Society; Washington, DC **1982**

[116] Lipkowitz, K.B.; Allinger, N.L. *QCPE Bull.* **1987**, 7, 19

[117] Beckhaus, H.-D.; Ruchardt, C.; Anderson, J.E. *Tetrahedron* **1982**, 38, 2299

[118] Jaime, C.; Osawa, E. *J. Chem. Soc., Perkin Trans. 2* **1984**, 995

[119] Forrester, T.R.; Smith, W. *DL_POLY_2 Reference Manual*; Daresbury England, **1998**, pp 15

[120] Jorgensen, W. L.; Tirado-Rives, J.; *J. Am. Chem. Soc.* **1988**, 110, 1657-1666

[121] Sprous, D. *http://linus.chem.wesleyan.edu/~mbjc/force.html* **1996,** Wesleyan University

[122] Allinger, N. L.; *J. Am. Chem. Soc.* **1977**, 99, 8127-8134

[123] Allinger, N. L.; Kok, R. A.; Imam, M. R.; *J. Comp. Chem.* **1988**, 9, 591-595

[124] Lii, J-H.; Gallion, S.; Bender, C.; Wikstrom, H.; Allinger, N. L.; Flurchick, K. M.; Teeter, M. M.*; J. Comp. Chem.* **1989** 10, 503-513

[125] Allinger, N. L.; Yuh, Y. H.; Lii, J-H.; *J. Am. Chem. Soc.* **1989**, 111, 8551-8565

[126] Hay, B. P.; Yang, L.; Lii, J-H.; Allinger, N. L. *Theochem: J. Molecular Structure* **1998**, 428, 203-219

[127] Lii, J-H.; Allinger, N. L. *J. Am. Chem. Soc.* **1989**, 111, 8566-8575

[128] Lii, J-H.; Allinger, N. L. *J. Am. Chem. Soc.* **1989**, 111, 8576-8582

[129] Lii, J-H.; Allinger, N. L.*; J. Comp. Chem.* **1991**, 12, 186-199

[130] Lii, J-H.; Allinger, N. L.; *J. Comp. Chem.* **1998,** 19, 1001-1016

[131] Damm, W.; Frontera, A.; Tirado-Rives, J.; Jorgensen, W. L. *J. Comp. Chem.* **1997**, 18, 1955-1970

[132] Jorgensen, W. L.; Maxwell, D. S.;Tirado-Rives, J. *J. Am. Chem. Soc.* **1996**, 118, 11225-11236

[133] Kaminski, G.; Duffy, E. M.; Matsui, T.; Jorgensen, W. L. *J. Phys. Chem.* **1994**, 98, 13077-13082

[134] Tecklenburg, M.M.J.; Villarreal, J.R.; Laane, J. *J. Chem. Phys.* **1989**, 91, 2771

[135] Allinger, N. L.; Geise, H. J.; Pyckhout, W.; Paquette, L. A.; Gallucci, J. C. *J. Am. Chem. Soc.* 1989, 111, 1106-1114

[136] Gerenser, L.J.; Goppert-Berarducci, K.E.; Baetzold, R.C.; Pochan, J.M. *J. Chem. Phys.* **1991**, 95, 4641

[137] Casewit, C.J.; Colwell, K.S.; Rappé, A.K. *J. Am. Chem. Soc.* **1992**, 114, 25, 10047
[138] Mayo, S.; Olafson, B.; Goddard, W. *J. Phys. Chem.* **1990**, 94, 8897
[139] Rappé, A.K.; Casewit, C.J.; Colwell, K.S.; Goddard, W.A. III.; Skiff, W.M. *J. Am. Soc.* **1992**, 114, 25, 10025
[140] Rappé, A.K.; Casewit, C.J.; Colwell, K.S. *Inorg. Chem.* **1993**, 32, 16, 3438-3450
[141] Allen, M.P.; Tildesley, D.J. *Computer Simulation of Liquids* **1987**
[142] Born, M.; v. Karman, T. **1912** in 141
[143] Singh, U.C.; Kollman, P.A. *J. Comput. Chem.* **1986**, 7, 718
[144] Warshel, A.; Levitt, M. *J. Mol. Biol.* **1976**, 103, 227
[145] Field, M.J.; Bash, P.A., Karplus, M. *J. Comput. Chem.* **1990**, 11, 700
[146] Vasilyev, V.V.; Bliznyuk, A.A.; Voityuk, A.A. *Int. J. Quantum Chem.* **1992**, 44, 897
[147] Théry, V.; Rinaldi, D.; Rivail, J.-L.; Maigret, B.; Ferenczy, G. *J. Comput. Chem.* **1994**, 15, 269
[148] Thompson, M.A.; Glendening, E.D.; Feller, D. *J. Phys. Chem.* **1994**, 98, 10465
[149] Thompson, M.A.; Schenter, G.K. *J. Phys. Chem.* **1995**, 99, 6374
[150] Stanton, R.V.; Hartsough, D.S.; Merz, K.M., Jr. *J. Comput. Chem.* **1995**, 16 , 113
[151] Bernardi, F.; Olivucci, M.; Robb, M.A. *J. Am. Chem. Soc.* **1992**, 114, 1606
[152] Åquist, J.; Warshel, A. *Chem. Rev.* **1993**, 93, 2523
[153] Bash, P.A.; Field, M.J.; Karplus, M. *J. Am. Chem. Soc.* **1987**, 109, 8092
[154] Dewar, M.J.S.; Thiel, W. *J. Am. Chem. Soc.* **1977**, 99, 4899
[155] Dewar, M.J.S.; Thiel, W. *J. Am. Chem. Soc.* **1977**, 99, 4907
[156] Dewar, M.J.S.; Zoebisch, E.G.; Healy, E.F.; Stewart, J.J.P. *J. Am. Chem. Soc.* **1985**, 107, 3902
[157] Field, M.J.; Bash, P.A. Karplus, M. *J. Comput. Chem.* **1990**, 11, 700
[158] Svensson, M.; Humbel, S.; Froese, R.D.J.; Matsubara, T.; Sieber, S.; Morokuma, K. *J. Phys. Chem.* **1996**, 100, 19357-19363
[159] Humbel, S.; Sieber, S.; Morokuma, K. *J. Chem. Phys.* **1996**, 105, 1959
[160] Bakowies, D.; Thiel, W. *J. Phys. Chem.* **1996**, 100, 10580-10594
[161] Antes, I.; Thiel, W. *J. Phys. Chem. A* **1999**, 103, 46, 9290
[162] Zhang, Y.K.; Lee, T.S.; Yang, W.T. *J. Chem. Phys.* **1999**, 110, 1, 46
[163] Bakowies, D.; Thiel, W. *J. Comp. Chem.* **1996**, 17, 1, 87

[164] Antes, I.; Thiel, W. In *Combined Quantum Mechanical and Molecular Mechanical Methods*; Gao, J.; Thompson, M.A. Eds.; Ser., vol 712, American Chemical Society, Washington, DC **1998**, p50
[165] Philipp, D.M.; Friesner, R.A. *J. Comp. Chem.* **1999**, 20, 14, 1494
[166] Maple, J.R.; Hwang, M.-J.; Stockfish, T.P.; Dinur, U.; Waldmann, M.; Ewig, C.S.; Hagler, A.T. *J. Comp. Chem.* **1994**, 15, 2, 162
[167] Thole, B.T. *Chem. Phys.* **1981**, 59, 341
[168] Winter, N.W. Pitzer, R.M. *J. Chem. Phys.* **1999**, 103, 1, 46
[169] Thole, B.T.; van Duijnen, P.Th. *Theor. Chim. Acta.* **1980**, 55, 307
[170] de Vries, A.H.; van Duijnen, P.Th.; Juffer, A.H.; Rullmann, J.A.C.; Dijkman, J.P.; Merenga, H.; Thole, B.T. *J. Comp. Chem.* **1995**, 16, 1, 37
[171] van Duijnen, P.Th.; de Vries, A.H. *Int. J. Quant. Chem.* **1996**, 60, 6, 1111
[172] de Vries, A.H.; van Duijnen, P.Th. *Int. J. Quant. Chem.* **1996**, 57, 6, 1067
[173] Matsubara, T.; Maseras, F.; Koga, N.; Morokuma, K. *J. Phys. Chem.* **1996**, 100, 2573
[174] Dapprich, S.; Komaromi, I. Byun, K.S.; Morokuma, K.; Frisch, M.J. *J. Mol. Struc.(Theochem)* **1999**, 461, 1
[175] Eichler, U.; Koelmel, K.M.; Sauer, J. *J. Comput. Chem.* **1996**, 18, 463
[176] Woiterski, A. *QM/MM (DL_POLY_2) Users Guide*, TU München, **2003**
[177] Belling, T.; Grauschopf, T.; Krüger, S.; Nörtemann, F.; Staufer, M.; Zenger, C.; Rösch, N. *High Performance Scientific and Engineering Computing, Bungartz, (H.-J., Durst, F.; Zenger, C.; Eds.), Lecture Notes in Computational Science and Engineering*, 8, Springer, Heidelberg, **1999**, p. 439
[178] Dunlap, B.I.; Rösch, N. *Adv. Quantum Chem.* **1990**, 21, 317
[179] Dunlap, B.I.; Conolly, J.W.; Sabin, J.R. *J. Chem. Phys.* **1979**, 71, 4995
[180] Nasluzov, V. A.; Rivanenkov, V. V.; Gordienko, A. B.; Neyman, K. M.; Birkenheuer, U.; Rösch, N. *J. Chem. Phys.* **2001**, 115, 8157-8171
[181] Fuchs, M.; Shor, A. M.; Rösch, N. *Int. J. Quantum Chem.* 2002, 86, 487-501
[182] Belling, T.; Grauschopf, T.; Krüger, S.; Nörtemann, F.; Staufer, M.; Mayer, M.; Nasluzov, V.A.; Birkenheuer, U.; Hu, A.; Matveev, A.V.; Fuchs-Rohr, M.; Neyman, K.M. Ganyushin, D.I.; Kerdcharoen, T.; Woiterski, A.; Rösch, N. PARAGAUSS Version 2.2, Technische Universität München, 2001
[183] Kerdcharoen, T.; Birkenheuer, U.; Krüger, S.; Woiterski, A.; Rösch, N. *Theor. Chem. Acc.* **2003**, in press

[184] Desmarais, N.; Jamorski, C.; Reuse, F.A.; Khanna, S.N. *Chem. Phys. Lett.* **1998**, 294, 480

[185] Perdew, J.P.; Wang, Y. *Phys. Rev. B* **1986**, 33, 8800; Erratum: *Phys. Rev. B* **1989**, 40, 3399

[186] Perdew, J.P. *Phys. Rev. B* **1986**, 33, 8822; Erratum: *Phys. Rev B* **1986**, 34, 7406

[187] Seemüller, T.; Krüger, S.; Rösch, N. in preparation

[188] Cu basis: Wachters, A.J.H., *J. Chem. Phys.* **1970**, 52, 2224 + Gianolo, L.; Pavani, R.; Clementi, E., *Gazz. Chim. Ital.* **1978**, 108(5-6), 181 (contractions)
S basis: Veillard, A. *Theor. Chim. Acta* **1968**, 12, 404
C, H bases: van Duijnefeldt, F.B. *IBM Res. Report RJ 945*, **1971**
Contracted by standard procedure: Dunlap, B.I.; Rösch, N. *Adv. Quantum Chem.* **1990**, 21, 317

[189] Dunlap, B.I.; Rösch, N. *Adv. Quantum Chem.* **1990**, 21, 317

[190] Becke, A.D. *J. Chem. Phys.* **1988**, 88, 2547

[191] Lebedev, V.I. *Zh. Vychisl Mat. Mat. Fiz.* **1975**, 15, 48

[192] Lebedev, V.I. *Zh. Vychisl Mat. Mat. Fiz.* **1976**, 16, 293

[193] Lebedev, V.I. *Proc. Conf. Novosibirsk* **1978**, Ed. Sobolev, S.L. (Nauka Sibirsk. Otdel., Novosibirsk, **1980**)

[194] Flechter, R. *Practical Methods of Optimization Wiley*, Chichester, **1981**

[195] Davidon, W.C.; *Variable Metric Method for Minimization. Technical report, AEC Res. And Dev.* **1959**, Report ANL5990 (revised)

[196] Flechter, R.; Powell, M.J. *Maths. Comp.* **1963**, 29, 1067

[197] Broyden, C.G. *J. Inst. Maths. Applns.* **1970**, 6, 70

[198] Fletcher, R. *Computer J.* **1970**, 13, 317

[199] Goldfarb, D. *Maths. Comp.* **1970**, 24, 23

[200] Shanno, D.F. *Maths. Comp.* **1970**, 24, 647

[201] Eckert, F. *Ab Initio Geometrieoptimierung großer Moleküle in kartesischen und internen Koordinaten*, Diplomarbeit, Universität Stuttgart, **1996**

[202] Edwards, P.P.; Johnston, R.L.; Rao, C.N.R.; *Metal Clusters in Chemistry* (Eds. Braunstein, P.; Oro, G.; Raithby, P.R.), Wiley-VCH, **1998**

[203] Messmer, R.P.; Knudson, S.K.; Johnson, K.H.; Diamond, J.B.; Yang, C.Y. *Phys. Rev. B* **1976**, 13, 4, 1396

[204] Jug, K.; Zimmermann; B.; Calaminici, P.; Köster, A.M. J. Chem. Phys. 2002, 116, 11, 4497

[205] Massobrio, C.; Pasquarello, A.; Dal Corso, A. *J. Chem. Phys.* **1998**, 109, 16, 6626

[206] Calamici, P.; Köster, A.M.; Russo, N.; Salahub, D.R. *J. Chem. Phys.* **1996**, 105, 21, 9546

[207] Ziegler, T. *Chem. Rev.* **1991**, 91, 651-667

[208] Görling, A.; Trickey, S.B.; Gisdakis, P.G.; Rösch, N., in : Topics in Organometallic Chemistry, Vol. 4; Brown, J.; Hoffmann, P., Eds.; Springer: Heidelberg 1999, p. 109-165 and references therein

[209] Shannon, R.D. *Acta Crystall. Sect. A* **1976**, vol. 32, part 5, 751-767

[210] Kittel, C. *Introduction to Solid State Physics*, Wiley, New York, **1986**

[211] Jander, G.; Blasius, E.; Straehle, J.; Schweda, E. *Lehrbuch der analytischen und präparativen anorganischen Chemie*, Hirzel, Stuttgart, **1995**

[212] Holleman, A.F.; Wiberg, E.; Wiberg, N. *Lehrbuch der Anorganischen Chemie* Gruyter **1995**

[213] Beyer, H.; Walter, W.; Francke, W. *Lehrbuch der organischen Chemie* , Hirzel, Stuttgart, **1998**

[214] Jug, K.; Zimmermann; B.; Calaminici, P.; Köster, A.M. J. Chem. Phys. 2002, 116, 11, 4497

[215] Nörtemann, F. *A Parallel Implementation of the Density Functional Method: SCF Part, Optimization Package and Application to Gold Clusters*, thesis, TU München, **1999**

[216] Douglas, B.E.; Hollingsworth, C.A. *Symmetry in Bonding and Spectra*, Academic Press, Inc. , Orlando, **1985**

[217] Wilson, E.B. Jr.; Decius, J.C.; Cross, P.C. *Molecular Vibrations*, Dover, New York, **1980**

[218] Winter, B.J.; Parks, E.K.; Riley, S.J. *J. Chem. Phys.* **1991**, 94, 12, 8618

[219] Genest, A. Diploma thesis, *Thiolatstabilisierte Goldcluster Eine Modellstudie mit der Dichtefunktionalmethode*, TU München, **2002**

[220] Hu, Z.-M.; Boyd, R.J. *J. Chem. Phys.* **2000**, 112, 21, 9562

[221] Akinaga, Y.; Nakajima, T.; Hirao, K. *J. Chem. Phys.* **2001**, 114, 19, 8555

[222] Pan, C.; Pelzer, K.; Philippot, K.; Chaudret, B.; Dassenoy, F.; Lecante, P.; Casanove, M.-J. *J. Am. Chem. Soc.* **2001** 123, 31, 7584

[223] reference calculations using the MM3 force field

[224] Krystian, S.; Pulay, P. *Chem. Phys. Lett.* **1994**, 229, 175

[225] Pérez-Jordá, J.M.; Becke, A.D.; *Chem. Phys. Lett.* **1998**, 241, 469

[226] Lewis, G.V.; Physica B **1985**, 131, 114

[227] Forrester, T.R.; Smith, W. *DL_POLY_2 Reference Manual*; Daresbury England, **1998**, pp 40

[228] Williams, D.E.; *Acta Crystallogr.* **1974**, A30, 71

[229] Modugno, G.; De Natale, P.; Bellini, M.;Inguscio, M.; Di Lonardo, G.; Fusina, L. *J.Opt. Soc. Am. B* **1996**, 8, 13, 1645

[230] Smirnov, S.N.; Braun, C.L. *Rev. Sci. Instr.* **1998**, 69, 2875-2887

[231] Sherwood,P. *Hybrid quantum-mechanichal/molecular-mechanical approaches*, in Grotendorst, J. (Ed.) *NIC Series Vol. 1*, FSZ Jülich, **2000**

[232] Williams, D.E. *J. Comput. Chem.* **1988**, 9, 745

[233] Ponder, J.; subroutine for charge – dipole interaction in [127-129]